UNIVERSITÀ
DEGLI STUDI
FIRENZE

PhD in CHEMISTRY
(Chemical Science)

CYCLE XXXIV

COORDINATOR Prof. Baglioni Piero

Reconstructing climate and environmental variability using East Antarctic ice records from the last millennium

Academic Discipline (SSD) CHIM/01

Doctoral Candidate
Dr. Nardin Raffaello

_____
(signature)

Supervisor
Prof. Traversi Rita

_____
(signature)

Coordinator
Prof. *Baglioni Piero*

_____
(signature)

Years 2018 /2021

Contents

1 Introduction **1**

1.1 Antarctica and Ice Cores 1

1.2 Horizontal tie points 7

1.2.1 Plutonium Isotopes from NWT 7

1.2.2 Sulphate in ice cores and Volcanic Signatures 9

1.3 Stratigraphic dating and Chemical markers 12

1.3.1 Stable isotopes ratio 13

1.3.2 Sulphate compounds ($nssSO_4^{2-}$ and MSA) . . 15

1.3.3 Nitrate in Ice cores 19

1.3.4 Sea-salt ions 23

2 Materials and Methods **27**

2.1 Samples collecting and samplings site 27

2.1.1 GV7 sampling site and sample retrieving . . . 27

2.1.2 DC3D sampling site 30

2.2 Decontamination Procedure 32

2.3 High Performance Liquid Chromatography - HPLC-IC 35

2.3.1 GV7(B) ice core samples 37

2.3.2 DC3D and snow surface samples 39

2.4 Total conductivity of DC3D samples 43

2.5 Inductively Coupled Plasma – Sector Field Mass Spectrometry Analysis (ICP-SFMS) 45
2.6 Analysis done outside University of Florence 46
2.6.1 Isotopic composition 46
2.6.2 Trace Element analysis 47
2.7 Identification of Volcanic signatures and Volcanic Flux 47
2.8 Dating of the records 50
2.8.1 Uppermost section of GV7(B) ice core 51
2.8.2 Layer counting dating of the GV7(B) ice core 52
2.9 Snow accumulation rate evaluation and trend analysis 54

3 Results **57**
3.1 Validation of decontamination procedure 57
3.2 Dating of Ice Cores 60
3.2.1 GV7(B) ice core dating 60
3.2.2 Dome C 3D ice core dating 74
3.2.3 Snow pits dating 77
3.3 Trace element analysis in DC3D core 80
3.3.1 Plutonium records 80
3.3.2 Metal records in the DC3D core 83
3.4 Snow accumulation rate across the East Antarctic Plateau 85
3.4.1 Accumulation evaluated at the GV7 site . . . 85
3.4.2 Accumulation evaluated at the DC site and the Antarctic Plateau 89
3.5 Volcanic Fluxes 91
3.6 Chemical variability across Antarctica 95
3.6.1 Sea-salt ions 95
3.6.2 Crustal ions 99
3.6.3 Nitrate 102

3.7 Dome C 3D ionic records 104
3.8 Chemical markers found in GV7(B) ice core 107
3.9 Correlation with Environmental Parameters and Chemicals found in the GV7(B) core 113
3.9.1 Total Solar Irradiance 114
3.9.2 Sea Ice Extent 118
3.9.3 Atmospheric circulation over Antarctica . . . 127

4 Conclusions **203**

Chapter 1

Introduction

1.1 Antarctica and Ice Cores

Antarctica is Earth's southernmost continent. It contains the geographic South Pole and it's located in the Antarctic region of the Southern Hemisphere, almost entirely under the Antarctic Circle (66°33'47.1" South of the Equator). Surrounded by the Southern Ocean (i.e., southern part of the Pacific, Atlantic and Indian Oceans) and with its 14 billion square kilometers (nearly twice the size of Australia for comparison) it is considered the fifth-largest continent. The continent is divided in two by the Transantarctic Mountains, which run between the Ross Sea and Weddell Sea. The mountain range divides Antarctica in East Antarctica (on the East of Ross Sea) and in West Antarctica (on the west of the same Sea). This division roughly correspond to the Western and Eastern Hemispheres in relation to Greenwich meridian.

Being on average, the coldest, driest, and windiest of continents, Antarctica landscape consist mostly of icy mountains, glacier and smooth ice sheet with little to no significant rivers, frozen and under-

ground lakes (most important of all being the Vostok lake, the largest sub-glacial lakes in the world) and almost no vegetation. Only the Antarctic Peninsula houses small areas of tundra with no grass or trees. Temperatures reach a minimum between -80 and -90°C during the winter and a maximum of -20°C inland during the summer, with few places near the coast that can reach temperatures of few degrees above 0°C. The lack of solar radiation reaching the continent due to its position plays a role in its extreme temperatures (i.e. during winter, in a period lasting approximately 4 months, the sun doesn't rise above the horizon) and in fact it has been reported that less than 100 W m^{-2} of annual mean shortwave radiation reaches the coast (Obryk et al., 2018), but compared to its Northern Hemisphere counterpart, South Pole is definitely colder. This is due to mostly two reasons:

- The height of the continent above the sea level: having an elevation of 2500m on average, Antarctica is the highest continent on Earth. The highest point on the icecap is in the Australian Antarctic Territory at 4100 m (82°20'S, 56°30'E), the highest mountain is Mount Vinson with a height of 4892m.

- The distribution of land and seas around the continent. Unlike the North Polar zone, which is covered by the Arctic Ocean and its warmth can get transferred to the icepack, most of Antarctica is a solid land surface, preventing this heat exchange in most of the inland continent.

Antarctica's surface is mostly covered in ice, with an ice sheet with a thickness of at least 1.9 km on average, reaching 4.7 km at the thickest point (Fretwell et al., 2013). As already stated, the majority of the Antarctic ice is considered continental ice. Major exceptions are the Ronne Ice Shelf, the Ross Ice Shelf and other minor zones in

the coast where the ice is floating on top of the sea level as reported in Figure 1.1. Since almost 70% of the world's freshwater reservoir is stored in Antarctica in the state of ice (90% of the continental ice), the surface mass balance (SMB) of the continent plays a critical role in Earth's climate and sea levels rising. It has been noticed that if all of Antarctica's ice melted down, average seas' level would rise of almost 60m. This makes understanding the evolution of the continent critical to understand the potential of its variation in SMB to impact the climate. Despite its position, as well as being one of the most isolated continents in the world, in fact, Antarctica and its tropospheric circulation play an important role in the regulation of the continent's climate and have significant influence over the world's general atmospheric circulation. Furthermore, not only does the presence of snow on the continent makes it a key component in the water balance of the planet, but it also significantly influences the global radiation balance due to its high albedo. Lastly, Antartica's role in the Earth's climate it's critical because the continent has a role in the heat transfer with higher latitudes, making it an essential part to the Earth's climate.

Despite the huge efforts of internationals programs (e.g. International Trans-Antarctic Scientific Expedition, ITASE, East Antarctic International Ice Sheet Traverse, EAIIST), a large part of the Antarctic sheet is still unexplored and additional data are needed to understand the role of the continent's surface mass balance (SMB) in the sea-level rise in recent decades and in the near future (DeConto and Pollard, 2016; Krinner et al., 2007). In particular, the last millennium is a critical time period to understand and put the more recent human related climate change into a longer temporal context, but for Antarctica, this time perios is still poorly investigated at high resolution. The goal of this work is to investigate this key time

Figure 1.1 – Map of Antarctica. Figure from (team LIMA, 2019)

period using ice cores and other snow and ice records from the East Antarctic plateau. Precipitations on the continent are low, with most areas inland receiving as little as 20 mm yr^{-1} of equivalent water and coastal sites reaching approximately 200mm yr^{-1}. Thus, from coastal sites is possible to retrieve cores with a high enough accumulation rate (which, in turns, correspond to a high temporal resolution). It must be noted that one of the most important consequence of the extreme cold temperatures is the formation of a constant low-pressure zone over the continent. This leads to air masses that rotate clockwise around the continent and generate what is known as circumpolar vortex (particularly intense in the winter's months) that can isolate air masses in the Pole from those from middle and low latitudes. This,

together with the lack of anthropogenic pollution on the continent makes it one of the few places on Earth where it's possible to obtain uncontaminated information about the past in the form of ice core records. Components of the atmosphere are, in fact, locked in the snow and ice of both poles; for gaseous components, air bubbles are trapped in the compressing layers of snow and are then preserved into ice (Brook, 2007) allowing the study of the air chemistry throughout millennia and going back up to 800,000 years (Augustin et al., 2004; Jouzel and Masson-Delmotte, 2010). Similarly, particulate matter and other component of the atmosphere can be found in the Antarctic snow thanks to dry and wet deposition phenomena that scavenges these compounds from air and make it deposit on the snow. In sites where external contamination, post depositional processes are low, and the snowfall is relatively constant, it's possible to retrieve cores in whic these markers are permanently fixed in the ice (progressive layers of snow "lock" atmospheric compound in the ice that forms through compression of the previous layers) and use them as proxies in the reconstruction of the past climate. In this work, most of the focus was given to these records that have already been extensively used to reconstruct atmospheric composition and temperatures of the past, spanning from few years up to hundreds of thousands (Abram et al., 2013; Delmonte et al., 2002; Fischer et al., 2007; Traversi et al., 2012; Watanabe et al., 1999; Wolff et al., 2010). In order to maintain the exact stratigraphy of the snow, cores are drilled on top of plateau where the snow accumulated undisturbed or on top of "domes" where the ice flow is perpendicular to the snow bed (although it's worth pointing out that this is not always the case e.g., Vostok ice core). This provides an ordinated record of progressively older layer of snow and compressed ice as described above. The ordinated stratigraphic layering of snow is also a main component to one of the key aspects

in the reconstruction of past climate, which is the age of the ice being analyzed. Different methods were developed since the second half of the last century (Hammer et al., 1980) and now include, for example:

- identification of seasonal patterns in chemical and physical stratigraphies (Alley et al., 1997; Cole-Dai et al., 1997; Extier et al., 2018; Sigl et al., 2016) that provide an accurate year-by-year dating

- analysis of ice flow models (e.g. Parrenin et al. 2001, 2004) based on deriving an accurate chronology from physical equations consistent with accumulation and thinning rates hypothesis on the continent

- identification of temporal horizons such as volcanic eruptions that brings spikes in the acidity of an ice layer and/or trace elements concentration (Castellano et al., 2005; Igarashi et al., 2011; Winstrup et al., 2012, 2019).

It must be noted, that due to the stratification process and the pressure of the upper layers, a thinning of the deeper layers of the core is always present and could bring to a loss of a the aforementioned seasonal patterns. Identification of these temporal horizons thus become the primary way to correctly assign a date to an ice layer and therefore to correctly interpret the chemical signal. In this work, particular interest was given to the chemical concentration vs. depth profile (also referred as stratigraphy in the main text with the similarity with the physical stratigraphies of ice cores) of different ions across multiple cores and shallow snow pit of Antarctica with the purpose of understanding the chemical and environmental variability in the last millennia of the continent.

1.2 Horizontal tie points

Most areas of the Antarctic continent receive little snowfall, with some areas investigated in this work with as low as 70mm w.e. of snow accumulation on average during a year. Thisis normally too low to allow the identification of single ice layers for the dating purpose of a core, especially at the deeper sections. In this work, the sulfuric acid signatures from past volcanic eruptions left in the core and the 240Pu traces from the second half of the 20th century's Nuclear Weapons Testing (NWT) were used to assign an exact date to the layer of ice.

1.2.1 Plutonium Isotopes from NWT

Plutonium is a man-made transuranic element first produced and isolated in the late 1940 by deuteron bombardment of ^{238}U at the University of California, Berkeley. It was extensively used in the making of nuclear weapons in the second half of the 20th century and in the atmospheric NWT of the same time period (the number of tests and the locations in which they were carried out are reported in Figure 1.2 and 1.3 respectively). It is present in the environment and deposited on the Antarctic continent via atmospheric transport. It exists in six isotopes (^{238}Pu ^{239}Pu, ^{240}Pu, ^{241}Pu, ^{242}Pu and ^{244}Pu with the latter having the longest half-life and ^{239}Pu being the most abundant in the environment) and it has been estimated that 6.5PBq of ^{239}Pu were released globally after the 1945 -1980 CE atmospheric NWT (United Nations Scientific Committee on the Effects of Atomic Radiation, 2000)).

Other anthropogenic sources are present for Pu and other man-made radioisotopes, but these are usually more local and can't produce a clear signal in ice cores (Waters et al., 2016; Galuszka and

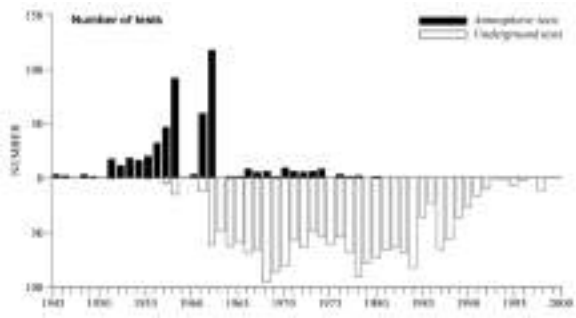

Figure 1.2 – Number of reported NWT across the globe in the second half of the 20th century as reported by (United Nations Scientific Committee on the Effects of Atomic Radiation, 2000)

Migaszewski, 2017). This, combined with the long half-lives (24110 years for ^{239}Pu), low solubility and high particle reactivity makes it one of the most suitable radioisotopes for reconstructing anthropogenic activities from ice cores and other records (Waters et al., 2016) In this work major attention was given to the NWT fallout traces in ice core. NWTs occurred in three distinct phases here briefly described. Phase one occurred from 1953 to 1959 CE and was dominated by the United States with tests in the low latitude of the Pacific and in Nevada. It is in this phase that one of the most well-known tests (Bravo test) was conducted in February of 1954 CE at Bikini Atoll, with a total yield of 15 Mt. Phase two occurred from 1961 to 1962 CE and was dominated by the former Soviet Union (USSR), whilst Phase three started in 1960 and ended in 1980 CE with the majority of tests conducted by France and China. Later tests were conducted underground with minimal input of radioactive nuclei in the atmosphere. In the atmosphere, radioactive debris attach to ambient aerosol particles which determine the mechanism governing their atmospheric transport both in the troposphere and in the stratosphere, with residence times in the order of days (Alvarado

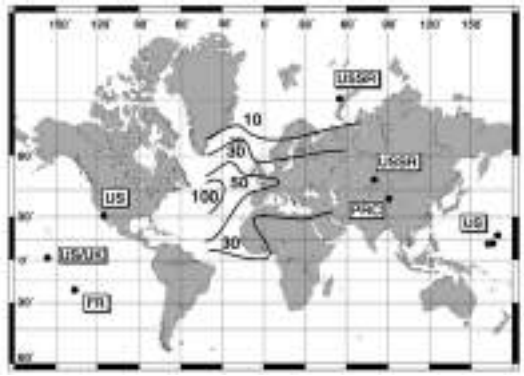

Figure 1.3 – Locations of the main atmospheric test sites as reported by Warneke et al. (2002) with Nevada Test Site follout (1953) radioactive distribution reported by the contour lines (relative units as reported by Eisenbud and Gesell (1997)

et al., 2014) and up to years for the smaller particles who reach the stratosphere (Martell, 1966; Allkofer and Fox, 1966) due to the thermal stratification. It's worth nothing that only 20% of the total nuclear weapon's fallout reached the SH (Hardy et al., 1973) but accidents like the SNAP-9A of 1964 introduced large amounts of ^{239}Pu found for the majority (up to 95%) in the SH (Hardy et al., 1973).

1.2.2 Sulphate in ice cores and Volcanic Signatures

When not considering sea spray and the presence of sulphate coming from sea sprays, two major sources of sulphate in ice cores can be identified and will be discussed in this work. Biogenic sulphate and volcanic sulfuric acid. Marine emitted (here referred as biogenic) sulphate mainly arise from the atmospheric oxidation of their precursor dimethyl sulfide (DMS), which in turn is produced by metabolic activities of marine phytoplanktonic species (Stefels et al., 2007). This brings a strong seasonality of DMS and, in turns, an

analogous seasonal behavior of nssSO_4^{2-} with the highest concentrations found during the phytoplanktonic bloom, occurring in austral spring-summer (November-March) (Becagli et al., 2012). MSA (see below) displays a similar seasonal pattern due to the shared precursor with biogenic sulphate.

Volcanic traces of sulfuric acid on the core are superimposed over this biogenic signal and can be identified in the core using statistical methods. In the aftermath of an explosive volcanic eruption, in fact, two kinds of compounds are emitted. A coarser fraction of magmatic material (essentially siliceous material emerging as solid particles of tephra (Robock, 2000) and different gaseous compounds. Amongst the latter, H_2O, CO_2 and SO_2 are the most abundant and have the possibility, unlike the coarser fraction to i) persist in the atmosphere for a longer time period (up to years) and ii) affect the climate on a larger scale. Sulfur species are then quickly oxidized to H_2SO_4 (Kremser et al., 2016; Yue, 1981) and due to their low water solubility can persist in the atmosphere for longer, and thanks to well-known tropospheric and stratospheric circulation pathways, the Brewer–Dobson circulation (Trepte and Hitchman, 1992; Langway et al., 1995; Robock, 2000; Gao et al., 2007; Delmas et al., 1985) can reach the polar regions in the form of H_2SO_4 and are then deposited on the ice sheets (e.g. Robock 2000) in the years following the eruption (Sigl et al., 2015). It must be noted that the exact date of the deposition varies widely not only when considering the location of the volcano but also the location in which the core was retrieved (e.g Marshall et al. 2018).

Identification of volcanic signatures in the ice of Antarctica is a well-investigated topic studied since the second half of the last century. A first, simple method, using the correlation between the acidity and the electrical current (ECM) measured in ice cores was

proposed by Hammer et al. (1980). ECM technique (Hammer, 1983), a continuous way to identify acidity levels on non-melted ice core. Lower acidity period (or even alkaline period due, for example, of large amount of dust into the atmosphere) could also be recorded in this way. Since acidity levels could also arise from the mixing of different acidic species (that may not be characterized by a real seasonal pattern) the presence of large acidity levels from volcanic eruption could alter ECM pattern. Direct chemistry such as ionic chromatography as proposed in this work is also extensively used (e.g. Sigl et al. 2016; Castellano et al. 2004, 2005) in the identification of volcanic signatures that are then used in paleoclimatic reconstructions and to understand their role in the climate. Despite their extensive use in synchronization of ice core timescales (Severi et al., 2007, 2012; Winski et al., 2019) and being widely used to assign an absolute date to ice layers in a core (Castellano et al., 2005; Sigl et al., 2013) in conjunction with the annual layer counting, the correlation between volcanic activity and climate and environmental variability (Zielinski, 2000; Robock, 2000) is still unclear. Although some environmental parameters seem to be unaffected by explosive eruptions, there is a general consensus on their contribution to a cooling of the climate from regional to global scale. This is due to either presence of volcanic matter in the atmosphere in the following months of the eruption or the formation of acidic clouds from tropospheric H_2SO_4 that can act as condensation nuclei for the formation of clouds. Main consequence of this, is a cooling of up to 1°C (Sigurdsson, 1990; Rampino, 1982) as a result of the reflection of incoming solar radiation in the troposphere.

Furthermore, specific trace elements such as Tl and Bi have been proposed to be associated with dust deposition from volcanic eruptions (Candelone et al., 1995; Kellerhals et al., 2010). Due to

the univocally source of these elements, unlike nssSO_4^{2-} that has different sources, the identification of the concentration peak of these elements can confirm the volcanic nature of a spike in sulphate concentration and be used in dating of the core. As reported by Hwang et al. (2019) this deposition of dust normally occurs earlier when compared to the deposition of sulphate material. It must be noted that not all eruptions are suitable to be used for the dating; for minor, not explosive volcanic eruptions, the long-range inter-hemispheric transport of volcanic material (with the exception of small gaseous molecules with long residence time in the atmosphere) is prevented by the tropical circulation belt (Hammer, 1980). This has as a direct consequence that only those eruptions from volcanoes in between the 20°N and 20°S latitudes are able to affect both hemispheres and reach both poles, with eruptions from volcanoes from middle to high northern latitudes not having an effect on the Antarctic continent (Lamb, 1970). This is not necessarily true for all volcanic eruptions and has been shown that high latitude eruptions can reach the Antarctic continent. This is the case of the Puyehue-Cordón Caulle volcano in Chile, whose volcanic material (tephra) reached the WAIS Divide within a few weeks of the eruption (Koffman et al., 2017).

1.3 Stratigraphic dating and Chemical markers

As already stated, unlike marine sediment cores, which despite allowing to investigate hundreds of thousands of years of past history, that due to the constant disturbance of the sea floor by deep ocean current don't allow to investigate at high resolution the past climate (annual to sub annual resolution) ice cores are able to provide detailed

information about the past. In sites where snowfall is high enough throughout the year can bring to the identification of annual to sub annual patterns. Since the presence of a correlation between the atmospheric components' concentration and the one found in the Antarctic ice has been proven true (e.g. Lambert et al. 1983; Pourchet et al. 1983), and many components of the atmosphere show seasonal pattern, it's possible to use these signals found in the core to date the ice.

1.3.1 Stable isotopes ratio

The variation in concentration between stable isotopes of the water is correlated with the temperature and investigating the isotopic composition of the ice is one of the most reliable and extensively used methods used to date an ice core (Extier et al., 2018). In this work, major interest was given to the ^{18}O excess found in the Antarctic snow that (i.e., the ratio between ^{18}O and ^{16}O found on the icecap) with the goal of identify a clear seasonal pattern for the dating of ice cores. The ratio is compared to a standard value (sea composition) and expressed as the deviation (δ) from said standard in permille values. $\delta^{18}O$ in falling snow varies with seasons (Dansgaard, 1964), due to the different rate with which different isotopes condense and therefore precipitate. From equatorial regions, when the majority of evaporations from sea and the formation of clouds occur, to the Antarctic regions where the water is then fixed in snow, the ratio between isotopes varies; heavier isotopes precipitate with ease, especially during winter months when their content in the snow is progressively depleted as schematically reported in Figure 1.4.

This brings a seasonal pattern with winter minimum and summer maxima that was widely used since firstly introduced (Dansgaard,

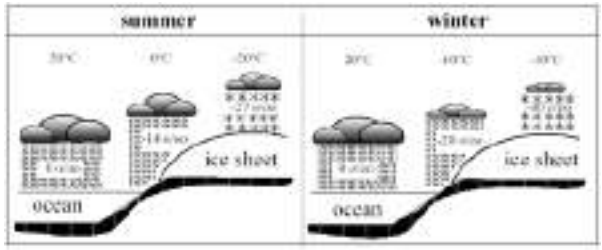

Figure 1.4 – $\delta^{18}O$ depletion during winter and summer months

1964; Hammer et al., 1980) to date cores by assigning to each maximum the start of the austral summer.

Since snow layers progressively deposit onto the previous ones and compressed the firn into ice through a densification process, each annual layer is compressed. The isotopic pattern and the possibility of identifying summer maxima not only is influenced by the physical thinning of the ice layers (i.e. the resolution becomes smaller in the deeper sections of a core) but also by the smoothing process visible under the firn zone. This is due to the diffusion of stable isotopes in the firn and snow layers (Whillans and Grootes, 1985; Cuffey and Eric, 1998). This process that strongly depends on the depth of the ice layers (diffusion is faster in the uppermost layers of the core) and the temperature (Jouzel and Merlivat, 1984), but that has the potential of masking the seasonal pattern and for deeper core, a correction of said smoothing could be needed (Holme et al., 2019) for the correct interpretation of the isotopic signal. The variability of the isotopic ratio is fixed in the snow, and as such the isotopes here considered work as a direct proxy of the relative depletion of water vapor in the transport from the evaporation source to the site. For this reason, is possible to find a correlation between $\delta^{18}O$ in the snow and the temperature of the cloud at the time of condensation. Indeed, several studies have investigated this relationship with the aim of

understanding the past climate (e.g. (Ekaykin et al., 2017; Stenni et al., 2004)). Whist beyond the scope of this work, and although a correlation between temperature and $\delta^{18}O$ is indeed present, it is worth noting that the variation of temperature is not the only parameter influencing the isotopic ration. (Noone and Ian, 2004) investigated the effect of the sea ice on the water isotope transport over Antartica, suggesting that the variation in temperature over the ice can affect more strongly the isotopic ratio rather than just the final temperature of the vapor mass. Similarly, Steig et al. (2013) didn't used $\delta^{18}O$ ad a direct proxy for ttemperature, but rather it noted that $\delta^{18}O$ in West Antarctica covaries with atmospheric circulation on the continent and it's influenced by the presence of sea ice as well (in particular, $\delta^{18}O$ in West Antarctica precipitation is increased when sea ice extent is reduced). Here, due to the limited amount of high-resolution data for $\delta^{18}O$ main focus was given on its use in the dating of one of the deep ice cores, GV7(B), without investigating the correlation with temperature on site.

1.3.2 Sulphate compounds ($nssSO_4^{2-}$ and MSA)

Inside ice cores, alongside sulfuric acid (H_2SO_4 in the form of non-sea-salt sulphate) arising from the oxidation of sulfuric gaseous materials (primarily SO_2) in the atmosphere, the main component of sulfur-oxidized compound is methanesulphonic acid (MSA). On the Antarctic continent, anthropogenic sources of sulphate are low, making the uncontaminated sea water surrounding it the main source of these compounds. The role of sulphate in biochemistry and in this work has been already discussed in previous sections where its potential in the dating of ice core has been explored. Due to their common precursor (DMS), the same is true for MSA.

Volatile sulfuric compounds like DMS in the atmosphere are the

result of numerous production and consumption processes occurring in the marine ecosystem. It's hard to predict via models the temporal and geographical distribution of these compounds due to the complex nature of the ecosystems and array of microorganisms producing them, but it's estimated that for polars regions, DMS (Stefels et al., 2007) up to 50 - 60% of the total. With an estimate emission ranging between 15 and 38 Tg S yr^{-1} (Kettle and Andreae, 2000), oceans are the main source (up to 95%) of the DMS that reaches the atmosphere. Both phytoplankton, mainly Dinocyceae dinoflagellates and Prymnesiophycear (Keller et al., 1989; Caruana and Malin, 2014), and in high-latitude marine areas sea-ice algaes (Levasseur et al., 1994; Becagli et al., 2016) produce dimethylsulphoniopropionate (DMSP), which is, in turn, the main precursor of DMS in complex cycles of reaction summarized in Figure 1.5

Concentration of DMS in the water column and in the marine atmosphere seems to be correlated with a number of factors influencing two different regimes of productions, one defined as "bloom-forced", the other "stress-forced" (Toole and Siegel, 2004). In the first one, phytoplanktonic bloom dictates DMS production (occurring primarily in regions characterized by mono-species blooms of phytoplanktonic species producing DMSP such as the subpolar North Atlantic Ocean and the Southern Ocean) and DMS is strongly correlated with the production of chlorophyll. A positive correlation is also found between the phytoplanktonic biomass in the sea (Vallina and Simo, 2007) and DMS (and by extent, MSA). For the stress-forced regime, the production of DMS is mostly correlated with high UV radiation doses and more typical for temperate seas. In polar seas, the two conditions can coexist, and the latter may follow the bloom regime (Galí and Simó, 2010). Similarly, other kind of stressors have been proven to increase DMSP and DMS production; both Iron limitations

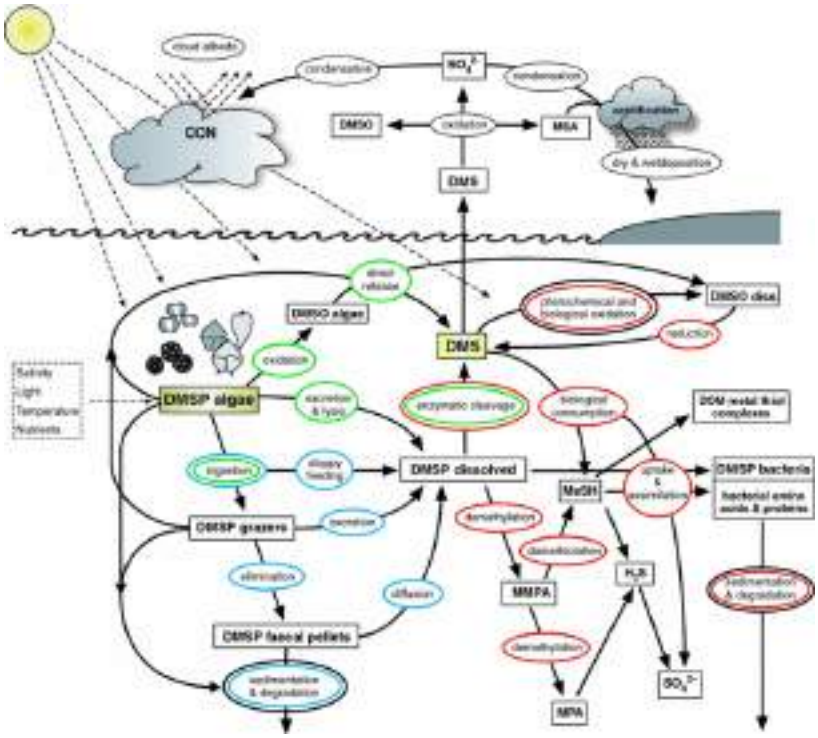

Figure 1.5 – Schematic representation of the process and pools involved in marine biogeochemical cycling of DMSP and DMS. Main functional groups are highlighted in colored ellipses: green, phytoplankton; blue, zooplankton; red, bacteria; black, abiotic factors (Stefels et al., 2007)

(Bucciarelli 2013) and nutrients limitations either increase cellular DMSP or its lysis to DMS (Sunda et al., 2002). In polar regions, the presence of Sea Ice adds complexity to the system. Melting of ice is associated with increased primary production and higher levels of DMS (Becagli et al., 2016), but the influx of fresh water into the sea can create a colder layer that isolate the upper layers of water, serving as a lid on the more productive waters underneath (Galí and Simó, 2010; Arrigo et al., 2008) further contributing to the regulation of DMS in the atmosphere. In ice cores' records, the

seasonality patter of MSA production is kept, but it must be noted that the low concentration of MSA in ice makes it so that its summer maxima can be less pronounced than the one shown by sulphate. Furthermore, despite the similar patter between nssSO_4^{2-} and MSA, the two summer maxima don't match, and a shift in the maxima peaks have been found not only in cores, but also in other sampling sites (Becagli et al., 2012). This is possibly due to the difference in the photochemical oxidation rate and size distribution and transport pathway (Preunkert et al., 2008). Due to its marine origin, and since unlike SO_4^{2-} which has multiple sources, MSA only arises from the oxidation of DMS, it is possible to use concentration records of MSA in ice core to reconstruct pythoplanktonic productivity (e.g. Legrand et al. 1991) in the last glacial-interglacial climate cycles. More importantly, in polar waters the production of MSA is strongly influenced by sea-ice extension and coverage: lowest concentration normally occurs beneath heavy ice pack (Leck and Persson, 1996). This leads to the suggestion of using MSA as a potential ice core proxy for sea-ice extend, for which only few decades of data are currently available (satellite data records only started in 1979 CE) and multiple studies have, indeed, found a correlation between MSA levels registered from ice core from both the Arctic and the Antarctic continent. Positive correlations were found with changes in the sea-ice extent for cores drilled in Greenland (Legrand and Mayewski, 1997; Whung et al., 1994) and Antarctica (Curran, 2003; Welch et al., 1993; Foster et al., 2006), but it must be noted that this is not true for all sites on the continent. Negative correlations were also found from records coming from both Poles (Pasteur et al., 1995; O'Dwyer et al., 2000), suggesting that the relationship between production and transport of MSA and Sea Ice Extend is not as simple as initially thought and does not follow a linear correlation. This is also because

of different production regimes (Isaksson et al., 2005) that can affect the final concentration of MSA in the core. Furthermore since MSA concentration is correlated to the phytoplanktonic bloom, large sea fluctuations that bring an upstream of nutrients can be correlated with such concentration as well. This was first hypothesized by Legrand et al. (1991) who correlated the Southern Oscillation Index (SOI) with MSA concentration in ice cores. Indeed, higher MSA concentrations were found in correspondence with the extended 1991 - 1993 CE El-Niño event when considering cores drilled both from the South Pole (Dibb and Whitlow, 1996) and more coastal sites (Isaksson et al., 2001) with the ratio between MSA and biogenic sulphate more than double during such events than what found in the background . It has been proposed (Legrand et al., 1991) that the reduced upwelling of Antarctic water during an El-Niño Southern Oscillation (ENSO) event could enhance productivity (i.e., nutrient rich water reaches the sea surface where light is more abundant) and therefore DMS and MSA production.

1.3.3 Nitrate in Ice cores

Atmospheric Nitrate mainly arise from the oxidation of reactive nitrogen species (e.g. $NOx \longrightarrow NO + NO_2$), the complete cycle of nitrogen compounds in the atmosphere is not important for the purpose of this work) and together with NH_4 and N_2O in gaseous form trapped in ice in form of bubbles, NO_3 constitute the majority of the nitrogen trapped on the Antarctic continent (Legrand et al., 1999). For the Antarctic continent, due to its position, most of the oxidated species come from stratospheric sources (oxidation of N_2O and N_2 photochemistry) and lightning action on the tropospheric atmosphere at the tropical latitudes(Legrand and Kirchner, 1990). Due to post depositional processes (see below), the snowpack itself

can be considered a source of Antarctic Nitrate (Savarino et al., 2007) as well and studies on atmospheric nitrogenous compounds' concentration have revealed a non-negligeable amount of organic nitrate (Jones et al., 1999; Dibb et al., 1998) inside the cores. Nitrate's abundance in snow makes it relatively easy to detect in the cores and a large number of nitrogen ice-core data are available or the continent, but despite the abundance of data, their interpretation is still unclear (Wolff, 1995). Some of the characteristics of the NO_3^- concentration records obtained from ice core were explained (e.g. the rise of Nitrate since 1940 CE is well known to be caused by rising in fossil fuel combustion as reported by Neftel et al. (1985)), others, such as the discrepancy between North and South Pole's cores' records, are still not fully understood. Unlike Ammonium (which is prone to external contamination from laboratory atmosphere), the concentration of Nitrate in the core once the ion is fixed in the ice layers and post-depositional processes can't affect its final concentration any longer, is relatively stable during both sampling and shipping of the core. The same is not true for the nitrate on surface snow, whose stability and the processes affecting its final concentration are still unclear and for which both depositions, post depositional loss and recycling processes (e.g. Röthlisberger et al. 2002; Shi et al. 2015; Zatko et al. 2016) are all contributing factors to the final concentration. In both Poles, in fact, the deposition of Nitrate has been proven to be reversible and a in the first meters of snow, a net loss of nitrate is observable. Both re-evaporation of nitrate in the form of volatile nitric acid (Dibb et al., 1998; Mulvaney et al., 1998; Röthlisberger et al., 2000b) and photolysis of Nitrate in the first centimeters of snow (Noro and Takenaka, 2020; Meusinger et al., 2014) contribute to the loss of nitrate. The latter occurs following the

$$NO_3{}^- + hv\,(^+H^+) \longrightarrow NO_2(aq) + OH(aq)$$

$$NO_3{}^-\,(aq) + hv \longrightarrow NO_2{}^-\,(aq) + O(^3P)\,(aq)$$

pathways (Zatko et al., 2016) in the liquid-like region of the ice grains. Both processes occurr in the snow, but the former is though to be the more dominant one (Grannas et al., 2007; Meusinger et al., 2014). It has been noted that allloss and formation of Nitrate, are also correlated with the temperature on site (Röthlisberger et al., 2000b) as well as the snow accumulation and wavelength irradiating the snow on site (Röthlisberger et al., 2000b, 2002; Berhanu et al., 2014, 2015), with lower temperatures bringing higher NO_3^- concentration in the snow. The Nitrate decomposition in the superficial layers leads to re-oxidation processes in the atmosphere to NO_3^- when sufficient amount of oxidant and sunlight are available (Grannas et al., 2007; Erbland et al., 2013). Since these phenomena are more intense during the Austral summer (highest irradiance and highest oxidation capacity of the atmosphere), a seasonal behavior seems to be present in both aerosol and snow concentration (Traversi et al., 2014). This would be in line with the seasonal character of Nitrate sources and transport mechanism, enhanced during the spring and summer's months (Legrand and Delmas, 1986; Traversi et al., 2004).

One last relevant source of nitrate in the polar caps are stratospheric processes (Legrand and Kirchner, 1990; Savarino et al., 2007) involving extraterrestrial fluxes of energetic particles and Solar Irradiation. These processes generate Nitrate in the upper atmosphere as a result of the action of ionizing cosmic radiation, in a chain of reactions starting with NO, making Nitrate records in ice core a potential quantitative marker for solar activity in the past (Kocharov et al., 2000; Dreschhoff and Zeller, 1998). Solar activity does vary indeed widely through the years, with deep minimum (e.g. Maunder Minimum) with almost no visible sun spots for decades to period

of extreme activity (Eddy, 1976). Written records of the number of solar spots as a direct record of solar activity do exist and covers approximately the last four centuries of history, but understanding solar variability on longer time scale can bring important information on how it affected (and by consequence how it will affect) the climate. Periods characterized by grand maxima of solar activity see also an influx of cosmic rays reaching the Earth, these can interact with the atmosphere and produce radionuclides in a series of chain reactions (Masarik and Beer, 2009).

Solar Activity can be reconstructed from a number of proxies, but the most used radionuclei that are stored in polar ice cores are ^{10}Be and ^{14}C . The two isotope follow independent paths once produced but they do show similar patterns in ice core, although it has been shown that they disagree on a decadal and millennial scale (Usoskin et al., 2009) with ^{10}Be signal thought to be possibly distorted by the regional circulation over the polar regions at a decadal to multi decadal scale (Steig et al., 1996). Despite being univocal markers of the solar activity, two major drawbacks are to be considered when investigating the possibility of using isotopic signals in paleo reconstructions: firstly, the relatively short half life of the ^{14}C. This means that, despite being a suitable proxy for investigating the last 10kyr time period, concentration of ^{14}C in deep cores rapidly decreases, potentially making impossible to quantify it in the samples. Similarly to ^{14}C and unlike Nitrate which comes from a number of sources, ^{10}Be records in ice core would constitute an unique marker for solar activity, but the extremely low concentration in ice cores and therefore the extensive volume of sample needed, could mean a reduced temporal resolution when analyzing their profile. Findings of any independent proxy of the past solar activity is therefore extremely valuable and levels of Nitrate, due to its atmospheric origin has been

proposed and successfully correlated with the past solar activity (Traversi et al., 2012).

1.3.4 Sea-salt ions

The primary source of sea-salt ions (e.g. Sodium) found in Antarctica is sea-salt aerosol (SSA) from bubble bursting at the open ocean surface (de Leeuw et al., 2011). When a wave breaks, air is introduced inside the water and then quickly rise to the surface. When these bubbles burst, two kinds of particles are created: first, film droplets from the bursting of the bubble itself are ejected in the atmospere Then, since the cavity by the bubble is quickly filled by water, a "jet", i.e. a column of water, is created and ejectes smaller particles in the atmosphere (Thorpe, 1992; Löndahl, 2014) as reported in Figure 1.6.

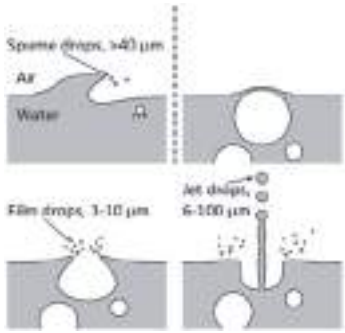

Figure 1.6 – Creation of sea-spray aerosol from spume and jet droplets. Figure from Löndahl (2014)

Since sea spray contributes to the majority of the aerosol reaching Antarctica (e.g. Delmas et al. 1992; Wagenbach et al. 1998) this is the primary sources for chemical species on the Antarctic snow. However, a secondary source of SSA over the continent can be identified in the form of the sea ice itself. This was firstly investigated when studying

the fractioning of the Sulphate in the Antarctic aerosol. Sulphate can precipitate on the Sea Ice as Mirabilite (Na_2SO_4*$10H_2O$) and gets collected in frost flowers (Rankin et al., 2000, 2002). This depletion of Sulphate when Sea Ice forms at temperature below -8°C is also noticeable in the aerosol (Wagenbach et al., 1998; Rankin et al., 2004) brought from air masses blowing over frost flower rich regions of the Antarctic Sea ice (Rankin et al., 2002) suggesting frost flowers and sea ice in general as a source of SSA. In this work, sea-salt ions (mainly, Sodium, Magnesium, Chloride and on lesser extent, Potassium Calcium and Sulphate) were used both in the dating of the high-resolution core and as a way to investigate the chemical variability of the past. It has been shown (Bergin et al., 1998) that sea-salts' concentration in South Pole ice cores display a seasonal patter with maxima in synch with the minimum of the $\delta^{18}O$ profile (Legrand and Delmas, 1984; Whitlow et al., 1992). This increase of concentration in early winter has been correlated with the number of storms that can penetrate the Antarctic continent (van Loon, 1967) and the same winter-spring maximum was observed in the aerosol of coastal stations (Mulvaney and Wolff, 1994; Weller et al., 2011). Due to their well resolved seasonal pattern in ice cores, Sodium (and to a lesser extent Magnesium and Calcium) concentration profiles have been used to date ice cores using an annual layer counting procedure (i.e. by identify each winter maximum, e.g. Herron and Langway 1979; Winski et al. 2019; Cole-Dai and Mosley-Thompson 1999; Ferris et al. 2011). It must be noted that the origin of the SSA combined with the increase of SIE during the winter months could increase the distance from the primary source, resulting in a loss of aerosol from the ocean during the long-term transport (Abram et al., 2013), potentially masking or dampening the aforementioned pattern in some sites. On the other hand, the presence of Sea Ice as

a secondary source of SSA on the continent raises the possibility of using sea salts' concentration records in the core as a potential proxy for the sea ice extent in the past e.g. Wolff et al. 2003; Severi et al. 2017). Unlike MSA, in fact, which has been proven being subjected to post depositional processes in sites with low accumulation rate (Weller et al., 2004) with a loss of up to 50%, levels of Sodium in the ice core are fixed in the snow. Unlike MSA, that requires a careful site planning, SSA can ensure a reconstruction of the SIE that is not biased by non-marine parameters, and of all the SSA components, Sodium has been noted to be the most reliable one. Unlike Calcium and Magnesium, whose sources are not univocally marine, Sodium levels found in ice core can be considered having only marine sources (Legrand and Delmas, 1984; Maupetit and Delmas, 1992). Sodium can, in fact, coming from crustal sources, but both in inland (Röthlisberger et al., 2002) and coastal sites (Benassai et al., 2005; Nyamgerel et al., 2020) these can be considered negligeable. Similarly, despite its marine sources, Chloride is affected by post depositional effects, especially in sites with low accumulation rate (Röthlisberger et al., 2003) and fractioning processes, leading to a less reliable seasonal pattern in ice cores that can be used for the dating procedure.

Chapter 2

Materials and Methods

2.1 Samples collecting and samplings site

In this work, multiple deep ice core, shallow firn snow pits and surface snow samples were analyzed for the purpose of understanding the spatial and temporal variability across the East Antarctica in the last millennium. In particular, two deep ice core (GV7(B) and DC3D), five shallow snow pits sampled during the 2018/19 EAIIST traverse and surface and bulk samples of snow sampled during the same traverse, were analyzed. All samples sites are highlighted in Figure 2.1.

2.1.1 GV7 sampling site and sample retrieving

GV7 (70°41'S, 158°51' E) is a drilling site located in the Oates Coast, in East Antarctica characterized by a mean annual temperature of -31.8°C and originally investigated in the framework of the 2001/2002 ITASE traverse. During that time period, a 55-m firn core was retrieved, and the characteristic of the site investigated. The snow accumulation rate on site (241 ± 13 mm w.e. yr^{-1} over the

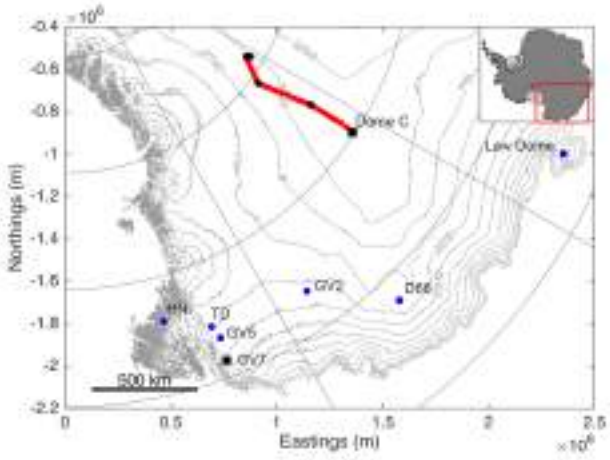

Figure 2.1 – Sampling sites across the East-Antarctic plateau. In black, sites analyzed in this word (square, cores, circles, snow pits). Red circles highlight the path of the EAIIST. In blue are highlighted different cores used with comparisons and named in the core

past 50 years) was evaluated by using the 1965-1966 CE radioactive horizon associated to NWT (Frezzotti et al., 2007; Stenni et al., 2002; Magand et al., 2004). Its snow accumulation rate, 3 times fold the one found on Talos dome and 10 times higher than EPICA Dome C, together with the thickness of the ice (approx. 1700 m), the limited post depositional processes due to the reduced force of katabatic winds along the ice divide (Becagli et al., 2004; Frezzotti et al., 2007; Magand et al., 2004) and the excellent stratigraphy (chemical and isotopic Caiazzo et al. 2017; Delmonte et al. 2015; Frezzotti et al. 2007) makes it the perfect site to retrieve ice core to investigate the past climate at high resolution (annual to sub-annual). Preliminary models based on the snow accumulation rate and the snow density at the site predicted that the upper 500 m might span back in time more than 2000 years. The expected time resolution for the site was

found to be about 2 yr m^{-1} at the surface, 4 yr m^{-1} at 50 m, and 6 yr m^{-1} at 500 m (Caiazzo et al., 2017). Thanks to these characteristics and to its high snow accumulation rate, GV7 was chosen as a site to investigate the last millennia in the framework of the PNRA projects IPICS 2kr – IT, which represent the Italian contribution of the project "The IPICS 2k Array: a network of ice core climate and climate forcing record for the last two millennia". The latter is one of the four topics of the International Partnerships in Ice Core Sciences (IPICS) that coordinated several drillings out in the Oates Coast, East Antarctica. Furthermore, spatial distribution of snow accumulation from GPR layer upstream GV7 site shows that internal layering and surface elevation are continuous and horizontal up to 10 km from the site, revealing low ice velocity 0.3 $\pm$ 0.01 m yr^{-1}. Distortions of isochrons due to ice flow dynamics are absent and the site present a very low snow accumulation spatial variability (less than 5%, Frezzotti et al. 2007). Further information on the site and the extensive chemical dataset covering 7 years of deposition on site obtained from the analysis of two snow pits are already elsewhere (Caiazzo et al., 2017). The drilling operations were carried out during the 2013/2014 Antarctic summer using an electromechanical drilling system (Eclipse Ice drill Instrument) which was able to extract a 247.2 m long core from the bottom of a snow pit down to a depth of 250.7 m. Drilling fluid (Exxsol D40) was introduced in the bore hole from a depth of 80m (close off 75 m) and kept at a level of 4m over the drilling system to ensure the best quality of the core. Despite this and the care taken during the drilling operation, the Eclipse instrument experienced problems and multiple cracks and breakage were found in the ice when retrieving the lower section of the core (from a depth of approx. 100 m). This led to problems when it came to interpret the data, and it's further discussed in later

sections of this work. The core, cut in 60cm samples and logged accordingly, was then shipped at the EUROCOLD lab at University of Milan Bicocca (Italy) where the sections were further divided (cut longitudinally) and distributed among different research group. The section destined to the determination of ionic content (4x4x60 cm strips) was kept in the cold room of the University of Florence until the moment of analysis in sealed PE bags.

2.1.2 DC3D sampling site

Dome C (75°C 06'S, 123°21'E) is the fourth highest dome in Antarctica, reaching a height of approx. 3233 m a.s.l. and housing the permanent Italian French Antarctic Station (Concordia). Situated approximately 1100 km from the coastline on the Antarctic plateau, Dome C is an elliptical dome with the minor axis (NO-SE) about 70% shorter than the major axis. This makes the SW-NE wind direction prevalent (Remy and Tabacco, 2000; Urbini et al., 2008), although the typical katabatic winds of the continent aren't prevalent on site. The site is characterized by an average temperature of the ice cap of -54.5°C and a thickness of the ice cap of 3250 $\pm$ 25 m with an annual accumulation rate of 25 mm w.e. yr^{-1} as evaluated by analysis of volcanic events (Traversi et al., 2009; Urbini et al., 2008). In the framework of the PNRA-MIUR 3D (Dome C Drilling for Dielectric measurements) project, a 120 m deep core was retrieved and shipped to Italy, where the 10cm long sub-samples were kept in the cold room of the University of Florence until analysis. Preliminary studies have shown that the core should cover the last 2500 years. The site was also chosen as a starting point for the 2019-2020 ITASE traverse campaign, with the aim of understanding and integrate the surface mass balance of the Antarctic plateau and the impact of very low and highly variable accumulation on the SMB. The traverse started on

the 7th of December 2019 at Dome C and ended January 1st of 2020. It followed the 123°E meridian on a route chosen to minimize any variability due to elevation (sampling site range in elevation between 2900 m and 3250 m), crossing a region receiving air masses from both the Atlantic/Indian Ocean and Ross Sea (Sodemann and Stohl, 2009; Scarchilli et al., 2011). During the traverse, 32 sampling site for collecting bulk and surface snow and 5 sites for collecting shallow snow pit samples were identified. The ITASE traverse reached the south pole, but for the purpose of this work only the first section is considered, with the last sampling site being Megadune (80°34'S, 121°38'E), 660 km away from Dome C, reached on the 27 th of December 2019. Surface samples were collected at a distance from the convoy and considering for wind direction in order to avoid external contamination. Pre-cleaned PE vials were used to sample both the surface and bulk samples. For the surface samples (first 10 cm of snow) the vials were introduced directly in the snow. For the bulk samples, the uppermost 1 m of snow was collected using a stainless-steel corer, the mixture of snow and firn was homogenized, and the final samples collected in the same pre-cleaned PE vials used for the surface samples. In order to further analyze the spatial and temporal variability across the east Antarctic plateau, during the traverse 4 sampling sites were chosen to collect 5 shallow snowpit using pre cleaned PE vials. The sites are here briefly described:

- AGO5 (77°14.29'S, 123°28.59'E): ex American geomagnetic station (Automatic Geophysical Observatory) situated 1050km from McMurdo Station and 250km from Dome C
- Paleo (79°38.79'S, 126°08.25'E): site with a regular snow deposition rate
- Wind Crust (80°42,97'S, 122°10.23'E): site with null or negative

snow accumulation rate due to the strong wind

- Megadune (80°34.26'S, 121°38.58'E): site characterized by megadune structures and sampled on both the zone of accumulation and erosion. The area is characterized by drastic variation on snow accumulation rate at a scale of few km, with the erosion zone having a null or negative accumulation

2.2 Decontamination Procedure

With the exception of the surface snow samples and the snow pit samples, collected in pre cleaned plastic vials, all firn and ice samples had to be decontaminated before ion chromatography and trace elements analysis. This was done under the widespread knowledge that the drilling, handling and shipping of the samples can, indeed, introduce a level of external contamination inside the core samples (Chisholm et al., 1995; Gabrielli et al., 2006; Tao et al., 2001). Numerous studies have already showed that this kind of contamination, only affects the most external layer of ice and that by removing the first few cm of sample, it is possible to restore the pristine concentration of the sample. Studies conduct on the snow pits drilled on site showed that removing the first 1 cm of ice from the core strips (Caiazzo et al., 2017) is enough to restore the original concentration of the core's samples for the GV7 site. Samples were stored before the decontamination in Polyethylene (PE) sealed bags inside the cold room of the University of Florence and kept frozen at -20°C. For the GV7 the decontamination of the ice samples (4x4x60 strips of ice) was accomplished for the majority of the samples by manually scraping the external layer of ice with a pre-cleaned ceramic knife. The strips where then cut into sub samples (average resolution 4.5 cm) and stored into pre-cleaned

Polystyrene vials until the moment of analysis and then melted at room temperature under a class-1000 flow hood. Due to problems in the drilling procedure, multiple ice core strips showed breakage and cracks that made difficult to manually remove the outside layers of ice from the samples. These samples were kept frozen in sealed PE sampler holder until the moment of analysis. Shortly before that, the external layer of ice was removed by quickly submerging the sample 3 times in ultra-pure MilliQ water. The samples were then left melting at room temperature under a class-1000 flow hood. For the DC3D ice core, two different approached to the decontamination of the samples were tested. One of the main drawbacks of manually decontaminating samples, is the handling of the samples itself that could bring external contamination. In order to investigate how different procedures can affect the final concentration of ions in the samples, the core samples (10 cm in diameter, 10 cm on average height) were split in two longitudinally.

- One section was decontaminated as with the GV7(B) samples, by manually scraping the first few cm of firn/ice using pre cleaned ceramic knifes. These samples were kept as a reference.
- The other section was re-cored using a stainless-steel corer (see Figure 2.2) insert in the firn sample to isolate the inside section of the sample.

Preliminary tests on the corer to ensure that adequate levels of purity and cleanliness were carried out before using them in the decontamination procedure and re-coring the ice samples. The corers were cleaned using the following procedure: grease and organic traces left on the metal by the lathe used to sharpen it, were removed using a 1% Extran AP detergent solution (Merk). Then ultra-sound assisted wash with ultra-pure water MilliQ was carried for at least

Figure 2.2 – Decontamination procedure of the DC3D samples inside the Cold Room of the University of Florence. Ph. Alessia Saracino

three times. The level of cleanliness achieved was checked by washing the corer with approx. 30 mL of Ultra-Pure water (18.3 MΩ) and analyzing the wash with the same Chromatographic method used for the samples until the level of contamination were comparable with the laboratory blanks. One of the main drawbacks of this methods was the difficulty of removing $NH_4{}^+$ contaminations from the metal corer, due to the tendency of metals to adsorb gas from the atmosphere (Vaittinen et al., 2014). This tendency was investigated before the analysis of the samples by plotting adsorption kinetics in standard laboratory conditions and in the cold room where the samples were handled until the moment of analysis, finding that this process was hindered at low temperatures. Furthermore, the low porosity of the ice samples must be taken in consideration and in general, despite the tendency of the metal to assorbs ammonia from the atmosphere, the quantity of NH_4 transfered to the samples was found to be minimum.

2.3 High Performance Liquid Chromatography - HPLC-IC

All samples collected and analyzed for this work, such as snow and ice cores, share the common characteristic of extremely low concentration of analytes (most of the time, in the order of 100 ppb and at times lower than 1 ppb). The large number of samples, the limited sample volume (around 10-15 mL) and the extremely low level of ionic content of the samples, made so that all the samples had to be handled and analyzed in a clean laboratory (class-10000) to minimize the risk of contamination. Conductivity suppressed Ion Chromatography (IC) was chosen as sensitive, selective, fast and reproducible methods to analyze the high number of samples. IC is a HPLC (High Performance Liquid Chromatography) separation technique based on the ionic exchange between a stationary phase (ion-exchange resin) and the mobile phase (eluent) that carries the sample inside the column containing the resin. The R-X groups of the resin interact with the opposite charged analyte ions in the sample and are therefore allow for the separation of the analytes. The sample is injected into the separation system via an injection valve connected to either a concentrator column or a loop with the purpose of injecting a reproducible and set volume of sample inside the system. The separation system is comprised of a guard column (a shorter IC column with the purpose of avoiding organic compounds or ionic species that can't be separated to enter the separation column thus "poisoning" it by irreversibly binding with it) and a separation column following it. Once the analytes are being separated, the eluent solution passes through a conductivity suppression system (to decrease the high conductivity signal of the eluent itself, associated with a high background noise) and then the separated peaks get

detected by the conductivity cell used as a detector. Since all the analytes are ionic species, their presence in the eluent phase can be detected as an increase of the conductivity relative to the background. The presence of a conductivity suppression system increases the signal/noise ratio and exalt the analytical signals which is then integrated by the software. Dionex Chromeleon Chromatography software was used for instrument control and data acquisition. Samples and standards were injected in the chromatographic systems through an auto sampler (222XL Liquid Handler, Gilson, Middleton, WI, USA). This allowed for minimal contamination of the sample as the stainless-steel needle drill through the sample holder directly and the samples are then pumped into the systems via a peristaltic pump. On-line 0.45 um Teflon membrane were used to filter the samples and ensure that only the "soluble" fraction of each analyte was introduced in the system and avoiding the possibility of blockage in the capillary tubes of the system. Concentrations of the samples were evaluated by using calibration curves built with external standard solutions (at least 5 points, single replicates) used also to verify the correct working of instruments. Doing single replicates for each standard was found to be usually enough to ensure an accurate calibration and the choice of doing for each standard multiple replicates was ultimately discarded. This is due to two reasons: first, the time needed for completing a chromatographic run and the need to calibrate the instruments daily. Secondly, the system used was characterized by an extremely high reproducibility. Indeed, doing multiple replicates (e.g. 3) and averaging the signals of each standards would reduce variability and bring a more accurate measure, but the excellent reproducibility and the number of samples needed to be analyzed each day led to the choice of doing single replicates. Calibration curves were discarded if the correlation coefficient was found to be

too low to ensure an accurate evaluation of the ionic content of the samples ($R^2 > 0.9995$) Standard solutions for the calibration of the instrument were prepared in pre-cleaned polyethylene vials, diluting stock certified standard solutions (1000 mg/L, Merk Darmstadt, Germany) with ultra-pure Milli-Q water. Eluents were prepared using reagent grade Merk or Fluka products diluted in ultra-pure Milli-Q water.

Different procedures were used for different samples and were optimized in order to find the best balance between the need of lowering the time of analysis (due to the large number of samples, over 3500 for the GV7(B) ice core, over 500 for the DC3D core and in the order of hundreds for the snow pit and surface samples) and reaching an extremely low detection limits due to the nature of the samples.

2.3.1 GV7(B) ice core samples

Two Ion Chromatograph were simultaneously used for the analysis: DIONEX ICS-1000 for cation separations (Li^+, Na^+, NH_4^+, K^+, Mg^{2+}, Ca^{2+}) and DIONEX DX-500 equipped with a GP50 gradient pump for anion separation (F^-, Formate, MSA, Cl^-, NO_3^-, SO_4^{2-}). The gradient pump was necessary in order to achieve a good separation within a relatively small eluent run. It must be remembered that the high number of samples, made necessary to minimize the analysis time (about 10-11 minutes) with both maintaining a good separation between chromatographic peaks and a high level of reproducibility in order to obtain a significantly valid measurement without any repetition (also needed due the scarce quantity of the samples). Table 2.1 and Table 2.2 summarize the setting parameters and the chromatographic columns used for cation and anion separation. Table 2.3 reports the different steps for the separation of both

organic and inorganic anions. Figure 2.3 and 2.4 report examples of the chromatographic separation.

Table 2.1 – Analysis parameters and chromatographic columns used in the cathionic separation for the GV7(B) samples

Chromatograph ICS-1000	
Injection	Peristaltic pump (flow rate 1.3 ml/min, 1.5 min load)
Loop	800 µm
Guard column	Dionex®IonPac CG12 4x50 mm
Column	Dionex®IonPac CS12A 4x250 mm
Suppressor	Dionex®CERS 500
Eluent flow	1.5 ml/min
Mobile phase	22.5 mN H_2SO_4
Suppression	Electrochemical (180 mA) – recycle of eluent
Detector	Conductivity detector CD 20

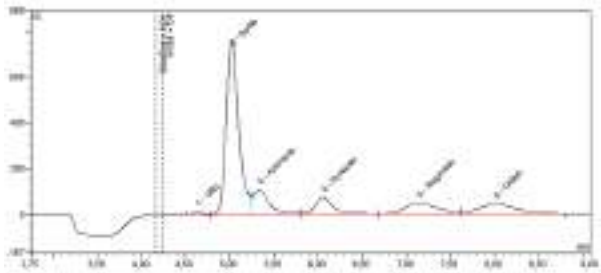

Figure 2.3 – Example of cations' separation for the GV7(B) core samples

More information about the analytical performance about the method used are reported in (Morganti et al., 2007; Caiazzo et al., 2016).

Table 2.2 – Analysis parameters and chromatographic columns used in the anionic separation for the GV7(B) samples

Chromatograph DX500	
Injection	Peristaltic pump (flow rate 1.15 ml/min, 1.5 min load)
Concentrator	Dionex®IonPac TAC-2 (3x35mm)
Column	Dionex®IonPac AS17C 4x250 mm
Suppressor	Dionex®AERS 500
Eluent flow	1.6 ml/min
Mobile phase	9.1 mM $NaHCO_3$ + 2.9 mM Na_2CO_3 buffer
Suppression	Electrochemical (180 mA) – recycle of eluent
Detector	Conductivity detector CD 25

Table 2.3 – Elution steps for the anionic separation

Time (min)	Milli-Q water (%)	$NaHCO_3/Na_2CO_3$	Note
0.00	94.0	6.0	Inject
1.00	94.0	6.0	Load
2.45	94.0	6.0	Inject
3.25	87.0	13.0	1^{st} Step
4.40	0.0	100.0	2^{nd} Step
7.91	94.0	6.0	
10.10	94.0	6.0	End

2.3.2 DC3D and snow surface samples

Two Ion Chromatograph were simultaneously used for the analysis: DIONEX ICS-100 for the cation separations (Na^+, NH_4^+, K^+, Mg^{2+}, Ca^{2+}) and DIONEX DX-500 for the anion separation (Cl^-, NO_3^-, SO_4^{2-}). Due to the number of samples, the systems were optimized to reduce as much as possible the run time, leading to

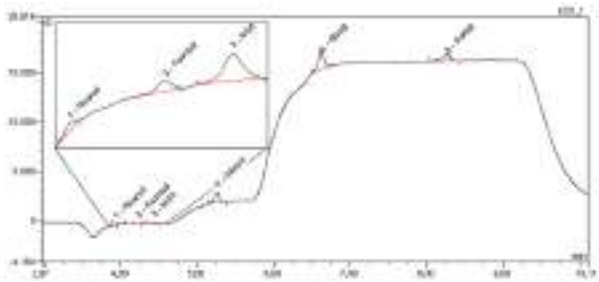

Figure 2.4 – Example of anions' separation for the GV7(B) core samples

the choice of not separate and quantify organic compounds in the samples. True FIC methods are able to separate and quantify ionic content in less than a minute and were used extensively for ice core samples (Severi et al., 2014; Traversi et al., 2002), but here, we focused on methods able to obtain a fast (under 5 min) separation with extremely low detection limits not only for the anionic content, but also for the cation of the core. This was accomplished by using a higher eluent flow, higher ionic strength of the eluent and shorter separation columns. Table 2.4 and Table 2.5 summarize the setting parameters and the chromatographic columns used for cation and anion separation. An example for each chromatographic separation is reported in Figure 2.5 and 2.6.

The analytical performance of these methods were tested and the linear range for the determination of each ion, the reproducibility and the detection limits were evaluated. For the linear range: standard solutions at known and progressively higher concentration obtained by dilution of stock certified solution (Merk, 1000mg/L for each ion) were manually injected in the systems and their signals recorded. The analytical signal (expressed in nS) was then plotted against the concentration of the samples and linear regression for each set of standards calculated. The linear range for each ion was expressed in

Table 2.4 – Analysis parameters and chromatographic columns used in the cathionic separation for the DC3D samples

Chromatograph ICS-1000	
Injection	Peristaltic pump (flow rate 1.3 ml/min, 0.8 min load)
Loop	200 µm
Column	2 Dionex®IonPac CS12 4x250 mm
Suppressor	Dionex®CERS 500
Eluent flow	2.1 ml/min
Mobile phase	12.5 mN H_2SO_4
Suppression	Electrochemical (100 mA) – recycle of eluent
Detector	Conductivity detector CD 20

Table 2.5 – Analysis parameters and chromatographic columns used in the anionic separation for the DC3D samples

Chromatograph ICS-1000	
Injection	Peristaltic pump (flow rate 1.3 ml/min, 0.8 min load)
Concentrator	Dionex®IonPac TAC-2 (3x35mm)
Column	2 Dionex®IonPac AS13 4x250 mm
Suppressor	Dionex®AERS 500
Eluent flow	2.0 ml/min
Mobile phase	2 mN $NaHCO_3$ + 3 mN Na_2CO_3 buffer
Suppression	Electrochemical (100 mA) – recycle of eluent
Detector	Conductivity detector CD 25

ppb and was evaluated as follows. For each ion, a low concentration calibration curve (usually in the range of 0 to 20ppb) was constructed and used as a reference. At these concentrations it's assumed that the column is not saturated by the analytes and that the response of the instrument to the variation of concentration is fully linear. Then, multiple calibration curves for each ion were produced with

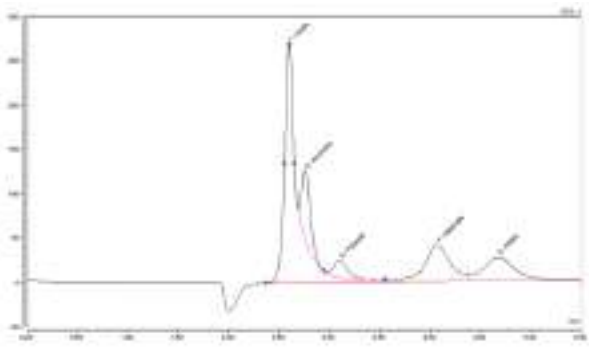

Figure 2.5 – Example of cations' separation for the DC3D core samples

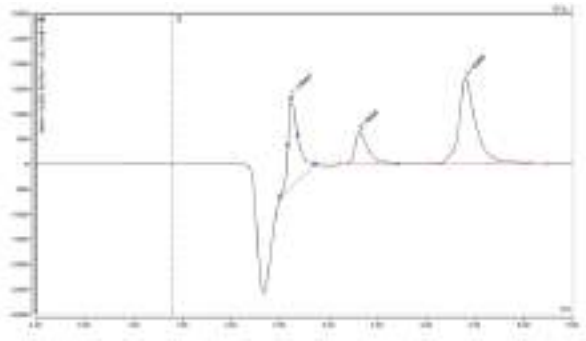

Figure 2.6 – Example of anions' separation for the DC3D core samples

a progressively higher range of concentration. The linear range was then taken as the highest concentration at which the slope of the calibration curve differs less than 5% from the one used as a reference. For evaluating the reproducibility and the detection limit of the methods, standards solutions of know concentration obtained by dilution of certified stock solutions (Merk, 1000 mg/L for each ion) were injected multiple times and analyzed. Reproducibility of the analysis for each ion was expressed as percentage standard deviation over the know concentration of the standard, whilst the Detection Limit of the method was expressed in ppb as 3 times the standard

deviation of a "fortified" blank i.e., a low concentration standard. This was used in place of a real blank because of the extremely low noise found in the blanks of Ultra-Pure MilliQ water that would have brought to an artificially high DL. An example of the evaluation of the linear range (NH_4^+) is reported in Figure 2.7, whilst Table 2.6 report the DL and reproducibility for each ion. All calibration curve displayed a linear range large enough to accurately quantity the ions found in the core even at extremely high spike concentration (mostly due to external contamination) with most of the calibration curves displaying a linear correlation between concentration and signal in the range between 0 and well above 500 ppb.

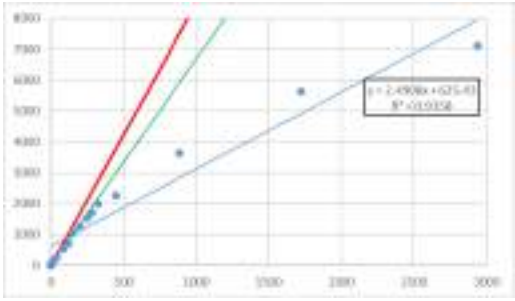

Figure 2.7 – Example of linearity range analysis, low calibration curve used as a reference (red), calibration curve in the linear range (green), calibration curve outside the linear range (blue) are reported

2.4 Total conductivity of DC3D samples

A DX120 Chromatographer's conductivity cell was used to measure the total conductivity of the samples. Due to the extremely low ionic concentration and total acidity of the samples (which it was assumed to be the main contribute to the conductivity of the melted samples), calibration of the conductivity cell was accomplished with standard solutions (Wu and Berezansky, 1995) prepared on the same

Table 2.6 – Detection Limits and reproducibility for each ion considered

Ion	DL (3*dev st, ppb)	RSD(%)
Sodium	0.12	1.88
Ammoniun	0.56	3.80
Potassium	0.30	2.94
Magnesium	0.23	1.60
Calcium	0.22	1.89
Chloride	4.90	3.44
Nitrate	2.95	2.68
Sulphate	2.10	1.26

day (Deleebeeck et al., 2020) with 96% acetic acid and 1000 ppm KCl solutions (Merk) diluted with ultra-pure Milli-Q water. The samples were left melting under a class-1000 flow hood and then introduced quickly after in the cell using a peristaltic pump (loading flow rate of 2.0 ml/min) to avoid external contamination. PeakNet software was used to plot the conductivity registered by the cell and evaluate the total conductivity of each sample. A small slope was always found in the analysis of the samples and the ultra-pure water used as a reference. This is most likely due to the presence of atmospheric CO_2 readily adsorbed into the water (creating carbonic acid which lowers the purity and the pH and, as a consequence, rises the conductivity). A concentration of 300-500 ppb of atmospheric CO_2 is typical for ambient air, which can cause an expected rise of the conductivity of the samples up to 1 µS/cm (compared to the 0.055 µS /cm^2 ensured by the ultra-pure production system). For this reason, measurements were taken at 30 seconds after the injection of the sample or after reaching plateau of conductivity (monitored via the acquisition software), whichever came first.

2.5 Inductively Coupled Plasma – Sector Field Mass Spectrometry Analysis (ICP-SFMS)

Due to the low concentration of metals in the samples, extreme care was taken not only during the decontamination procedure, but also during the analysis. Only the samples decontaminated with ceramic knives were analyzed for metal contents (Pu contamination should be non-existent in a laboratory setting but different metals were tested at the same time). The samples after being analyzed for ionic content, were re-frozen until the moment of analysis, upon which they were left melting under a class-100 laminar flow hood and acidified. Sub boiled (s.b.) HNO_3 acid purification system (DST-1000, Savillex, Minnesota, USA) was used to purify 65% nitric acid for analysis (Carlo Erba, Italy). The s.b. acid was then diluted to 1% HNO_3 using Milli-Q ultrapure water (18 MΩcm), which was used to both acidify the samples and used to regularly clean ampler and skimmer cones, ICP torch, spray chamber nebulizer and sample introduction tubes to remove any form of external contamination. Internal standard (^{115}I) was added to all the samples and standards to account for instrumental variation. For Pu, an indirect calibration was accomplished using with ^{238}U external calibration curve as described in (Gabrieli et al., 2013), making it a semi-quantitative analysis. As a first approximation, this is a valid approach, as the sensitivity of heavy elements in ICP – SFMS is correlated to the element's mass and the ionization anergy of the two elements are very close (for Pu, 6.06 eV, for U 6.19 eV) and as such they should show a similar behavior in the plasma and during the ionization. Furthermore, the lack of contaminant in the pristine environment of the Antarctic snowpack makes it so that the presence of heavy metals that could bring interferences is low. For ^{239}Pu, one possible

source of interference reported in (Gabrieli et al., 2013) at low U concentrations (< 40 pg g^{-1}) is UH^+, but this type of interference is minimal and when present, easily identified due to be extremely higher than the ^{239}Pu measurements (Arienzo et al., 2016). 73 subsamples and external samples were prepared and then placed in a high efficiency sample introduction system and directly analyzed using a Thermo Finnigan MAT, Element-2, ICP-SFMS (Bremen, Germany). The analysis was performed at low resolution (LR: 300 m/Δ m), laboratory blanks in the form of ultra-pure water acidified and treated in the same way the samples were, were used.

2.6 Analysis done outside University of Florence

2.6.1 Isotopic composition

Unlike the ones devoted to ionic content, samples for isotopic analysis were not decontaminated prior to the analysis as external contamination would not be a factor in evaluating $\delta^{18}O$. Both bag samples (60 cm resolution) and high-resolution samples (4 cm resolution) were analyzed for oxygen's isotopes ratio as follows. Bag samples were analyzed for $\delta^{18}O$ at the University of Parma, using a Thermo-Fisher Delta Plus Isotope-ratio Mass Spectrometer (IRMS) coupled with a HDO automatic equilibration device. Water-CO_2 equilibration (Epstein and Mayeda, 1953) technique was used. High resolution samples (4 cm) were analyzed for $\delta^{18}O$ at the Ca' Foscari University of Venice, using both the Cavity Ring-down Spectroscopy (CRDS) technique (Picarro L1102-I) and the IRMS water-CO_2 equilibration technique (Thermo-Fisher Delta Plus Advantage coupled with a HDO automatic equilibration device). The latter is char-

acterized by an analytical precision of 0.05‰ for $\delta^{18}O$, while the Picarro L1102-I has an analytical precision of 0.10‰ for $\delta^{18}O$. internal isotopic standards periodically calibrated against the certified International Atomic Energy Agency (IAEA) standards VSMOW2 and SLAP2 were used to calibrate all measurements. All the isotopic data in this work are reported in the SMOW-SLAP δ-scale.

2.6.2 Trace Element analysis

For the GV7(B) core, the ice samples after chromatographic analysis were shipped to the University of Venice. Here they were analyzed with an Inductively Coupled Plasma Single Quadrupole Mass Spectrometer (ICP-qMS, Agilent 7500 series, USA) equipped with a quartz Scott spray chamber. A 120-seconds rinsing step with 2% HNO_3 (Suprapure, Romil, UK) was performed after each sample to limit any possible memory effect, the vials used for standard preparation were cleaned following the same procedure adopted for ice samples. External calibration curves with acidified standards (2% HNO_3, Suprapure, Romil, UK) obtained from dilution of certified IMS-102 multielemental standard (10 ppm ± 1%, Ultra scientific) were used in the quantification of the trace elements. Detection limit of the method for Tl, U and Bi, calculated as three times as the standard deviation of the blank were calculated and were found to be 0.001 ppb for Tl and U while for Bi 0.004 ppb.

2.7 Identification of Volcanic signatures and Volcanic Flux

Volcanic signatures are superimposed over the biogenic background and are, therefore, statistically different from the oscillating

pattern of the nssSO_4^{2-} found in the core. Since volcanic eruptions bring large amount of sulphonic material to the Antarctic continent, it is possible to pinpoint past eruptions in the form of concentration spike. In order to reliably identify this concentration spikes, different procedures are available (e.g. Castellano et al. 2005; Sigl et al. 2016) and are based on the estimate of a biogenic background and a number of thresholds over which a sample point's concentration can be considered statistically higher than the background and therefore possibly associated with the deposition of volcanic material.

For this work, the procedure discussed in (Castellano et al., 2005) was followed and it's here briefly discussed. The biogenic background was estimated in the form of the average of the nSO_4^{2-} concentration after the 99^{th} percentile points (associated to external contamination and most likely non-statistically relevant to the estimate of the biogenic background) were discarded. For the GV7 ice core records, since the temporal resolution was found to be much higher than the other records analyzed in this work (sub annual compared to the decadal resolution of the DC3D core for example), a running average function (101 sample points centered on the 51^{st} sample) was used and plotted against the depth to evaluate the biogenic contribution of the nSO_4^{2-} in the core. For the other records, the average across all samples was used instead. A number of thresholds were then set and plotted: standard deviation added to the aforementioned biogenic background ($2\sigma$and 3σwere both used in this procedure) were choosen as a way to identify a statistically higher than background level of Sulphate. This procedure was therefore repeated: since every sample point over the threshold is considered statistically higher than the background, they should not contribute to the background at all and could, in fact, higher the background and lead to false negative. By removing from the dataset the points over the thresholds and

iteratively repeating the process of evaluating the background and setting up thresholds until no further points were removed, ensuring to properly identify every possible volcanic signature in the records. An example of this iterative process is reported in Figure 2.8.

A similar approach was used when evaluating the total amount of volcanic sulphate (i.e. volcanic flux f) in the form of total mass of sulphate deposited on site per square km. For each identified volcanic signature, the total $nssSO_4^{2-}$ flux was calculated by integrating the concentration of all the samples within a given depth interval (sufficiently large to take into account for background variability and the fact that volcanic deposition of sulphate could happen across multiple years). From this value, the integrated biogenic background (evaluated as described above) calculated in the same interval, was subtracted. By taking into account for ice core density and the thinning of the ice layers, the amount of volcanic material was then calculated. As it might be obvious, the most critical step of this procedure is to correctly identify a time window (centered on the sample point with the highest concentration of $nssSO_4^{2-}$) in which integrate the signals. The choice is somewhat arbitrary, and it's unavoidably affected by discretional choices and previous experience with dealing with such data (Castellano et al., 2004, 2005; Severi et al., 2007, 2012). Usually, thw window of years needed to properly integrate the signal was found to be 11 years. Similarly, the same procedure was used to evaluate the volcanic flux of the same volcanic signatures found in three other cores drilled in the same sector considered for this work GV7ITASE (158°52' E, 70°41' S, 1947 m a.s.l., 55 m, about 150 yrs (Frezzotti et al., 2007)), TD 96 (159°06' E, 72°48' S, 2316 ma.s.l., 89 m, about 800 yrs (Stenni et al., 2002)), and TALDICE (159°11'E, 72°49'S, 2315 m a.s.l., 1620 m, more than 200,000 yrs (Severi et al., 2012)). The procedure used to detect

the volcanic signatures for these are described in their publications, respectively (Stenni et al., 2002; Frezzotti et al., 2007; Severi et al., 2012).

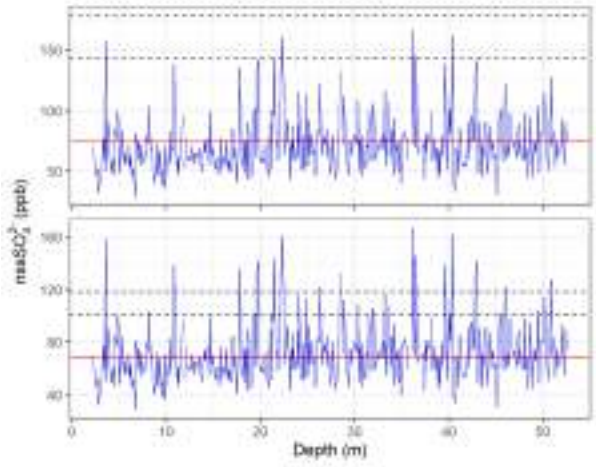

Figure 2.8 – Example of iterative process for the identification of the volcanic signatures Step 1 (up) and final step (down). Biogenic background is reported in red, statistical thresholds are reported in black

2.8 Dating of the records

Two different approaches were used in the dating of the ice records. First, since volcanic signatures (in the form of spikes in the nss$SO^4{}_2$- concentraton vs. depth profile) can be identified in multiple cores, it's possible to synchronize these by identify similar patterns and use a well resolved chronology to date another core. Secondly, the idenitification of well known signatures (e.g. 1816 CE and 1809 CE volcanic eruptions that form a very distinct "doublet" in the cores that makes it easy to identify them) can be used to assign an exact date to a given ice layer using historic records of volcanic eruptions. Since the majority of the Sulphate associate from volcanic eruptions

can be found in the form of of Sulphuric acid, the same pattern of spikes can be identified in the total conductivity/acidy profile of the core. Similarly, trace elements can be used to constrain the dating: for the GV7(B) ice core, volcanic ashes and dust deposition are associated with higher levels of U, Bi, Tl. These were found in the core and unlike the rise in $nssSO_4^{2-}$ which comes from a multitude of sources, their presence is specific for this kind of events. Their records were used to date the uppermost layer of ice by identifying, in a similar matter as done with the $nssSO_4^{2-}$ record, statistically higher-than background levels of trace elements in the core. For the DC3D core, the records of trace elements associated with nuclear tests such as Pu were used to aid the dating alongside the evidence of past volcanic signatures already identified in the core. The dating was therefore obtained by synchronizing the different temporal tie points with the one found in different core drilled on the same site or in sites with similar characteristic. A similar approach was used when dating the ice layers found in the snow pits drilled during the EAIIST 2018/2019 campaign, although only a few number of signatures were identified due to the limited amount of samples and depth covered by the core. For the GV7(B) ice core, where the temporal resolution was higher due to the higher mean accumulation rate on site, a more accurate dating was achieved by means of annual layer counting.

2.8.1 Uppermost section of GV7(B) ice core

As described in (Nardin et al., 2021), for the uppermost section of the core the records of $nssSO_4^{2-}$ and $\delta^{18}O$ were used due to their well pronounced seasonal pattern (Caiazzo et al., 2017), with maxima found in their concentration during the Austral summer (i.e. late December, early January). Two individual dating were first produced, one using $nssSO_4^{2-}$ and the other using $\delta^{18}O$ by two

different operators in order to avoid biases. The two dating were then aligned using the volcanic signatures found in then nssSO_4^{2-} and the trace elements concentration vs. depth records. Only the uppermost 38 m of cores for which the $\delta^{18}O$ records were available at high resolution were dated this way.

2.8.2 Layer counting dating of the GV7(B) ice core

Different procedures are reported in literature to date ice cores at high resolution (annual to sub-annual) and were considered for the dating of the lower section of the GV7(B) core. Due to their seasonal patter, sea salt ions and some of the non-sea salt ones were considered. Their concentration's profile was investigated by means of PC analysis and bin plots to test their potentials in the dating procedure. PCA (Principal Components Analysis) was performed using the software STATISTICA to understand the correlation between nssSO_4^{2-} and the different ions analyzed. NH_4^+, K^+, F^- and $Form^-$ were not included in PCA due to the amount of samples whit lower than DL concentration and their lack of seasonal pattern in ice. Since, as previously discussed, nssSO_4^{2-} shows a strong seasonal pattern, ions showing a similar patter should be either grouped with it or be anticorrelated with the sulphate (i.e., it shows a summer minimum rather than a summer maxima). $\delta^{18}O$ data were not included due to the different depth resolution of the samples. These patterns were further investigated with bin plots: each year was divided in 4 time periods (roughly corresponding to the Antarctic seasons, Jan-Mar, Apr-Jun, Jul-Sep, Oct-Dec) the presence of a seasonal pattern was highlighted, and considerations were made assuming a similar trend was then found in the lower sections of the core. These considerations only cover a small section of the core (approx. the 20% of its length and due to the compression of the snow and the ice layers, reasonably

even less when considering the ice's age), but the results were in line with the preliminary consideration made analyzing the profile of the ions through the core. One of the drawbacks of this approach is that the snow accumulation rate was assumed to be constant for the site throughout the year, which is not necessarily true. Most of Antarctica snowfall comes in the form of light precipitation, but Extreme Precipitation Events play a significant role in the snowfall balance of the continent (e.g. Turner et al. 2019) and it has been proven to be higher during the winter months. Using intervals of only 3 months was able to provide a good compromise between resolution needed to investigate the seasonal variability of the markers and avoid misinterpreting the ice layers' age. Three procedures found in literature were tested on the basis of the consideration made and are here briefly described.

- Multiparametric approach using the sum of MSA, NO_3^- and $nssSO_4^{2-}$ normalized concentrations as reported by (Udisti, 1996). Normalization means that every concentration is divided by the values of the nearest concentration maxima, in this way is possible to give the same relevance to maxima having different concentration values in the same data series and from different data series. Since by normalizing the three series (all showing similar patterns) each sample points would have the same "weight" in the dating procedure; this should be useful for nearby volcanic eruptions, where the high concentration of sulphate could potentially mask the seasonal pattern, but as highlighted by bin plot and PCA, MSA maxima do not exactly match the other ions. For NO_3^-, its maxima can also be shifted by nearby volcanic eruptions due to the high acidity from H_2SO_4 (Jiang et al., 2019; Röthlisberger et al., 2000a, 2002).

- Cation stratigraphies: although Na^{+} and Mg^{2+} stratigraphies were successfully used in the dating of ice cores (Herron and Langway, 1979; Winski et al., 2019) for the GV7 site they showed a less pronounced seasonal pattern both in the upper and lower portions compared to the nssSO_4^{2-} profile. The identification of winter maxima in their concentration profiles was found to be not univocal, making impossible the accurate core dating.

- As already seen in the first section of the core from the preliminary analysis of the different ions, the dating of the GV7 ice core using the nssSO_4^{2-} concentration vs. depth profile without any further data manipulation.

2.9 Snow accumulation rate evaluation and trend analysis

Ice cores' and snow pits' samples density was evaluated during their respective campaign directly on site by weighting the samples and estimating their volume. Due to the process of layering of snows on top of the Antarctic continent and the compression of the layers below after each snowfall, the density of the samples varies from approx. 0.3 mg/cm^3 of the uppermost layers (where the ice crystals are still intact and up to 80% of the layer is comprised of air) to 0.9 g/m^3 of the deepest sections. In Figure 2.9 and 2.10 are reported the different density vs. depth profiles of the samples analyzed in this work. Surface snow samples and bulk snow samples' density are not reported.

Once the dating was finalized for each record, the snow accumulation rate (i.e., the amount of snow that remained on site for each

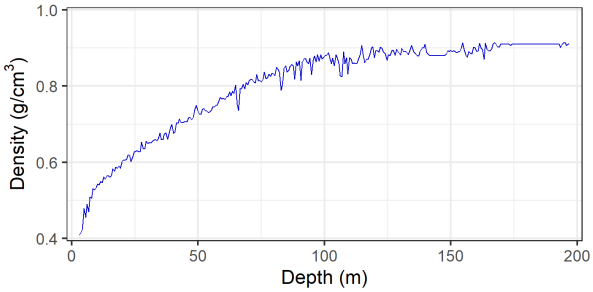

Figure 2.9 – GV7(B) ice core density

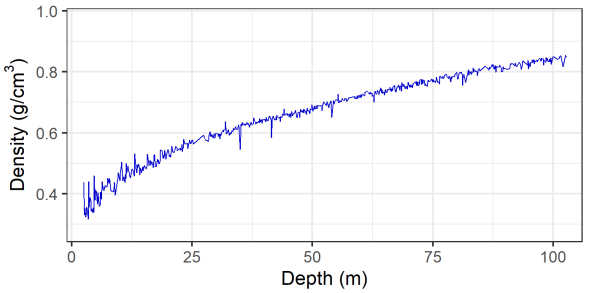

Figure 2.10 – DC3D ice core density

year rather than the one deposited on the ice cap) was calculated in the form of millimeters of equivalent water (mm w.e.) per year using the density record to take into account for the compression of the ice layers. For the GV7(B) ice core, due to the depth reached, the snow accumulation was also corrected for the ice layer thinning that would've otherwise brought a negative error and underestimation. In particular, a constant thinning function was applied to the snow accumulation rate considering an ice thickness of 1530 m for the GV7 site and aa constant vertical strain rate on the first 200m (see Nardin et al. (2021) for more details).

Chapter 3

Results

3.1 Validation of decontamination procedure

For the GV7(B) core, tests on the decontamination procedure were already performed on the snow pits (Caiazzo et al., 2016). For the DC3D core in order to ensure the two procedures used were not going to introduce external contamination, preliminary tests to evaluate the cleanliness of the material used were performed. By washing the inside of the corer with a volume of water equivalent of the volume of ice expected to sample, a laboratory blank was obtained. Despite the minimal interest given to the ammonium records when it came to interpret the chemical stratigrahies, it was noticed that the concentration on the corer rose with time as reported in Figure 3.1a and 3.1b and particular care was given to ensure that Ammonium from the core wasn't transfered on the samples.

Estimating a kinetic model for the adsorption of ammonium on the surface of stainless-steel corer is beyond the scope of this work, and the temporal correlation here reported were mostly used to confirm that, indeed, ammonia from the atmosphere (whose concentration

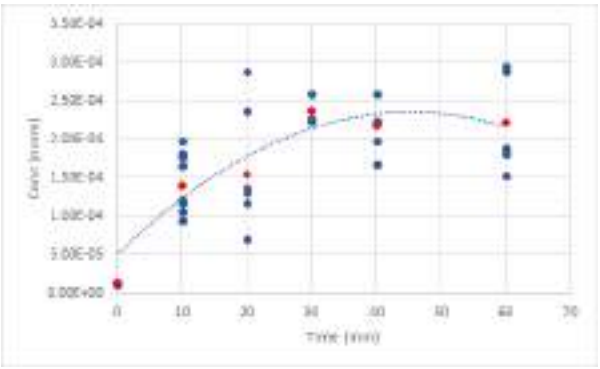

(a)

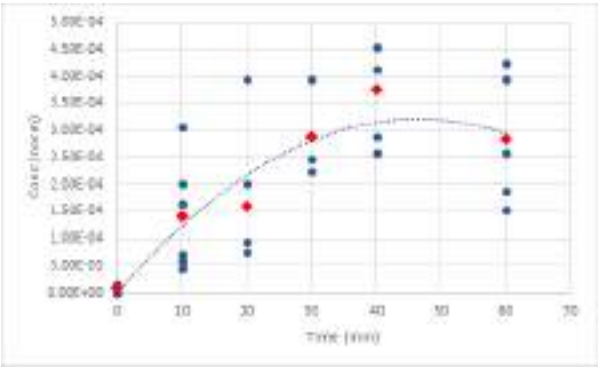

(b)

Figure 3.1 – Ammonium concentration rising in the stainless steel corer used in the sub-sampling of the ice core, quadratic interpolation used to estimate the adsorption of Ammonia on the stainless steel.

was hard to control during decontamination procedure and or stocking of the samples) could potentially bring a rise in the concentration in the sample. Further tests were performed on sample snow collected in Italy (mt. Cimone) that made possible to investigate whether or not sampling with the corer in the same conditions in which the samples would then be decontaminated, would introduce further contamination. Concentrations were plotted using box plots, with the aim of understanding whether or not there was a statistical difference between the two methods. Figure 3.2 reports these data.

Higher levels of contaminant were found, and even after removing those concentration clearly ascribed to external contamination (not to the corer), on average the samples cored with the stainless-steel corer displayed lower concentrations. This was somewhat unexpected and ascribed to the possibility of the corer to sample the innermost section of the snow samples, avoiding the more contaminated area (the surface) and the lack of direct manipulation of the samples by the operator. Furthermore, decontaminating samples with ceramic knives seemed to produce fine snow particles that, despite working under a flow hood, had the tendency to stick back to the samples, probably contributing to the higher concentrations. Lastly, the first 10 samples were analyzed after using both decontamination procedures. This small dataset was used to further confirm that no statistically relevant contamination could be introduced with the use of metal corer for decontaminating the samples. These preliminary results are not reported, but Figure 3.3 display the ionic concentrations' record for the DC3D core using the two procedures. The first 138 samples were decontaminated using the two methods described and the two datasets compared

With minor exceptions, no real statistical difference was found between the two methods, with the exception that using a metal

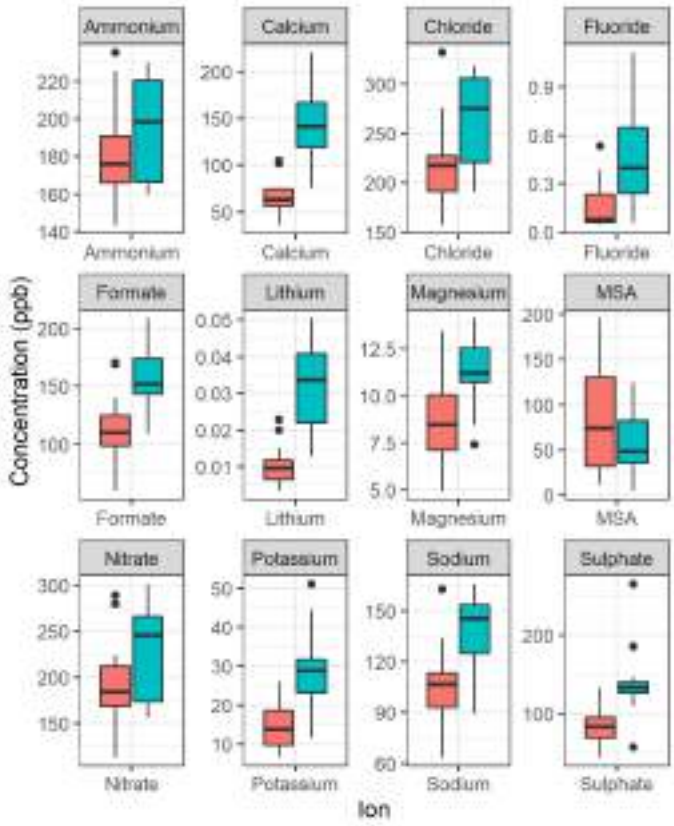

Figure 3.2 – Boxplot reporting the ionic content of the mt. Cimone samples, in red, samples taken with stainless steel corer, in teal, samples taken with plastic accuvette

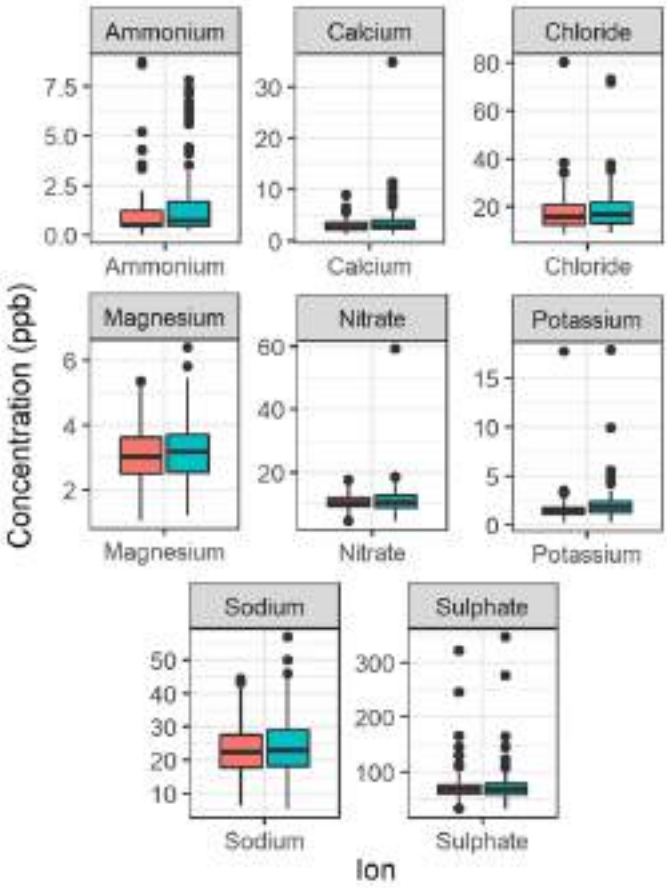

Figure 3.3 – Boxlots reporting the ionic content of the DC3D samples, in red, samples taken with stainless steel corer, in tea, samples taken with plastic accuvette

core proved to be quicker and more reliable. On the other hand, no tests for metal contaminations were performed on the samples, making impossible to understand the real extent of the contamination introduced by the corers, reason why for ICP-MS analysis, these samples were ultimately discarded. Furthermore, the brittleness and the hardness of the ice at lower depths made difficult to core and therefore decontaminate samples.

3.2 Dating of Ice Cores

The dating of ice cores is one of the most critical and key elements of paleoclimatology; in this work a mixture of annual layer counting and identification of temporal tie points (mostly past, well known and documented volcanic eruption) to assign an exact date to each ice layers. These tie points are used to constrain the dating and allow to assign a precise date with minimal uncertainty. In the case of volcanic signatures, since deposition can happen in the few years following the eruption as reported by Sigl et al. (2015), the uncertainty associated to the layers near eruptions should be considered as such. For the in-between dating (i.e. the one based on annual layer counting) the uncertainty is to be considered higher the further from a known temporal horizon.

3.2.1 GV7(B) ice core dating

For the GV7(B) ice core the volcanic signatures in the nssSO_4^{2-} concentration vs depth profile were identified. This, together with the identification of tephra layers and the trace elements associated with the eruptions lead to a first chronology of the core. Volcanoes signatures were compared to the one found in literature and identified in other cores (Castellano et al., 2005; Sigl et al., 2016; Simkin and

Table 3.1 – Known volcanoes used in the dating procedure and their location. Abbreviation used: Strat. (Stratovolcano), Cald. (Caldera), Pyrocl. (Pyroclastic cone).

Volcano	Location	Latitude	Longitude	Type
Pinatubo	Luzon	15°07' N	120°21' E	Strat.
Cerro Hudson	Chile	45°54' S	75°58' W	Strat.
Agung	Bali	8°20' S	115°30' E	Strat.
Krakatau	Indonesia	6°06' S	105°25' E	Cald.
Makian	Halmahera	0°20' N	127°22' E	Strat.
Cosiguina	Nicaragua	12°59' N	87°34' W	Strat.
Tambora	Indonesia	8°15' S	118°00' E	Stra.
Gamkonora	Halmahera	1°22' N	127°32' E	Strat.
Parker Peak	Philippines	6°11' N	124°89' E	Strat.
Huaynaputina	Perù	16°36' S	70°51' W	Strat.
Reclus	Chile	50°57' S	73°35' W	Pyrocl.
Samalas	Lambok	8°24' S	116°24' E	Strat.

Siebert, 1994). In particular in the GV7(B) core, 12 signatures associated with known past volcanic eruptions and 15 more yet-to be attributed signatures were found analyzing the core as in samples of concentration statistically higher than the biogenic background of the nssSO_4^{2-}. Here, these are briefly described and their position in the core and the volcanoes to which they're attributed, and basic information are reported in Table 3.1. More information about the recognition of the volcanic signatures are reported in Nardin et al. (2020).

The double peak found at a depth between 11.05 and 11.32 m was attributed to the Pinatubo/Cerro Hudson volcanic eruption. The former in particular is particularly well documented (Cole-Dai and Mosley-Thompson, 1999; Sigl et al., 2013, 2014, 2015; Proposito and Frezzotti, 2008) and lead to assign the the year 1992 CE to this

signature. The Pinatubo explosive eruption occurred in early June of 1991 CE and ceased volcanic activity only in September, but the volcanic material emitted in the atmosphere remained dispersed in the following wear up to the mid 1994 (Cole-Dai and Mosley-Thompson, 1999). The presence of a secondary eruption in this time period (Cerro Hudson) explains the double peaks: the eruption itself is very close to the Pinatubo's (early August of 1991 CE), but the volcano is in Chile, and volcanic matter could have reached the Antarctic continent earlier than the Pinatubo's. The two events are extremely close in time (separated by two months) meaning that differentiating the two volcanic eruptions inside an ice core is normally hard. Even for the GV7(B) ice core, whose drilling site is characterized by a high accumulation rate, the separation of the two is challenging. The year 1991 CE was attributed to the secondary peak found at a deeper depth, which was found to be consistent with the annual layer counting both using the sulphate record and the $\delta^{18}O$ record (see below). The presence of this volcanic signature was further confirmed when analyzing the trace elements' concentration profiles found in the core: following the procedure already used to identify the volcanic traces in the $nssSO_4^{2-}$ profile, with an identification of a background concentration and a statistical threshold (see Figure 3.4), a rise in concentration in both U, Tl and Bi was found in correspondence with the rise in concentration of sulphate. The peaks do not match exactly, but since volcanic ashes deposit prior to sulphate, the dating was maintained, and the year 1991 CE was associated to the rise in trace elements' concentration. Figures 3.5 and 3.6 report the entirety of the $nssSO_4^{2-}$ concentration profile for the GV7(B) core and the volcanic signatures found are here discussed.

A similar double peak was found at a depth of 22.02 and 22.62 m, but both of them were attributed to the 1963 CE eruption of

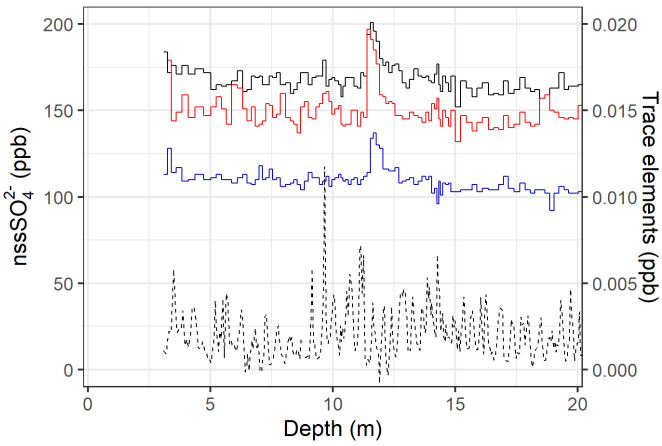

Figure 3.4 – $NssSO_4^{2-}$ (dashed black, left scale) and trace elements (right scale, solid black, ^{205}Tl, solid red, ^{209}Bi, solid blue, ^{238}U

the Agung volcano (Indonesia) and the presence of the double peak was attributed to snow reworking and layer mixing from winds on site and/or to diffusion processes on site. The attribution of the year 1964 and 1965 CE to these peaks is consistent with the annual layer counting (see below) and with the historical records of this past know volcanic eruption. Furthermore, its presence and this date assignment is in line with what already been done by other authors (e.g. Sigl et al. 2013) investigating different cores.

The peak found between 49.22 and 49.48 m is to be attributed to the explosive eruption of the Krakatau volcano, and it's considered of the most important horizons in ice core dating, whose traces are found both in Antarctic and Greenland ice cores (Cole-Dai and Mosley-Thompson, 1999; Traufetter et al., 2004; Sigl et al., 2013; Moore et al., 1991). The eruption itself began in late May of 1883 CE, but it peaked on the late morning of Monday, 27 August 1883 CE, when the explosive eruption destroyed over 70% of the island of Krakatoa and its surrounding archipelago, making the volcano

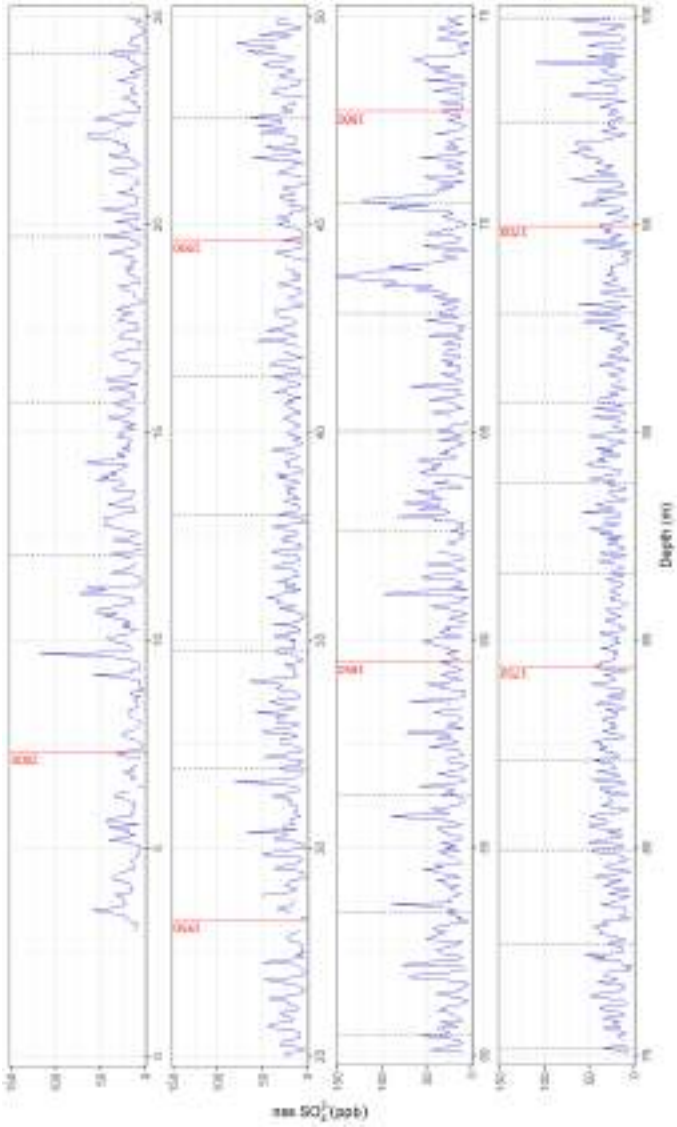

Figure 3.5 – $NssSO_4^{2-}$ concentration vs. depth plot. Final dating is also reported, with grey dashed lines placed every 10 years

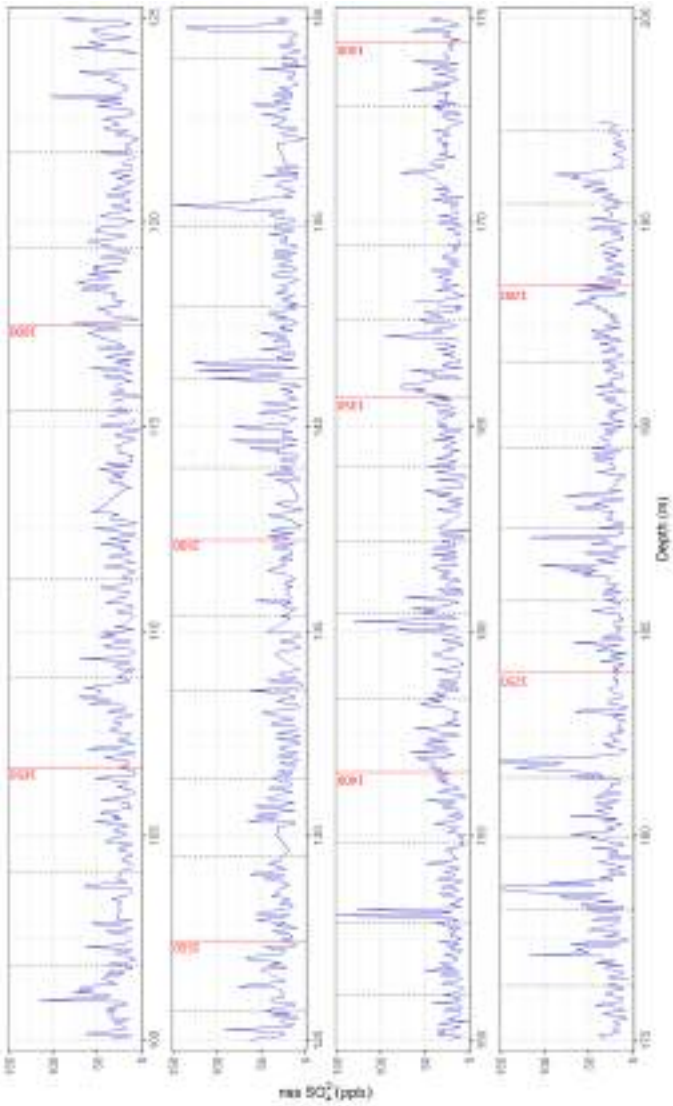

Figure 3.6 – cont. $NssSO_4^{2-}$ concentration vs. depth plot. Final dating is also reported, with grey dashed lines placed every 10 years and red solid lines every 50

collapsing into a caldera. The highest peak of concentration found in the core (at a depth of 49.35 m) was attributed the year 1884 CE, which is fully compatible with the time period in which the eruption occurred and the fact that deposition of volcanic aerosol ended in the year 1886 CE. Another massive, explosive eruption critical both in terms of its effect on the climate in the years surrounding the eruption and the relevance of it in the framework of dating ice core, is the 1816 CE Tambora, in the Indonesian island of Rakata. The eruption, occurring in April of 1815 CE is recorded as the largest in human history and in the Holocene, with consequences on the climate at a global scale. The year 1816 CE is commonly recorded as the "Year Without A Summer" due to the climatic consequences of approximately 60 mT of sulfur into the atmosphere (six times the one of the 1991 CE Pinatubo eruption) (Oppenheimer, 2003; Fasullo et al., 2017) with repercussions that provide important insights in the forcing phenomena caused by these events. Tambora eruption shortly followed another, probably smaller in scale, event. It is usually found in ice core records as a "doublet" that makes easy to identify the year 1815 CE, with the other peak dated 1809 CE. The volcano associated with this eruption is still unknown and it's usually reported in literature as "Unkn 1809". The same nomenclature is used in this work. The two volcanic signatures associated with these eruptions were found between 68.52 and 70.58 m deep in the core. The date 1816 CE was attributed to the highest of the two peaks (at a depth of 68.75 m) and 1809 to the nearby one, consistently with what found in other core and with the stratigraphic dating (Sigl et al., 2013; Moore et al., 1991; Dai et al.; Yalcin et al., 2006). Two other volcanic signatures are worth an in-depth discussion. The first one is the one found at a depth of 145.41 m in the core, originally assigned to the 1452 to 1453 CE eruption of the Kuwae underwater

caldera in the Vanuatu archipelago (Traufetter et al., 2004; Sigl et al., 2013; Severi et al., 2007, 2012). The eruption is thought to be one of the largest of the last millennium, with an amount of sulphate matter emitted in the atmosphere comparable or even superior to the one from the 1815 CE Tambora (Gao et al., 2006), but recently the attribution of the volcanic signature to this event has been questioned by using cryptotephra analysis on the SPICE core (Hartman et al., 2019) with the most plausible candidate for this record found in ice cores being Mount Reclus in Chile. Lastly, the peak found at 181.86 m was ascribed to the 1257 CE eruption of the Samalas volcano (Narcisi et al., 2019) whilst the nearby tephra layer as well as the tephra layer (Narcisi et al., 2001, 2012; Narcisi and Petit, 2021) is normally associated with the eruption of Mount Rittman in 1254 CE. The tephra layer in particular was easily to identify in the core, as the particulate matter deposited on site was in high enough concentration to make it visible to the naked eyes during the drilling operations. The volcanic eruption was dated 1260 CE (Sigl et al., 2013). Other minor eruptions were found in the core and are more in detail described in Nardin et al., 2020. The list of volcanic signatures used in the dating and the depth at which they were found is reported in Table 3.2.

Once the identification of the volcanic temporal horizon was accomplished, the dating of the core was finalized with the identification of the seasonal pattern of the ions in the core. By manual layer counting, the entire core was dated with a sub annual resolution. Here a discussion of the different method tested is reported. For the first section of the core, the combination of sulphate records, volcanic temporal horizons, and the high resolution $\delta^{18}O$, together with the high resolution of the core (up to 2 yr m^{-1} in the uppermost firn region of the core) made the identification of each year straight-

Table 3.2 – Volcanoes found in the core and used for the dating of the core. The interval in which a statistically higher than the background sulphate concentration was found and the associated maximum are reported (Interval and Max respectively). Both the Historical date and the Assigned dates used in the dating is reported. The signal associated to the Pinatubo* is a combination of the signal of both Pinatubo and Cerro Hudson eruption, occurring in the same year, but too close to be differentiated in the sulphate record.

Volcano	Depth (m)		Date (CE)	
	Interval	Max	Historical	Assigned
Pinatubo*	10.91 – 11.42	11.10	1991	1992
Agung	21.82 – 22.43	22.12	1963	1965
Krakatoa	49.01 – 49.53	49.35	1883	1884
Makian	55.55 – 56.12	55.75	1861	1863
Cosiguina	63.05 – 63.64	63.27	1835	1837
Tambora	68.16 – 69.18	68.75	1815	1816
Gamkonora	100.90 – 101.61	101.25	1673	1675
Parker Peak	108.18 – 108.77	108.39	1641	1642
Huaynaputina	117.38 – 117.62	117.48	1600	1600
Reclus?	145.05 – 145.61	145.41	1460	1460
Samalas	181.40 – 182.12	181.86	1257	1258
Tephra Layer	182.07 – 183.14	183.07	1253	1254

forward most of the time. The $\delta^{18}O$ and the Sulphate records as reported in Figure 3.7 do not always align and/or did not always show a pronounced summer maximum.

Most notably the peak at 4.67 m is characterized by an extremely low concentration of sulphate compared to the average found in the core and on the isotopic records is a shoulder of a secondary peak. This specific example is reported in Figure 3.8. In these occasions, the sea-salts concentration profile (mainly Sodium and Magnesium) together with the knowledge of the snow accumulation rate was used to accurately date the core. It is true that previous study (Caiazzo et al., 2017) have shown that the most accurate and in line with the isotopic composition of the snow was the $nssSO_4^{2-}$, but a strong seasonal pattern was found in most sea-salts concentration profile and the snow density of the core in this section is still low enough (and in turns, the temporal resolution is high enough) to ensure the goodness of the dating with different ions.

In particular, for the uncertain peak found at 4.67 m, a sharp decrease in Sodium concentration was found in correspondence of the shoulder peak in the isotopic profile, further confirming the dating firstly proposed. Furthermore, disregarding the peak as a summer maximum (minimum) would have brought two major consequences. Firstly, $nssSO_4^{2-}$ concentration spikes, already assigned to known past volcanic eruption would have shifted. This would have not been a problem in the deeper section of the core, but it would have a direct repercussion on the dating of the 1992 CE $nssSO_4^{2-}$ peak found at a depth between 11.05 and 11.32 m. A shift of one year would have made the highest peak more in line with the year of the eruption of the Pinatubo/Cerro Hudson (1991 CE), but both eruptions, as reported previously, occurred in the middle of the year. Despite the proximity of one of the volcanoes with Antarctica, it seemed more plausible

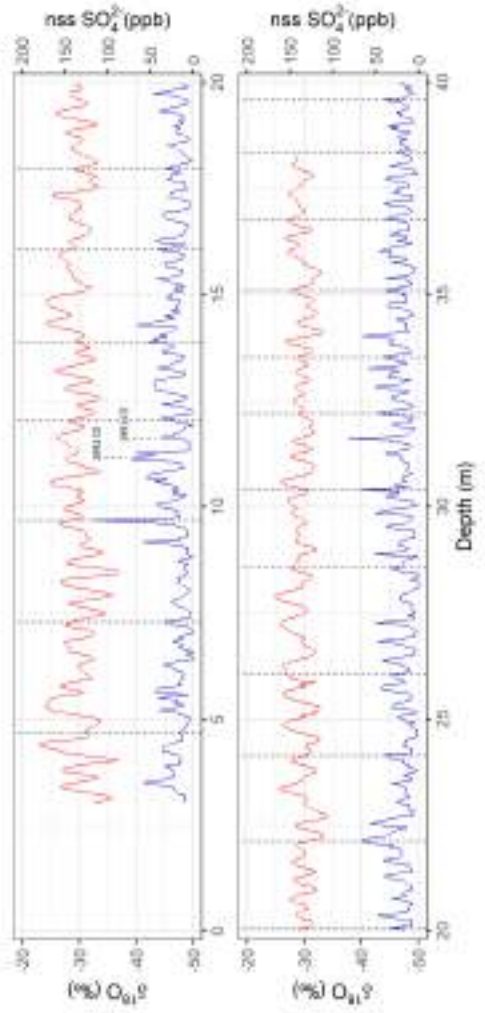

Figure 3.7 – $NssSO_4^{2-}$ (solid blue, right scale) and $\delta^{18}O$ in the first 40m of the GV7(B) core. 1992 CE Pinatubo/Cerro Hudson is also reported. Dashed vertical lines are placed every 5 years starting at 2005 CE

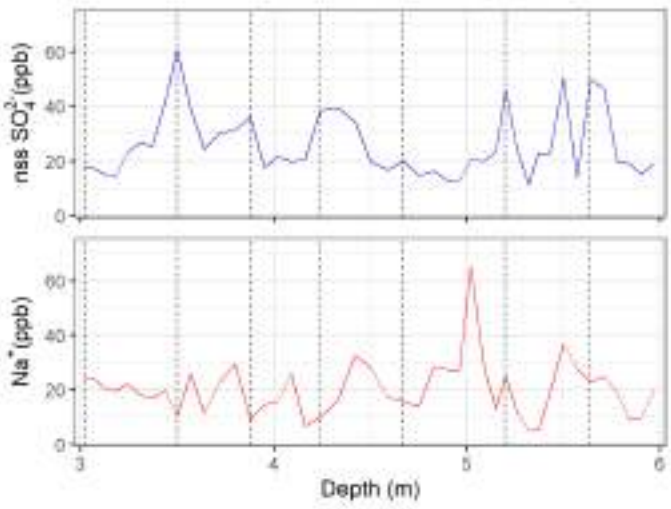

Figure 3.8 – $NssSO_4^{2-}$ (solid blue, right scale) and $\delta^{18}O$ in the first 40m of the GV7(B) core. 1992 CE Pinatubo/Cerro Hudson is also reported. Dashed vertical lines are placed every 5 years starting at 2005 CE

to justify the deposition of volcanic matters in the years following the eruption rather than explaining the peak during the summer enriched in sulphate matter from volcanoes due to diffusions in the snow layers and/or snow mixing due to wind blowing on the snow. Secondly, not considering the peak at 4.67 m as a summer maximum (minimum) would have mean that the snow accumulation rate for a single year on site would have reached values of approximately 500 mm w.e. yr^{-1}, more than double what has been found for the other years in the core (see below). Even considering annual variability and the uncertainty of the dating (resolution of this core is only 4.5 cm on average), and the fact that ice core only samples a small area of the continent (normally few centimeters in diameter) and can't take into account for small spatial variability, the possibility of having a single year of extreme snowfall over the continent seems unlikely. Similar considerations were made when dating the first section of

the core (the first uppermost 38 m) for which the $\delta^{18}O$ and the $nssSO_4^{2-}$ records were used effectively in the procedure. The lack of breakages and the relatively small number of uncertain layers made possible to date this section with relatively low uncertainty that made possible to investigate further procedures to date the entirety of the core. Firstly, the entirety of the dataset was considered and analyzed. Principal Component Analysis was performed on all ions that showed a potential for ice core dating and their profile investigated. Fluoride, Formate, Ammonium, Lithium and Potassium concentration records were discarded from PCA. This choice was made due to the fact that a high number of sample points displayed of concentration at detection limits or below. This initially lead to artificial correlation between these ions (samples characterized by a lower ionic concentration were more likely to have both these five ions under d.l.) and hide more interesting correlation between the ions displaying a seasonal pattern. As expected, and reported in Figure 3.9 and Table 3.3, sea-salt ions are grouped together in PCA when plotted, due to their common origin and the similar pattern throughout the year (with minimum during summer). Similarly, $nssSO_4^{2-}$ and NO_3^- displayed a similar pattern, and they were grouped in Factor 2 when PCA was performed, unlike MSA which despite showing a similar patter, did not seemed to be grouped with the other ions displaying a summer maximum. In Factor 2 NO_3^- and $nssSO_4^{2-}$ present the highest factor loading, but they are negative, highlighting the opposite seasonal pattern of the two factors: concentration maxima in winter and summer for Factor 1 and 2, respectively, further highlighting the possibility of using sea-salts record to date the core.

Despite this, when considering the profile of the ions throughout the years by means of box plot, all sea-salt ions seemed to show a less pronounced seasonal marker. Without claiming bimonthly

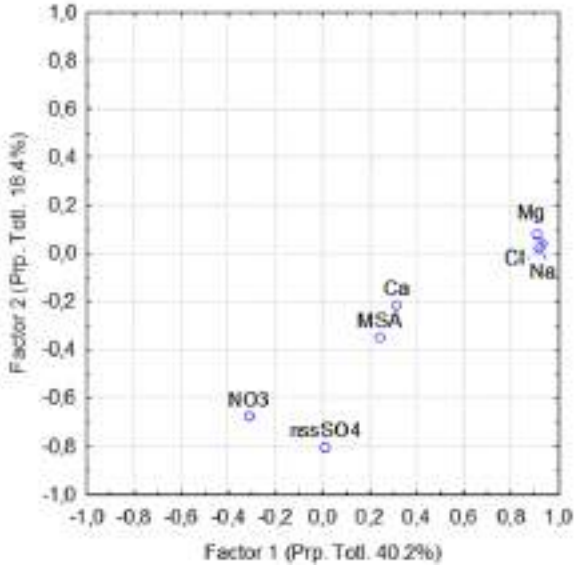

Figure 3.9 – PCA analysis for the first 38 m of the GV7(B) core reporting Factor 1 and 2

Table 3.3 – PCA analysis for the first 38 m of the GV7(B) core, values marked with a * are over .6

	Factor 1	Factor 2
Na^{+}	0.932818*	0.042949
Mg^{2+}	0.914067*	0.079863
Ca^{2+}	0.315526	-0.218724
MSA	0.245398	-0.349795
Cl^{-}	0.923317*	0.021686
NO_3^{-}	-0.311109	-0.677899*
$nssSO_4^{2-}$	0.013404	-0.806931*
Expl. Var.	2.814928	1.289574
Prp. Totl.	0.402133	0.184225

resolution of the dating of the first section of the core and assuming the snow accumulation as a constant throughout the year on site, each year was divided in 6 box and the concentration plotted as recorded in Figure 3.10. Each year was considered starting with the date 1st of January to be consistent with the dating, despite the Austral summer starting in December. Nitrate and nssSO_4^{2-}, as expected displayed an extremely pronounced seasonal patter with clear summer maxima and winter minimum, unlike MSA whose profile, despite the bin at the start and the end of the year being more populated than the one in the middle, didn't showed a clear seasonal pattern. This could be ascribed to both to the potential lack of seasonality in this core, which seems unlikely, or to the higher variability of the MSA records in the bin plot due to the lower concentration compared to the others that forced to use smaller bin sizes in order to avoid smoothing the signal. This led to a higher number of bins with a small population and consequentially a higher variability and a not clear minimum. When doing the same with sea-salt ions, their seasonality was highlighted, as both Chloride, Sodium and Magnesium showed a maximum in the middle of the year. On average, their maxima concentration was found to be less pronounced compared to the average concentration of the ions in this section of the core when comparing their profiles and maxima to the sulphate and Nitrate. Furthermore, when considering the profile of all the proposed methods (i.e., sulphate record, multiparametric dating and sea-salt records), as reported in Figure 3.11a, 3.11b, 3.12a and 3.12b it was made clear that using the concentration profile of either Sodium or Magnesium for the dating of the lower section of the core would have not been a suitable option.

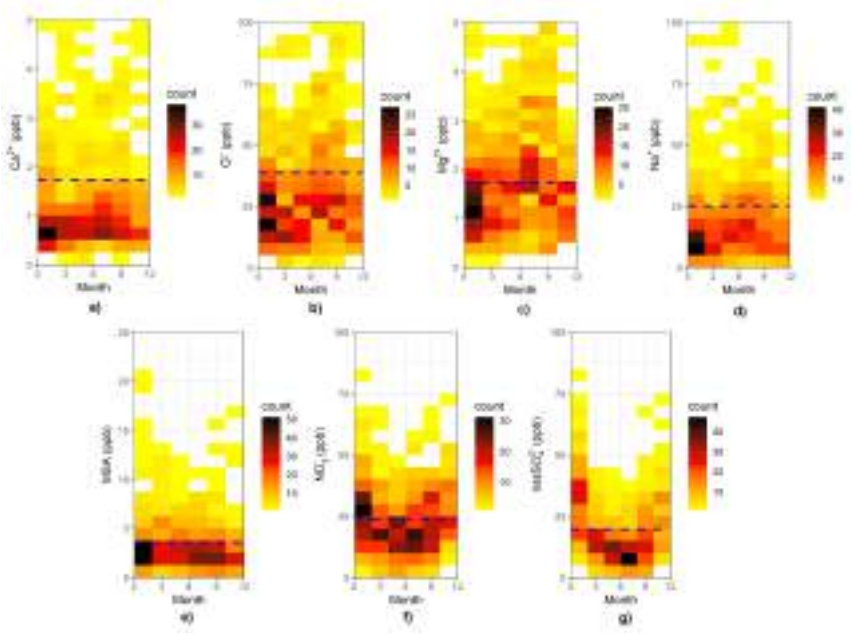

Figure 3.10 – Seasonal variability of sea-salt ions (Ca^{2+} (a), Cl^- (b), Mg^{2+} (c), Na^+ (d)) and non-sea-salt ions (MSA (e), $nssSO_4{}^{2-}$ (f), $NO_3{}^-$ (g)) found in the GV7(B) ice core. Concentration's bin are 3 "months" in width and 5 ppb in height except for MSA levels (1 ppb) and (Ca^{2+} and Mg^{2+} (0.25 ppb). Upper concentration limits and bin sizes were chosen to keep between each ion's plot the same proportions in order to facilitate the interpretation of the data. In blue, the average concentration of each ion in the time interval investigated

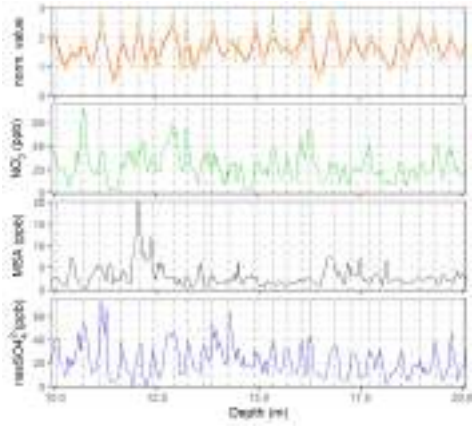

(a)

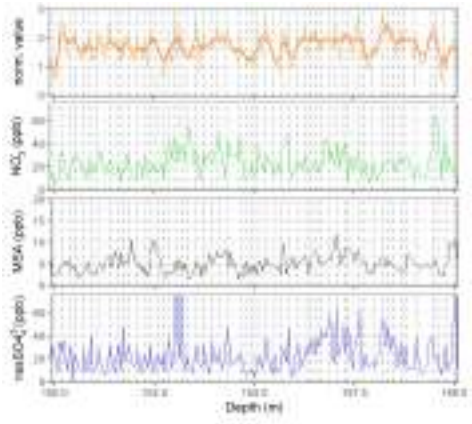

(b)

Figure 3.11 – Example of the dating of the core using the procedure described by(Udisti, 1996). Shades of red, multiparametric dating with different degrees of smoothing (raw, 3-year and 5-year running averages), Nitrate (green), MSA (black) and nssSO_4^{2-} (blue) are also reported. The final dating (dashed vertical lines) is reported as well. Both low depth (a) and higher depths (b) are reported to highlight the differences. Vertical dashed lines are placed every 1 year

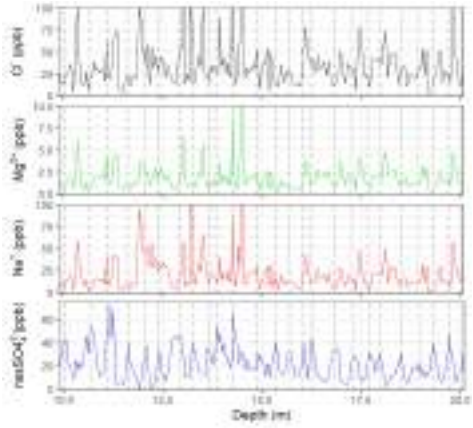

(a)

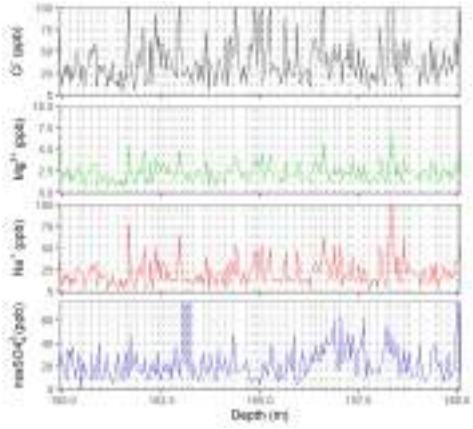

(b)

Figure 3.12 – Example of the dating of the core using the cationic records in the GV7(B) core. Both low depth (a) and higher depths (b) are reported to highlight the differences. Vertical dashed lines are placed every 1 year

Ultimately, the choice of continuing the dating using solely the $nssSO_4^{2-}$ concentration profiles were made. The sea salts' concentration profile was reserved to confirm the dating and/or in for those section of the core where the $nssSO_4^{2-}$ (either due to low concentration or because of external concentration spikes) profile was too compromised to be of use in the dating procedure. Figure 3.13 reports the complete dating of the rest of the core, up to a depth of 197 m with a sub-annual resolution. Three main reasons made impossible to accurately proceed the dating

- Low number of known volcanic records in this section: Sigl et al. (2013) reports a number of volcanic eruptions prior the year 1100 CE but only a few here are associated with known volcanoes, e.g. the Hekla 1007 CE eruption. This stratovolcano is in Iceland, but traces of its eruption have been found in core drilled in the Wais Divide, Antarctica. In the GV7(B) ice core, the volcanic flux found was low, making it a unreliable record to use in the accurate dating. Similarly, Castellano et al. (2005) identifies a number of volcanic signatures in this time period investigating the Dome C site, but most of them display a low volcanic flux. Major exception is the event 22, but the work date it to the year 699 CE, most likely not in the time period covered by GV7(B).

- High number of breaks and missing section of the core. Missing sections of the core were present in the section dated (see below), but here the lack of known volcanic eruptions to constrain the dating made so that the dating has to rely entirely on the annual layer counting, which requires an uninterrupted record to accurately date the core.

- The presence of cracks and breakages led the drilling fluid

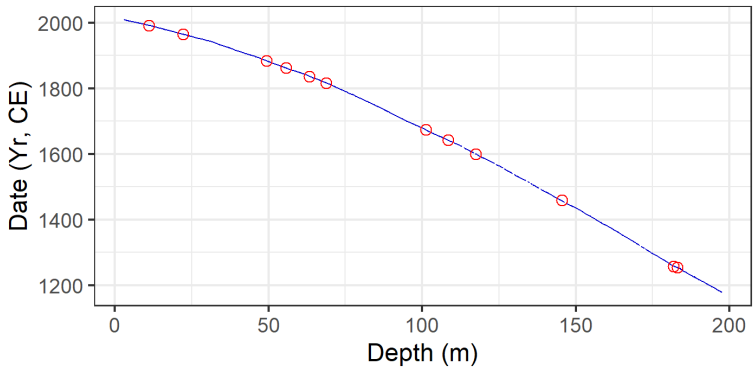

Figure 3.13 – Age - depth correlation for the GV7(B) ice core. Red circles highlight each volcanic eruptions found in the core

inside the core, this, together with the fractioning of the core in small section reduced the temporal resolution, which, in turn, could lead to missing years in the dating. For these samples, the decontamination procedure, which involves multiple steps, has the potential to introduce external contamination despite working under a class 100 flow hood.

The latter, since breakages in the core were found from a depth of approx. 80 m, was investigated in detail, to make sure that the concentration samples in the section investigated weren't affected by the decontamination procedure and/or by external contamination.

Ionic content in the core isn't expected to be constant throughout the years and the scope of this work is to investigate their variability in the last millennia, but if a contamination is indeed introduced, it is to be expected to see a rise in the number of "spikes" concentration. Five sections, each 2 m in length, were chosen and the concentration of each ion plotted using box plots as reported in Figure 3.14. Section 100-102 m and 150-152 m were used as a reference for sections of the core decontaminated using ceramic knives and without

breakage. The other sections are characterized by an increasingly higher number in cracks, with the last two presenting visible traces of drilling fluid on the surface of the melted samples despite the decontamination procedure. Despite this, all sections displayed a similar level of concentration for all ions, although the number of spikes in concentration seems to rise in the deeper sections of the core. This confirmed the goodness of the decontamination of the samples analyzed.

For the sections of the core missing, the dating was obtained by averaging the age/dept ratio of the 10 years before and after the breakage and therefore estimating the number of years present. This was made under the assumption that snow accumulation rate over Antarctica is relatively constant but lead to higher levels of uncertainty for those sections of the core too badly damaged. For annual layer counting, an estimate of the uncertainty of the dating is difficult to accomplish and it's normally either based on the uncertainty associated with the algorithm used to identify each layer (Sigl et al., 2016; Winski et al., 2019) and/or with the uncertainty of the records used as a reference in the dating (Winski et al., 2019). Here, the total uncertainty in a time period delimited by two volcanic events, is estimated to be the sum of the layer uncertainties as found in the identification of each summer maxima, estimated to be 0.5 ± 0.5 years (Rasmussen et al., 2006). This allowed to account for both underestimation and overestimation of summer maxima. The same level of uncertainty was given to the missing sections of the core. Each known volcanic eruption is considered here to be dated with an uncertainty of $\pm$ 1 years from the recorded eruption due to the amount of time needed to reach the continent and the site. In Table 3.4 is reported the uncertainty level of the dating of the core across the length analyzed together with the amount of missing ice for

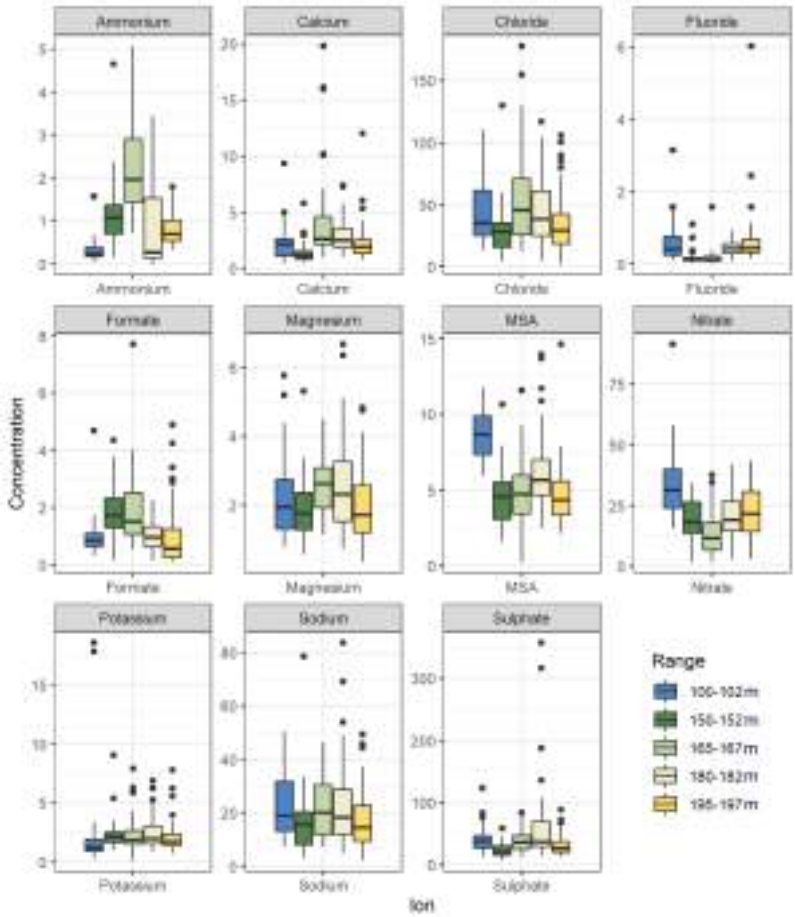

Figure 3.14 – Bin plots for major ions found in the GV7(B) core, sample size of 2 m were used to investigate the possible contamination of drilling fluid, avoiding major volcanic signatures

Table 3.4 – Uncertainty levels on the GV7(B) dating. For each section of the core, the amount of missing ice is reported. Uncertainty is reported both in Absolute years and Percentage levels

GV7(B) (m)	Missing %	Layers		Yrs	Error	
		Max	Certain		Abs.	%
3.00 – 11.10	0.37	17	17	17	-	-
11.10 - 22-12	0.18	28	26	27	1.0	3.7
22.12 – 49.35	0.48	86	76	81	5.0	6.2
49.35 – 55.75	0.31	27	21	22	3.0	13.6
55.75 – 68.75	0.38	50	42	48	4.0	8.3
68.75 – 101.25	2.15	146	136	141	5.0	3.5
101.25 – 108.39	2.46	34	31	32	1.5	4.6
108.39 – 117.48	2.53	44	37	41	3.5	8.5
117.48 – 145.41	8.80	142	133	142	4.5	3.2
145.41 – 181.86	3.76	200	188	200	6	3.0
181.86 –183.07	0.82	4	4	4	-	-
183.07 – 197.00	0.18	75	69	75	3	4.0

reference. As expected, the highest uncertainty was found for those sections of the core where the number of volcanic eruptions is lower. The uncertainty should be considered minimum in correspondence with the known volcanic eruption and at its maximum in between two.

3.2.2 Dome C 3D ice core dating

Due to the characteristic of the site (Dome C only receives about 70 mm w.e. yr^{-1}) and the low resolution of the core (10 cm), the stratigraphic dating proposed for the GV7(B) ice core and described in the previous section of this work was not possible. Instead, the dating was accomplished by identifying specific tie points (either volcanic or anthropogenic in nature) and temporal horizons. The

same procedure for the identification of the volcanic signatures in the GV7(B) ice core was used for the DC3D, with the identification of a biogenic background in the nssSO_4^{2-} (Castellano et al., 2005) and a statistical threshold over which a point sample could be attributed to a volcanic eruption. Two major differences with the procedure applied to GV7(B) are worth noting.

- Due to the low resolution of the core and the relatively low number of samples (approx. 500) so far analyzed and here investigated, using a running average function to smooth the biogenic background would have not given further information on the variability in the core. Instead, thanks to the relatively stable signal found, a single value of nssSO_4^{2-} background was used, averaging the signal over the entirety of the core section here considered.

- Any given signature was ascribed to a potential volcanic eruption even if only one single sample was above the set thresholds. This is due to the lower snow accumulation rate and the relatively low resolution of the samples (10 cm). This led to most of the volcanic signatures being concentrated inside a very short length of ice, and applying the same algorithm as done before (i.e., a rise in the nssSO_4^{2-} profile was ascribed to a volcanic eruption only if two consecutive sample points displayed a concentration over the set threshold) could have led to false negative.

The volcanic signatures identified in the core are reported in Table 3.5, whilst the complete record of the nssSO_4^{2-} profile and the total conductivity of the melted samples of the core are reported in Figure 3.15. Both records were used to create the DC3D chronology and do not differ significantly: this was expected, since free acidity

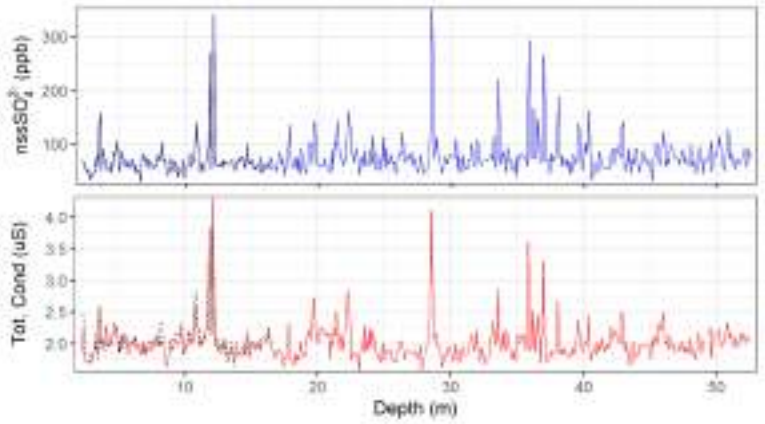

Figure 3.15 – Total conductivity and $nssSO_4^{2-}$ profile for the DC3D core. In black is reported also the corresponding record obtained by the cored samples

should contribute to the majority of the total conductivity of the sample, especially for those section of the core where volcanic material is present. Indeed, when considering the average of all samples, the free acidity (see Figure 3.16, the free acidity was evaluated on the basis of the major ions analyzed and is therefore affected by a higher uncertainty due to the lack of records of all ions in the core) is definitely a major component in the ionic balance together with Sodium levels. When considering the sulphate contribution as reported in Figure 3.17, a clear correlation between sulphate and free acidity is present. The ratio between the two (the correlation index of the trend line) is lower than the theoretical one, as expected due to the sea-salt component of the sulphate and the fact that both HCl and HNO_3 contribute to the acidity of the snow, but clearly indicates how H_2SO_4 is a majority component of the free acidity, and in turn of the total conductivity, record.

An in-detail description of the eruption that brought them on

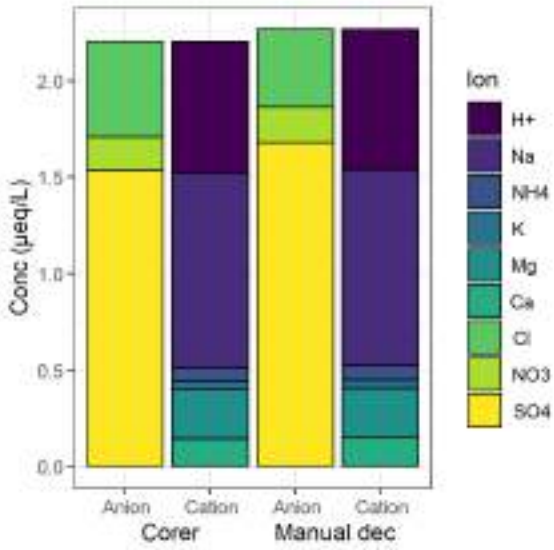

Figure 3.16 – Ionic balance and evaluated free acidity for the DC3D core. Both saples treated with the corer and manually decontaminated are reported here

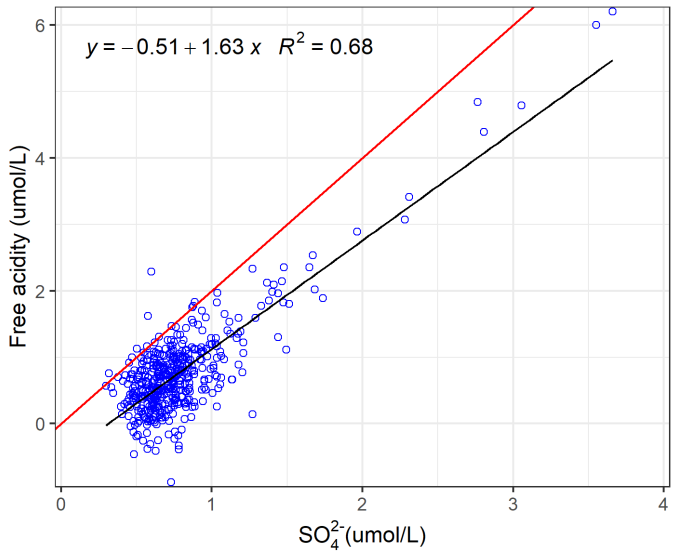

Figure 3.17 – Free acidity - sulphate correlation for the DC3D core. The theoretical ratio assuming all free acidity came from H_2SO_4 is reported in red

Antarctica is reported above and here the attribution of the signatures is only briefly described. Major exception is the 1835 CE eruption of the mt. Cosigüina, in Nicaragua. The eruption occurred in January and is explosive in nature, with a large amount of volcanic material erupted in the atmosphere and an assigned volcanic Dust Veil Index higher than both the Krakatau and the Tambora (Self et al., 1989). Despite its violent nature, the eruption had a modest magnitude and its effect on the climate seems to be limited compared to the amount of volcanic material. Furthermore, the amount of volcanic material that reached the GV7(B) site was found to be modest, and the rise in concentration was found to be not high enough and diluted across multiple years, making it a non-reliable reference for the dating. For the DC3D ice core, this was not the case and a sharp rise in concentration at a depth of 10.83 m was found, consistently with what found in another core drilled at the same site. For the deeper section of the core (over 30 m deep), a number of possible volcanic signatures was found (see section below) but they are yet to be attributed to know past volcanic eruptions. The lack of historical records makes harder to assign a date to these, but a common patter was found for at least five when comparing it to another DC core (Castellano et al., 2005). These are reported in 3.5 and marked as Unknown, and using the chronology extrapolated by flow models and on the basis of known past volcanic eruptions, were dated and used in this work.

The age depth relationship doesn't exactly match the one found in EDC96 ice core, even when taking into account for the snow deposition in the year between the two projects, but the previous work on the same site was taken as a reference to create an exact chronology for this core. The differences with EDC96 are highlighted in Table 3.6. By using the 1815 CE Tambora eruption as a tie point

Table 3.5 – Volcanoes used in the dating of the DC3D core. Unknown volcanoes marked with a ? are dated by comparing the nssSO_4^{2-} profile of the DC3D core with the records described in Castellano et al. (2005)

Volcano	DC3D Depth (m)	Historical date (CE)
Agung	3.61	1963
Krakatau	8.20	1887
Tambora	11.85	1816
Unkn 1809	12.16	1809
Serua	17.83	1696
Gamkonora	19.78	1675
Sub A	21.42	1624
Huaynaputina	22.34	1601
Kuwae	28.55	1460
Unkn ?	33.54	1347
Unkn ?	35.84	1288
Unkn ?	38.04	1230
Unkn ?	39.59	1190
Unkn ?	40.37	1170

reference (in DC3D found at a depth of 11.85 m and with a maximum concentration of sulphate lower than the one found for Unkn 1809, something that was ascribed to the low resolution of the core that, potentially, could diluted the signal) it was possible to estimate how much the two records differentiate in the form of distance between known volcanic eruptions. The difference between the two is further highlight in Figure 3.18 where the two dating are plotted point-by point. An excellent correlation is indeed found between the two, but the correlation is lower than expected, suggesting that either the layer of ice shifted slightly or, more likely, the drilling process compressed them, bringing a slight shift to the dating. Regardless, the excellent stratigraphy and almost perfect correlation with the EDC96 core, made possible to obtain an accurate dating for the DC3D core in the section investigated.

3.2.3 Snow pits dating

The snow pits sampling started in Concordia, with the traverse moving towards the inland of the continent following the 123°E. Therefore, snow accumulation is expected to be low for all of the five snow pits here considered, especially for those characterized by strong winds and/or ablation phenomena that could lead to an even lower accumulation in areas where the deposition is relatively high. For this reason, the identification of seasonal patterns in the ionic composition of the samples, despite the relatively high resolution (approx. 3.5 cm, the diameter of the vial used to collect them), was not a viable option to the dating. Furthermore, neither the isotopic composition nor dust records for these samples are yet available, and therefore estimate a chronology was only possible with the identification of volcanic signatures. Most records average a depth of 2 meters, with the deepest being the Wind Crust, reaching a depth of 2.38 m (although

Table 3.6 – Volcanoes used in the dating of the DC3D core. Unknown volcanoes marked with a ? are dated by comparing the nssSO_4^{2-} profile of the DC3D core with the records described in Castellano et al. (2005)

Volcano	Depth (m)		Distance Tambora (m)	
	EDC96	DC3D	EDC96	DC3
Agung	2.95	3.61	9.39	8.24
Krakatoa	8.00	8.20	4.34	3.65
Coseguina	10.83	-	1.02	-
Tambora	12.34	11.85	0	0
Unknown	12.68	12.16	0.34	0.31
Serua	18.62	17.83	6.28	5.98
Kuwae	29.77	28.55	17.43	16.7
Unkn 1347	34.55	33.54	22.21	21.69
Unkn 1288	36.96	35.84	24.62	23.99
Unkn 1230	39.22	38.04	26.88	26.19
Unkn 1190	40.79	39.59	28.45	27.74
Unkn 1170	41.52	40.37	29.18	28.52

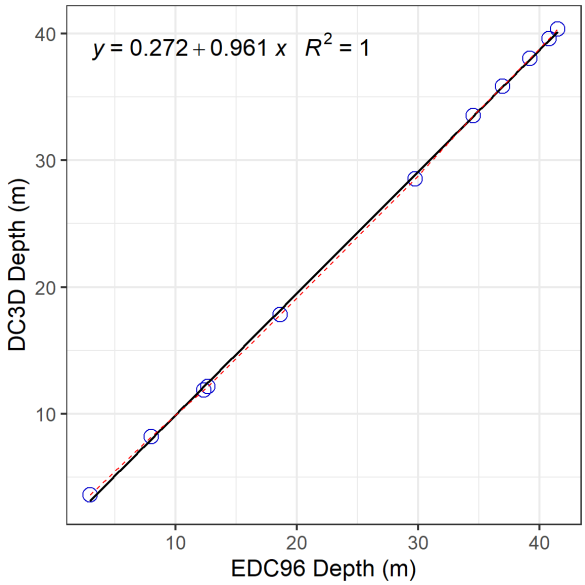

Figure 3.18 – Free acidity - sulphate correlation for the DC3D core. The theoretical ratio assuming all free acidity came from H_2SO_4 is reported in red

its resolution is lower, 7 cm), making difficult to obtain an exact chronology. Even in those areas where the accumulation is lower (and therefore identification of more volcanic signature would be possible depth-wise), the mixing of the snow layers in those areas would make it hard to obtain a clear profile. Regardless, the same procedure applied for the other records was here applied with the aim of identifying the two most recent historical eruptions identified in ice cores (1991 CE Pinatubo and 1963 CE Agung). In Figure 3.19, the $nssSO_4^{2-}$ profile for each snow pits is reported, together with the biogenic background and the statistical thresholds used to identify which sample points concentration were statistically high enough to be attributed to volcanic eruptions. The same consideration made for DC3D were applied here, mainly i) a single value for the biogenic $nssSO_4^{2-}$ biogenic background was used and ii) a single sample point above the threshold was sufficient to potentially ascribe the snow layer to a year in which a volcanic eruption was present. As reported in Figure 3.19, only two of the five investigated sites (AGO-5 and PALEO) display $nssSO_4^{2-}$ signals that could be ascribed to volcanic signatures. For ME and MA site peaks at a depth of 139.5 and 61.5 cm depth respectively are found above the set thresholds but taking into account for a snow accumulation rate of 8.0 cm of snow per year (Traversi et al., 2009), as found in a different snow pit drilled at Dome C during the 2005/06 CE campaign, the first peak would have been dated approx. 2002-03 CE and the second one approx. 2013-12 CE. No clear evidence of deeper volcanics' eruptions were found, and the two signals do not seem to correspond with any known past volcanic eruptions. This lack of volcanic signatures was ascribed to relative homogeneity in the concentration of the samples taken in the MA site and for the ME site to the high variability and noise in the core. Indeed, for the ME snow pit, the biogenic

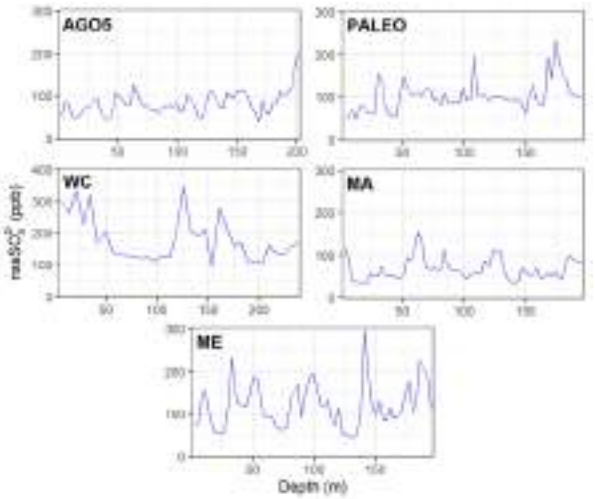

Figure 3.19 – $NssSO_4^{2-}$ profile for the five shallow snowpits of the EAIIST traverse, AGO5, Paleo, WC (Wind Crust), MA (Megadune Accumulation), ME (Megadune Erosion)

background was found to be particularly high (260 ppb of $nssSO_4^{2-}$) from with the "spike" in concentration differentiate only for 36 ppb in concentration, more likely to be ascribed to external contamination or biogenic contribution than to a volcanic signature. For the two other records, only the deeper peaks (199.5 m for AGO-5 and 172.5 m deep for Paleo) were ascribed to past volcanism, with the peak found at 106.5 m in the Paleo snow pit record discarded from the dating based on consideration of the snow accumulation rate in the area (Traversi et al., 2009).

3.3 Trace element analysis in DC3D core

Alongside ^{239}Pu, a number of metals were analyzed with the same procedure described for Pu, here the temporal profiles of these components are discussed. It must be noted that the system used

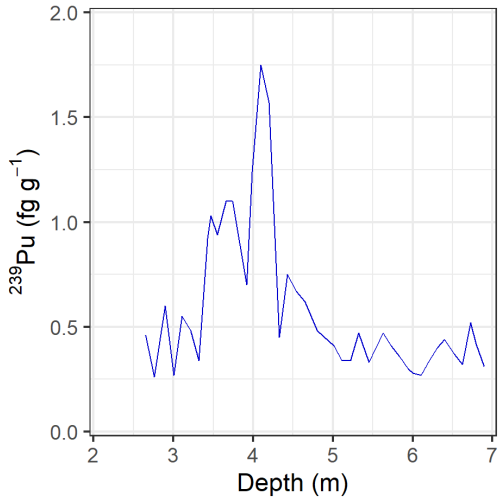

Figure 3.20 – ^{239}Pu concentration vs depth profile for the DC3D core

experienced problems during the run of each sample, mainly due to a damage in the cooling system of the instrument that forced a constant shutdown of the set-ups used. This introduced a larger error for most of the metal analyzed and forced, in the case of ^{239}Pu, to manually select individual peaks. Rare Earths' content was analyzed, but their profile was ultimately discarded as with most of the elements considered.

3.3.1 Plutonium records

For ^{239}Pu, the concentration profile (in fg g^{-1}, concentration needed to compare the record here produced with the ones found in other cores) is reported in Figure 3.20.

When comparing the two local maxima (found at 3.70 m and 4.09 m deep) in the concentration of Plutonium with the chronology obtained, it is possible to further confirm the goodness of said chronology. Indeed, the two peaks are dated to the years 1961-1964

CE and 1954-1958 CE respectively and this coincide with the two time periods in which the highest number of NWTs is reported. Both the year 1958 and the 1961 CE are associated with either the end or a start of a new phase of last century NWTs, with a total number of over 200 single tests (over 90 and 120 respectively), further confirming the dating produced with the volcanic signatures in the DC3D core. By taking into account for the relative ^{239}Pu specific activity (2.9*10Bq g^{-1} Baglan et al. (2000)) the data here presented were converted in mBq Kg^{-1} for easy comparison with other cores. In particular the profile found in another core drilled at the same site (Cutter et al., 1979) for the combined yield of 240Pu and 239Pu on Dome C was considered. In order to compare the two, it was assumed that the same quantity of ^{240}Pu and ^{239}Pu reached the site and a specific activity for ^{240}Pu of 8.39 *10^{9}Bq g^{-1} (Baglan et al., 2000). The comparison between the two is reported in Figure 3.21, where the two records are plotted against the date associated to each sample.

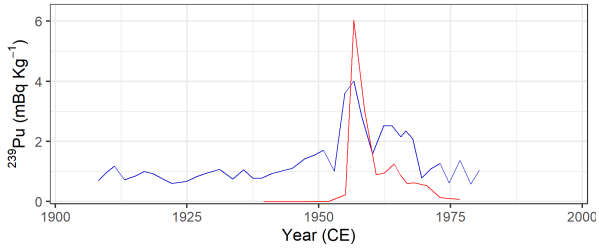

Figure 3.21 – Comparison of the Pu content in different cores from DC3D site. In red, Cutter et al. (1979) data, in blue, this work.

The two profile display similar characteristics and peaks, with a higher background found in the DC3D core (most likely due to the problems displayed with the instrument rather than an actually higher concentration of Pu in the core), and significantly higher

concentration of ^{239}Pu in the DC1997 snow pit samples. The latter, it must be noted, is characterized by a lower resolution than the core here analyzed and it's an extrapolation of a combined record of both ^{240}Pu and ^{239}Pu. Both display a first maximum in conjunction with the end of the first period in which significant atmospheric tests were conducted (1952 – 1958 CE) with the one recorded in the DC3D core most likely attributed to the Mike test in Einwetok Atoll (1952 CE) and the Bravo test (1955 CE). The increase in concentration of 239Pu, with a maximum value of 4.01 mBq Kg^{-1} is found in the 1956 - 1960 CE time year period, where the largest tests in the Southern Hemisphere were conducted by the U.S. shortly followed by the Limited Test Ban Treaty that coincides with the decline in the concentration of ^{239}Pu. The concentration never dropped to the base line levels most likely due to the longer residence time of ^{239}Pu in the atmosphere (Arienzo et al., 2016), but also to the following tests. It must be noted that the post-moratorium period (post 1960 CE) also concurs with the resumption of the tests by the Soviet Union, most specifically at the Novaya Zemlya (NH) site. Despite the total yield of the tests, the transports pathways from the Russian Arctic to Antarctica are not efficient and no real evidence of these experiments is recorded in the ^{239}Pu profile, with the last two peaks most likely associated with the late 1960 to 1970 CE French and Chinese NTWs. Indeed, composite records (Arienzo et al., 2016) show how in this phase, more than 10 times higher concentration of ^{239}Pu was found in Antarctic records when comparing to similar ones drilled in the Arctic. In general, due to the position of the test sites, higher levels of ^{239}Pu are found in the Arctic, with even Phase one-associated levels of plutonium in the Arctic core twice as high as the one found in the Antarctic ones. When comparing the data here presented, the total yield of ^{239}Pu is closer in the time period

1960 1965 CE was found closer to the one recorded in the Arctic composite record (Arienzo et al., 2016). Even taking into account the higher background in the DC3D core, the Pu concentration in this core seems to be higher than what found in other records (up to 2.5 mBq Kg (Arienzo et al., 2016) compared to the 0.6 mBq Kg (Arienzo et al., 2016) and 4.9 mBq Kg (Arienzo et al., 2016) for the Antarctic and Arctic composite record respectively in the post-moratorium period) across Antarctica.

3.3.2 Metal records in the DC3D core

As already stated, most of the records for metal content in the core were too unreliable to be used for environmental reconstructions and studies. Despite this, clear records of multiple isotopes of Lead (^{206}Pb, ^{207}Pb, ^{208}Pb) was obtained for the time period investigated (1908-1980 CE according to the chronology here proposed) as well as a clear the records for trace elements associated to volcanic eruptions (^{205}Tl and ^{209}Bi). In Figure 3.22 the profiles of ^{205}Tl and ^{209}Bi are reported. The peak found in the ^{209}Bi concentration profile at a depth of 3.8 m doesn't correspond with a similar peak in the ^{205}Tl profile, which excludes the possibility that this could be associated with volcanic materials. Two other peaks were found in the two records: the first one at a depth of 3.37 m and one at 6.27 m for ^{205}Tl. Indeed, similar peaks were found in the ^{209}Bi concentration profile, but the latter is shifted slightly to a depth of 6.16 m. In this section of the core, a only one volcanic signature was found in the nssSO_4^{2-} profile, the 1964 CE Agung eruption, but this signature does not coincide with the local maxima in the trace elements profile. When considering the sulphate chronology, the 3.37 m peaks would be dated to the year 1967 CE. Similarly, the other peaks at a lower depth in the core does not seem to coincide with any past volcanic

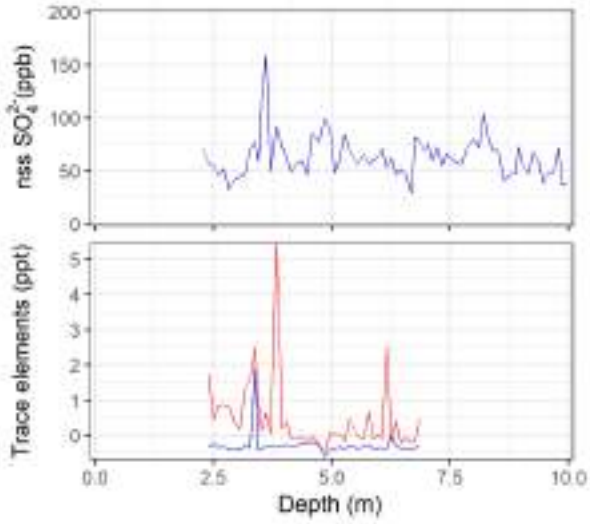

Figure 3.22 – $NssSO_4^{2-}$ profile (up) and trace elements (down, ^{205}Tl and ^{209}Bi

eruptions, making the trace elements' profiles less reliable to confirm the chronology produced with the volcanic peaks.

Of the four stable isotopes of lead, only three were considered for the DC3D core (^{204}Pb is present only in traces and the percentage in which is present is negligeable compared to the instrumental error), the total record of the lead concentration is reported in Figure 3.23. Concentration of lead from anthropogenic sources, bringing the levels of the metal above the natural background, have been rising since approx. 5000 years (Weiss et al., 1999) but a more significant rising in these has been observed in the last century. This is mostly due to mining and smelting activity as well as the introduction of lead in gasoline and fuels as tetraethyl lead in the second half of the 1900s, before its phase-out at the end of the century (Hurst et al., 1996). Despite the clear profile suggesting a rise in concentration in the last century, concentration of lead found in the core are low when

compared to what has been found in other records (Bertinetti et al., 2020) even when considering the levels in a pre-industrial period (pre 1900 CE). Indeed, the maximum concentration found in the DC3D core is found in the first sample (7.2 ppt), and when considering the rest of the core, none of the samples displayed a concentration above 2 ppt, less than a third than what found in other cores associated with anthropogenic pollution and more similar to the one found before the 20th century in the Antarctic snow (McConnell et al.) and even less than what found in the snow pits drilled in the same site. It is worth noting that the core only covers a small time period before the ban of lead in fuels and even if a clear rise in concentration is found, it is hard to estimate the clear extent of the lead pollution on site since the majority of the second half of the 20th century is missing in the record. When considering the ratio between ^{206}Pb and ^{207}Pb, a higher degree of variability is found in the first half of the 20th century, most likely due to the lower concentration recorded in the core. Indeed, the three lowest recorded ratios between the two isotopes are attributed to extremely low concentration of ^{206}Pb compared to the rest of core. Excluding these three sample points, the isotopic ratio remains mostly constant throughout the core, with slightly lower value in the first half of the 20^{th} century, but the discrepancy is non-significant when considering the variability of the data (0.92 ± 0.08 vs 0.88 ± 0.07 in the 1950 - 1980 CE and 1910 - 1950 CE time periods respectively), suggesting a single source for the lead contamination on site.

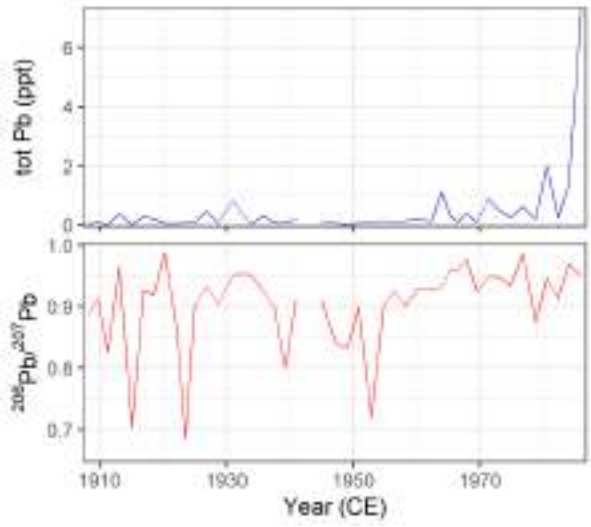

Figure 3.23 – $NssSO_4^{2-}$ profile (up) and trace elements (down, ^{205}Tl and ^{209}Bi

3.4 Snow accumulation rate across the East Antarctic Plateau

Due to the different resolution of the dating of the records so far presented, different approaches were used to evaluate the amount of snow accumulation for each of the three set of data.

3.4.1 Accumulation evaluated at the GV7 site

For the GV7(B) core, for which a yearly resolved chronology is available, the snow accumulation was evaluated with a resolution of one year despite knowing that the sample resolution (4.5 cm average) could have introduced a high level of uncertainty in the record of accumulation. Mainly, since in the lower section of the core are characterized by a higher density, this means that most

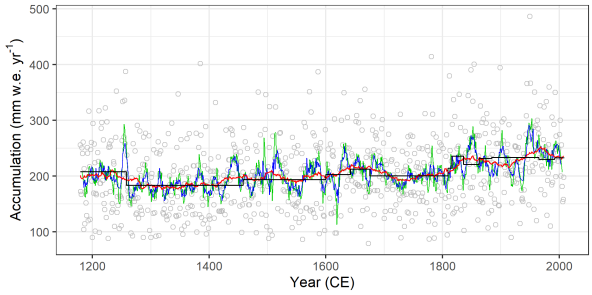

Figure 3.24 – Snow accumulation rate (in mm water equivalent per year) across the last millennia as calculated from the GV7(B) ice core. Grey dots, annual data, solid green, 3-year running average smoothing, solid blue, 7-years running average, solid red, 51-years running average, solid black, average snow accumulation rate evaluated between known temporal horizons (volcanic signatures)

years span across only a couple of samples (most of them after a depth of 100m, are comprised by two: a summer maximum and a winter minimum in the $nssSO_4^{2-}$ profile). Since the profile is made by discrete samples, overestimating (or underestimating) the length of a year becomes a more significant error in the deeper sections of the core. Regardless, an annually resolved record of the snow accumulation rate was produced as reported in Figure 3.24. In order to take into account for the overestimation (underestimation) of the accumulation a preliminary smoothing function in the form of running average was applied to the dataset. This assured to remove the possible noise present in the record due to post depositional processes such as sastrugi (Frezzotti et al., 2007) and both 7-, 11- and 51-year interval running average (centered on the middle of the interval) were applied to investigate the variability of accumulation rate in the last millennia.

On average, an accumulation of 242 ± 57 and 233 ± 64 mm w.e. yr^{-1} was found for the periods 1965 – 2000 CE and 1854 – 2004 CE

respectively. This confirmed the data found from other records on site, mainly the estimation of 241 ± 13 mm w.e. yr^{-1} based the atomic bomb horizon records (Magand et al., 2004), the stake farm measurements (252 ± 104 mm w.e. yr^{-1}) and other considerations made studying the seasonal variation in $nssSO_4^{2-}$ (Frezzotti et al., 2007) in the same the last 150 years (237 mm w.e. yr^{-1}). Particularly good agreement was found with the records of snow accumulation on site as found during the ITASE traverse. When comparing the data here presented, a good correlation ($R = 0.42$, $p<0.0001$) was found in the time period 1900 - 2001, but the degree of correlation decreases when considering the entirety of the ITASE record ($R = 0.3$ $p<0.0001$) mostly due to few incongruences between the years 1880 and 1850 CE. These were ascribed to differences in the dating mostly due to the different spatial resolution of the records. Conversely, when considering the entirety of the core analyzed in this work (1179 – 2009 CE time period), the snow accumulation found for the GV7(B) core was lower than what previously found in the last century (205 ± 63 mm w.e. yr^{-1}). More information about the snow accumulation rate for the GV7(B) site and the comparison with other cores drilled in the area are reported in Nardin et al. (2021), here, major focus is given to the accumulation record from GV7(B) itself. In particular, a significant trend in the accumulation on site was found both considering the entirety of the core and after break-points analysis, with a high increase throughout the 800 years period investigated (a rise of 47 mm w.e. yr^{-1}, approx. a rise of 23%). This was found to be somewhat consistent with other records on the Antarctic plateau: Law Dome (Roberts et al., 2015) in the same time period displayed a rise in accumulation, but of a lesser degree when compared to GV7 (20 mm w.e. yr^{-1} in the last 800 years, only 2% of the accumulation on site). This is in line with the clear increase

in the time period of the snow accumulation found in the coastal and slope regions (Frezzotti et al., 2013). Following the procedure highlighted in (Tome and Miranda, 2004), break point analysis on the accumulation record was performed in order to identify periods with significantly different trends. The algorithm uses a least-square approach to compute the best continuous set of straight lines in order to better fit a given time series, with a constrain on the number of break points and or the minimum distance between each of those points. Here a time period of at least 150 yrs was chosen as the minimum distance, in order to identify trends at a secular scale and to compromise the need for high computational power (for a low time period) and the risk of finding non-significant trends for a too large minimum distance. For GV7(B), four multi-centennial periods with different trends were highlighted, with an initial drop in accumulation (already low) from the beginning of the record up to the year 1341 CE followed by somewhat stationary period and a sharp increase starting around the year 1750 CE. Comparisons with other cores is not easy, especially because the number of cores in the area is still low. Thomas et al. (2017) reports 79 records of snow accumulation for the continent, but only 5 were drilled in Victoria Land (East Antarctic Plateau) and only few of those cover the last millennia, the time period here investigated. When considering the entire continent, an increase of the snow accumulation on the continent is found since the year 1800 CE, with the annual snow accumulation in the 2001-2010 decade is higher than the average at the start of the 19^{th} century. In contrast, Frezzotti et al. (2013) noticed a lack of significance in the increase of snow accumulation in the continent, in line with multi-millennial records in the area. Roberts et al. (2015) highlighted that in the time period covered by the Law Dome records (22 BCE - 2012 CE) that no clear long-term is found in the core.

However, this doesn't mean that anomaly periods of accumulation aren't present, most notably, considering the one overlapping the record object of this work, the 1429 – 1468 CE and the 1979 – 2009 CE period (low accumulation and high accumulation respectively). It must be noted, that despite similarities (and/or lack of) across the East Antarctic plateau in the snow accumulation rate, when considering the three deepest records for the area (Talos Dome, Law Dome and GV7), it's clear that their sites receive precipitations from different areas and are, therefore, influenced by different air mass atmospheric pathways. In particular both the Southern Indian Ocean (Caiazzo et al., 2017) and the Ross Sea (Sodemann and Stohl, 2009; Scarchilli et al., 2011) and their storms influence the precipitations over the area. Moreover, difference in behavior between the coastal sites, the one on the ice divide and the rest of Antarctica must be considered (Frezzotti et al., 2007). This is mostly due to the higher frequency of blocking anticyclones that increases the precipitation at coastal sites. This leads to the advection of moist air to higher areas; for windy sites, the blowing snow has the opposite effect with the erosion having a significant negative effect on the surface snow balance and accumulation. Comparison between these records and the break-point analysis are reported in Figure 3.25 and 3.26 respectively.

3.4.2 Accumulation evaluated at the DC site and the Antarctic Plateau

Similar consideration, due to the reduced resolution and the lack of a clear annual patter in the core (the dating was accomplished with the identification of volcanic signatures), were impossible to made for both the DC3D core and the snow pits records. For these, the same approach at the snow accumulation used in Nardin et al. (2020) for

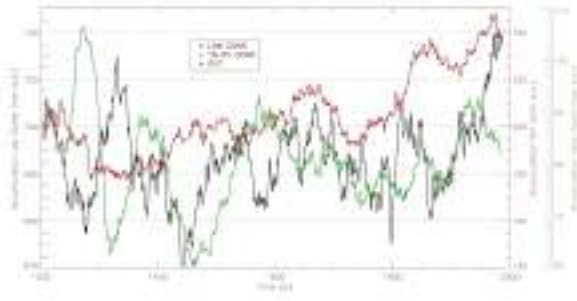

Figure 3.25 – Snow accumulation rate across Antarctica for the Law Dome (black, left scale), Talos Dome (green, right scale) and GV7 site (red, right scale).

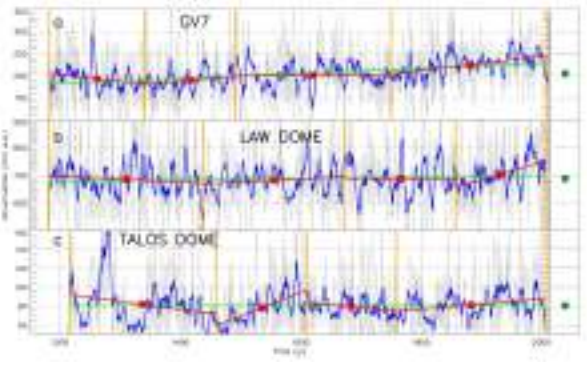

Figure 3.26 – Breakpoint analysis as reported in Nardin et al. (2021) investigating different sites across Antarctica

the preliminary investigation of the GV7 site, was used. Mainly, the snow/ice density was averaged across the length of the core/snow pit in between two horizontal tie point and used to evaluate the average accumulation in the same time period. This record for the DC3D core is reported in Figure 3.27, where no further smoothing was applied due to the limited numbers of volcanic signatures. This does not take in consideration the layer dating obtained with the age vs. depth relationship previously discussed; indeed, the obtained

chronology of the core that dated each layer of the core was tested to evaluate more accurately the accumulation rate (with a resolution of approx. 2 year). This was ultimately discarded, because it already works on the assumption that the accumulation rate is a constant function once the least-square interpolation is applied to the volcanic signatures. Indeed, the dating procedure does not take into account neither for the snow accumulation nor the snow density since it was obtained by merely interpolation of the historical date and the depth of any given volcanic signature. Furthermore, smoothing functions are normally applied to the accumulation record in order to remove possible noise. Here, it would have artificially smoothed the signal, making the evaluation of a yearly resolved accumulation record an extra step in this analysis.

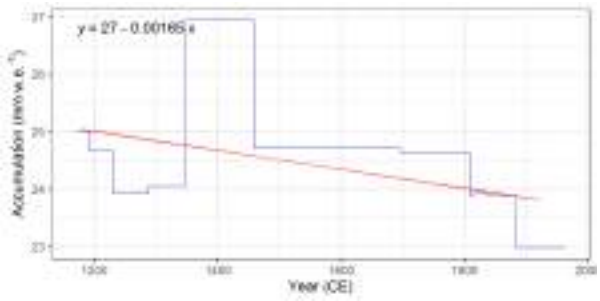

Figure 3.27 – Average snow accumulation rate (in mm of water equivalent per year) calculated using volcanic signatures found in the DC3D nssSO_4^{2-} profile. In red is reported the linear trend

For each snow pit that was successfully date, a preliminary evaluation of the snow accumulation was also performed in order to investigate the spatial variability across the East Antarctic plateau. By averaging the snow density and considering the two volcanic signatures in the nssSO_4^{2-} profile, the annual accumulation rate in mm w.e. yr^{-1} was estimated as reported in Table 3.7 together with

the density of the samples in the time considered.

Table 3.7 – Snow accumulation rate across the Antarctic plateau. Dome C accumulation rate, estimated in different campaigns (Traversi et al., 2009) is also report as comparison.

Site	Density (g cm^{-3})	Accumulation ($cm\ yr^{-1}$)	($mm\ w.e\ yr^{-1}$)
AGO-5	0.353	7.39	26.1
Paleo	0.357	6.39	22.8
DC 1997/98	0.43	8.2	35.0
DC 1998/99	0.42	8.8	37.0
DC 2000/01	0.37	8.3	31.0
DC 2005/06	0.35	8.0	28.0

These are in partial agreement with the records of snow accumulation obtained by investigating Dome C snow pits drilled during the 1997/98, 1998/99, 2000/01 and 2005/06 sampling campaign, also reported in Table 3.7. On Dome C, the average accumulation reported is slightly higher than the one found in this work across the traverse. The differences, particularly significant especially for the Paleo site could be ascribed with an actual difference in the precipitation between the two sites, even if the difference between the two is not high (approx. 230 km), since the origin of the air masses bringing precipitation on the two sites is the same. It must be noted that the records here investigated show a less clear profile than the one from the snow pits of Dome C, with the biogenic background of $nssSO_4^{2-}$ comparatively higher in both PALEO and AGO-5 sites and a spike in sulphate less clear when compared to the other records. Furthermore, no clear evidence of the 1991 CE eruption of the Pinatubo were found in neither of the records extracted from the ITASE campaign, making the dating less precise and reliable. Comparison with other records

in the area was not possible, mainly due to the scarcity of records in the area, which is essentially still unexplored when it comes to ionic composition records and deposition rates, making these first consideration an important first step to further explore the variability of the accumulation and the SMB in the Central Antarctic Plateau.

3.5 Volcanic Fluxes

The volcanic fluxes calculated as described above for the volcanic signatures found in the GV7 and DC3D ice core are reported in Table 3.8 and 3.9 respectively. For the known volcanic eruptions identified in the core, the Volcanic Explosive Index (VEI) (Simkin and Siebert, 1994; Newhall and Self, 1982) is also reported for reference. It must be noted that VEI index does not correlated with the volcanic flux, as some of the eruptions characterized by a low flux can be associated with a higher VEI than others, probably due to the geographical position of the volcano. Not all volcanoes were identified in both cores, in particular, a number of unknown or yet to be assigned signatures were found. Since most of the attributed volcanoes are from the Southern Hemisphere, it is possible that most of the unknown sources of sulphate reaching the cores is to be attributed to volcanic eruptions in these regions, but the lack of historical written records makes it sometimes difficult or even impossible to identify the source of the eruption. For these possible volcanic eruptions, the same procedure for the known volcanic signature was followed and the flux calculated. For the GV7(B) ice core records, an estimation of the uncertainty for the vulcanic flux as calculated in Nardin et al. (2020) is also reported, as in standard deviation of the sulphate background and the volcanic flux found analyzing the same site during the ITASE traverse (only the first few volcanoes found in the core were reported).

Table 3.8 – Volcanic fluxes f calculated from the nssSO_4^{2-} record of GV7(B) and GV7 ITASE cores. Both the uncertainty levels (in the form of σ) and Volcanic Explosive Index (Simkin and Siebert, 1994) are reported as a reference

Volcano	Depth(m)	GV7	σ	GV7 ITASE	VEI
Pinatubo/Cerro	11.10	5.28	2.88	10.46	6
Agung	22.12	5.29	0.16	8.15	4
Unknown	34.01	3.47	0.49	2.03	
Krakatau	49.35	8.06	0.56	11.51	6
Unknown	52.17	6.58	0.62	<2	
Makian	55.75	6.21	0.5	<2	4
Cosiguina	63.27	15.55	0.47	5	
Tambora	68.75	41.12	0.97	7	
Unkn 1809	70.53	23.32	1.66	?	
Unknown	73.97	6.09	0.75		
Gamkonora	101.25	12.91	0.48	5	
Parker Peak	108.39	11.14	0.58	?	
Huaynaputina	117.48	8.77	0.94	6	
Unknown	139.99	5.30	0.28		
Reclus	145.41	28.13	0.42		6
Unknown	160.25	12.12	0.69		
Unknown	166.01	16.69	0.09		
Unknown	178.73	38.84	0.14		
Unknown	180.03	8.09	0.11		
Samalas	181.86	53.36	1.01		7
Unknown	186.60	10.98	0.67		
Unknown	188.03	<2	0.40		
Unknown	193.07	10.99	0.66		
Unknown	196.17	8.15	0.29		

When compared with the volcanic flux as found in other cores drilled in the continent (Nardin et al., 2020) most of the one found in GV7(B) core were lower on average. The same was true when comparing the ration between the volcanic flux and the one of the

1815 CE eruption of the Tambora, used as a reference due to the importance of this specific eruption in the dating of cores and the understanding of the past climate in the last millennia. This was justified by the relatively closeness of the site with the sea, making the biogenic background higher compared to the maximum in concentration of the volcanic eruptions. For the DC3D core, a comparison with the records found in another core drilled at the site is reported (Castellano et al., 2005).

It must be noted that when comparing the two cores between each other and especially when comparing the volcanic flux of DC3D core with the one found in other studies, that the resolution of the core, breakages in it and the decontamination procedure can affect the total amount of volcanic material found in the samples. This is especially true for the DC3D core, where the temporal resolution is particularly low (10 cm) and where, due to the decontamination procedure chosen, a significant part of the sample went missing. Approx. 1.5 cm from the top and bottom of the sample, on average, were discarded due to the contamination procedure, leaving only 70% of the sample to be analyzed. Compared to the GV7 decontamination procedure, each 60cm strip of ice only the top and bottom 1 cm of ice were removed, making possible to analyze 95% of the ice for each strip (before cutting the strips in sub-samples) in the best-case scenario (lower percentage are to be expected when cracks in the samples were present). This could explain the extremely low fluxes found for some historically massive eruptions, most notably, the 1816 CE Tambora eruption, which for the DC3D core displayed a maxima concentration of nssSO_4^{2-} lower than the nearby Unknown 1809 CE eruption and a lower volcanic flux. Since no breakage is found at the depth at which the Tambora eruption was found, the most likely explanation for this is that the combined low accumulation rate on

Table 3.9 – Volcanic fluxes f calculated from the nssSO_4^{2-} record of different core drillet at Dome C. Volcanic Explosive Index (Simkin and Siebert, 1994) is reported for comparison as well

Volcano	Depth (m)	Flux DC3D	Flux EDC96	VEI
Agung	3.61	6.27	8.4	4
Krakatoa	8.20	2.84	3.1	6
Unknown	10.83	4.41		
Tambora	11.85	11.5	39.3	7
Unkn 1809	12.16	13.07	10.2	?
Serua	17.83	4.74	8.8	
Gamkonora	19.78	7.87	5.3	5
SubA	21.42	7.79	8.0	
Huaynaputina	22.34	15.1	13.4	6
Unknown	26.32	4.66		
Kuwae/Reculus	28.55	29.47	31.7	6
Unknown 1347	33.54	12.21	10.4	
Unknown 1288	35.84	27.78	22.4	
Unknown	36.20	8.58		
Unknown	36.51	7.06		
Unknown	36.96	22.34		
Unknown 1230	38.04	10.92	25.2	
Unknown 1190	39.59	6.07	18.0	
Unknown 1170	40.37	8.24	20.8	
Unknown	42.81	8.62		
Unknown	45.97	7.45		
Unknown	50.84	6.07		

site (and therefore an extremely reduced resolution with a single year accounting for less than 5 cm of snow/ice in the core according to the dating here proposed) and the need to remove a significant part of the sample to ensure the potentially contaminated layers of ice were discarded. This led to the possibility of discarding a significant part of the ice layers containing the majority of the sulphate material

of the eruption and therefore a reduced concentration of sulphate. The concentration of the samples reported are assumed to be the average of the 10 cm sample's concentration plotted on the middle on the sample, but in fact, are, to be more specific, the average concentration of the innermost 7 cm of each sample. The record is, therefore, not a continuous one but comprised of 7 cm of averaged concentrations separated by a 3 cm gap on average. There is no clear solution to this problem, since it's inherently tied to the way to core was sampled and the way it was stored and shipped to Italy, and even though the fact that a significant part of the core was addressed and kept in consideration, when plotting the concentration records, the 3 cm gap between each sample was not considered.

3.6 Chemical variability across Antarctica

The spatial and temporal variability across the East Antarctic sector was firstly investigated using the chemical records from the ITASE traverse. Both surface snow samples and snow pits were used to investigate the area from Dome C to the south pole and these preliminary results are here reported

3.6.1 Sea-salt ions

As previously stated, the primary sea spray is comprised by Na^+ and Cl^- with lower concentration of Mg^{2+}, K^+, Ca^{2+} and $SO_4{}^{2-}$, here a discussion of the first three is presented. Their concentration in the surface (first 10 cm) and bulk samples (uppermost meter, average) across the traverse is reported in Figure from 3.28a to 3.30b

Since the area receives air masses both from the Indian Ocean and the Ross Sea (Sodemann and Stohl, 2009), with the majority of the sea spray most likely coming from the former due to the presence

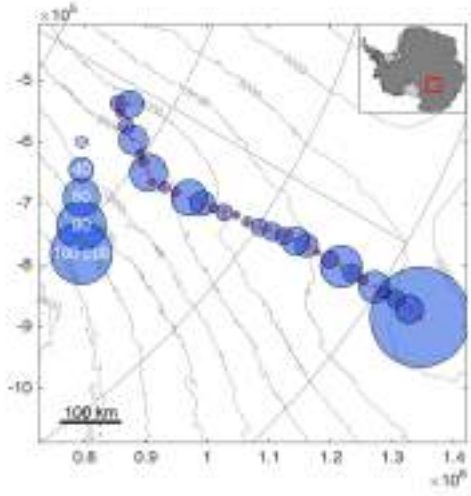

(a)

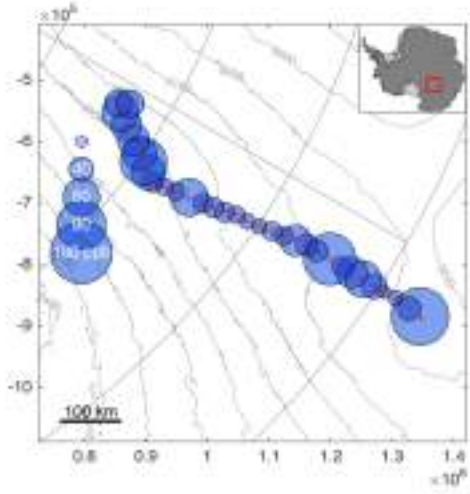

(b)

Figure 3.28 – Sodium concentration across the Antarctic plateau as found in the EAIIST surface (a) and bulk (b) traverse samples

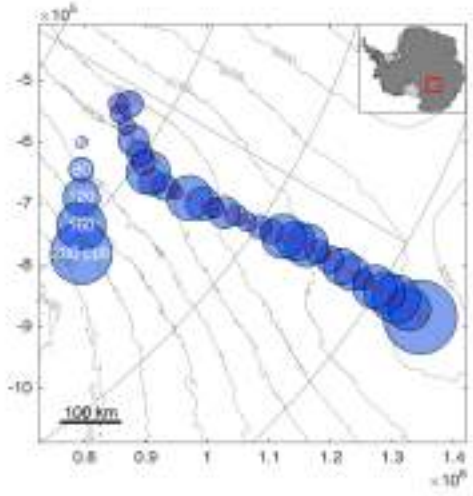

(a)

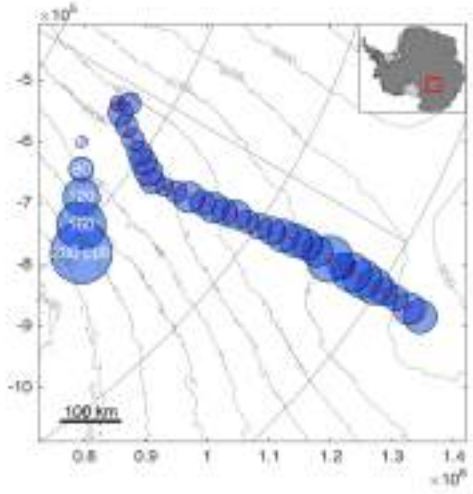

(b)

Figure 3.29 – Chloride concentration across the Antarctic plateau as found in the EAIIST surface (a) and bulk (b) traverse samples

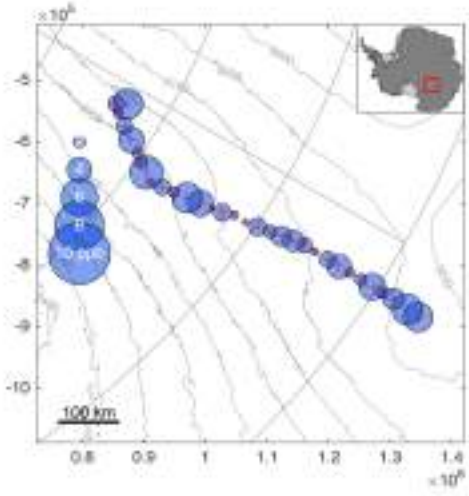

(a)

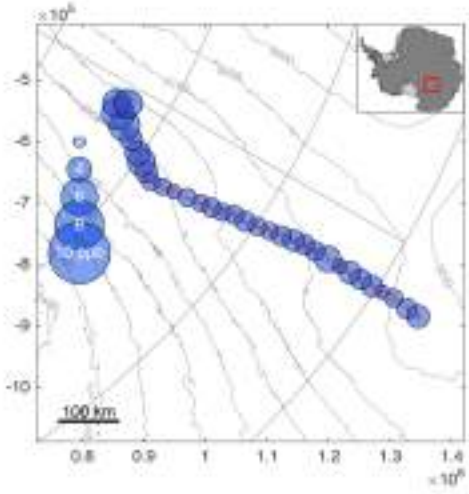

(b)

Figure 3.30 – Magnesium concentration across the Antarctic plateau as found in the EAIIST surface (a) and bulk (b) traverse samples

of the transantarctic mountains, concentrations were also plotted against the distance from the coast as reported in Figure 3.31. Sea ice, despite being an important secondary source for the sea spay, was not considered here, mostly due to the small window of time in which the samples were collected (less than a month), and the effect of the growth of sea ice was considered negligible compared to the distance from the sea itself.

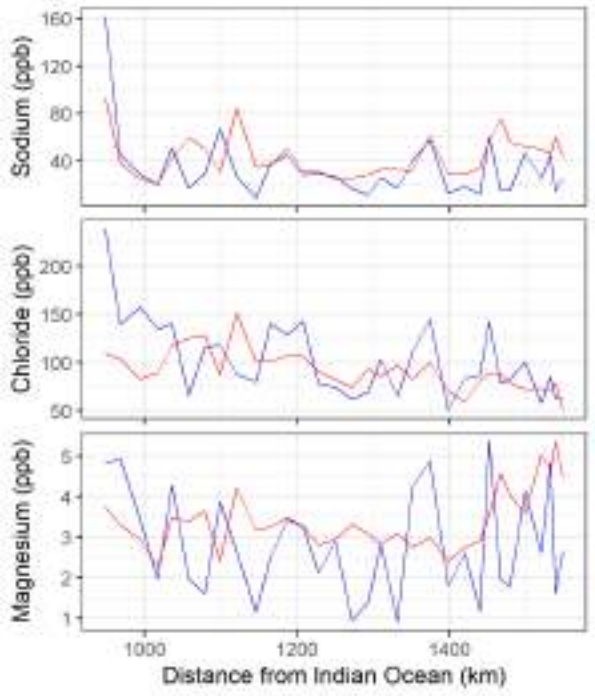

Figure 3.31 – Concentration of major sea-salt ions across the Antarctic Plateau plotted against the distance from the nearest coast (Indian Ocean)

Concentrations for all the ions were relatively similar when comparing the bulk samples with the surface ones as reported in Table 3.10 and 3.11, this was somehow unexpected for Chloride, as its concentration is thought to rapidly decrease in the snow due to

its volatile nature in the first layers of snow (Benassai et al., 2005; Röthlisberger et al., 2003; Udisti et al., 2004) although it has been noted that post-depositional processes can occur even at a depth of 4 meters (Udisti et al., 2004) possibly suggesting that the lack of clear difference between the first 10 cm of snow and the averaged 1 meter is mostly to be attributed to the fact that post-depositional processes are still occurring. With the exception of Magnesium, whose concentration remained mostly constant throughout the traverse (with a minor rise in concentration in the last stops, but with a minor to negligeable slope when considering the entire dataset), concentrations seem to decrease the further from the coast, with Chloride's concentration in particular displaying a higher, negative correlation (-0.087 and -0.074 for surface and bulk samples respectively) with the distance from the sea. Average concentrations for the samples are reported in Table 3.10 and 3.11.

Table 3.10 – Major sea-salt ions' concentration found in the EAIIST Surface samples

	Na^+	Cl^-	Mg^{2+}
Min (µg/L)	8.76	50.58	0.90
Max (µg/L)	75.72	155.10	5.37
Avg ± σ(µg/L)	29.76 ± 16.68	97.68 ± 31.87	2.86 ± 1.32

Table 3.11 – Major sea-salt ions' concentration found in the EAIIST Bulk samples

	Na^+	Cl^-	Mg^{2+}
Min (µg/L)	20.64	51.36	2.27
Max (µg/L)	93.43	151.41	5.36
Avg ± σ(µg/L)	43.52 ± 17.95	91.39 ± 20.76	3.43 ± 0.76

It must be noted that unlike Sodium, which mostly comes from the sea spray (only a small percentage of Sodium comes from crustal sources (Röthlisberger et al., 2002), Chloride has multiple sources and undergoes fractioning processes both on the atmosphere and in the first layers of blowing snow, mainly due to the interaction of acid species (H_2SO_4 and HNO_3). This produces volatile HCl that follows different transport pathways on the plateau (Teinilä et al., 2000; McInnes et al., 1994). Indeed, this fractioning of sea salt species was highlighted when considering the ratio between Chloride and Sodium when comparing it with the ratio found in the sea water (Nozaki, 1997; Bowen, 1979). All of the surface samples displayed a Cl/Na ratio higher than 1.8 and the same was found to be true for the majority of the samples when considering the bulk dataset s reported in Figure 3.32a and 3.32b. One major exception is that a minor slope was found when correlation the Cl/Na ratio with the distance from the Indian Ocean. The traverse ended on an area where the wind effect on the snow created large Megadune structures and the lower-than-expected ratio between the two ions in these areas could be potentially ascribed to the amplification of the post depositional processes due to the mixing of the snow layers. The opposite was found when comparing the characteristic ratio between Magnesium and Sodium in the snow and in the sea water, with the majority of samples displaying lower-than-expected ratio between the two ions both in surface and bulk ions as reported in Figure 3.33a and 3.33b. It must be noted that the analytical method used only evaluates the readily available and already dissolved Magnesium (in the form of free Mg^{2+}) and the non-soluble fraction is not taken here in account. The low ratio of the two ions was therefore associated with the precipitation of the Magnesium in the form of non-soluble carbonate and/or hydroxide and the presence of a not-null intercept

to a secondary origin of the Magnesium, for which the crustal origin is, unlike Sodium, a non-negligible source.

Similarly, when considering the five snow pits drilled during the traverse, most of the samples displayed a higher-than-expected Cl/Na ratio as reported in Figure 3.34, with the only exception being the Wind Crust site, but here the action of the wind could have easily further reduced the levels of chloride due to the constant mixing of the surface snow layers. This exposes the lower layers of snow to the action of the acidic species on the surface and produces more volatile HCl.

When considering the other sites, only one, Megadune Accumulation, displayed a significant ($R = 0.83$) correlation between the two ions ($R < 0.5$ in the other snow pits), but even for this site, higher levels of chloride suggest that an external, non-marine, source of chloride and/or a depletion of the marine one is present. The former seems to be more likely, especially when comparing the profile of the two ions with both displaying a similar pattern of spikes in concentration as reported in Figure 3.35.

The opposite is true for the records of Magnesium, which displayed an excellent correlation with Sodium. Figures from 3.36a to 3.40b report the correlation and the ratio between each pair of ion. As previously discussed, low correlation is found between Chloride and Sodium, with ratio extremely different from the one found in the sea water. For Magnesium and Sodium the ratio between the two ions closely resemble the one found in the sea water, suggesting that for the five sites considered, the majority of the aerosol seems to come from the sea-spray. This is in direct contradiction with what has been noticed for the surface samples, but when performing PCA analysis on the Surface snow sample, a stronger correlation, more in line with the results found in the analysis of the snow pits was

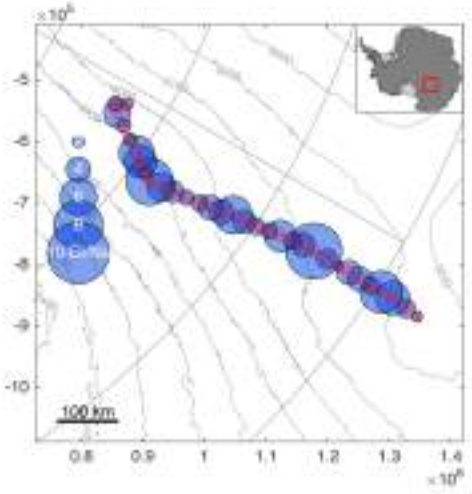

(a)

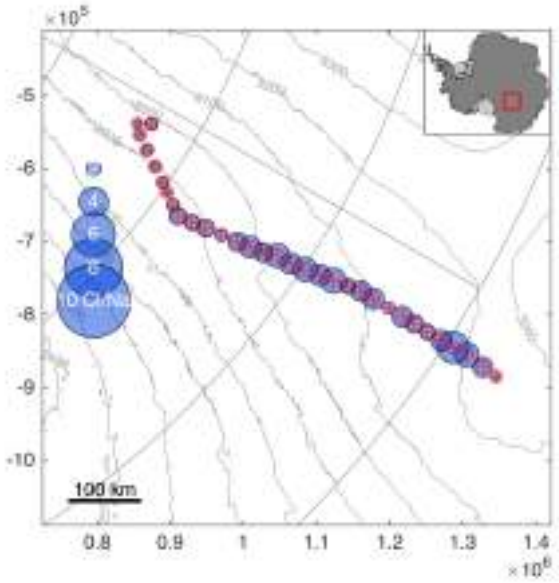

(b)

Figure 3.32 – Chloride/Sodium ratio across the Antarctic plateau as found in the EAIIST surface (a) and bulk (b) traverse samples. Red circles indicate the 1.8 ratio found in the sea water.

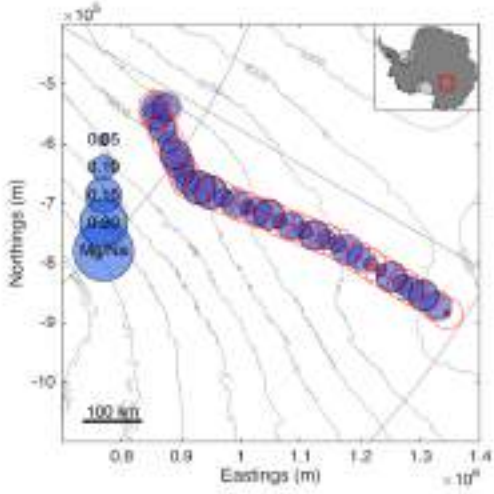

(a)

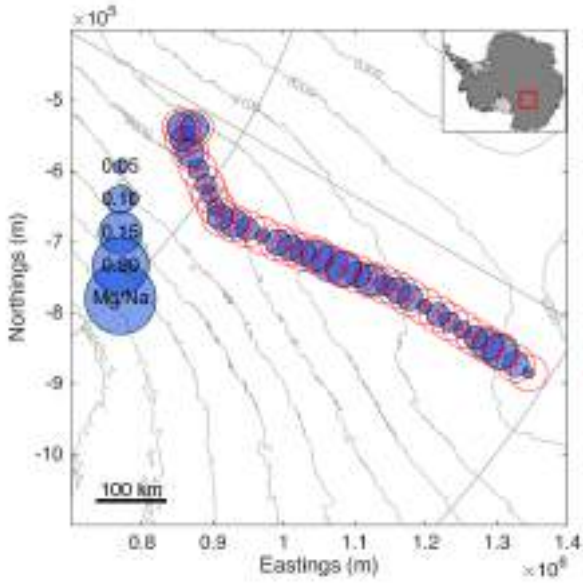

(b)

Figure 3.33 – Magnesium/Sodium ratio across the Antarctic plateau as found in the EAIIST surface (a) and bulk (b) EAIIST traverse samples. Red circles indicate the 1.8 ratio found in the sea water.

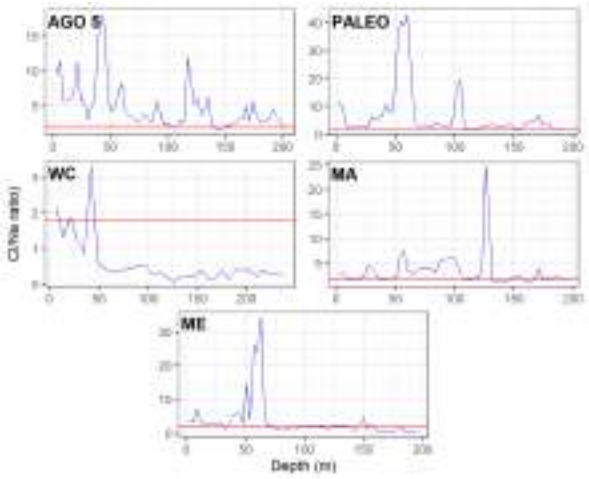

Figure 3.34 – Chloride/Sodium radio as found in the EAIIST snow pits. The red line reports the ratio found in sea water

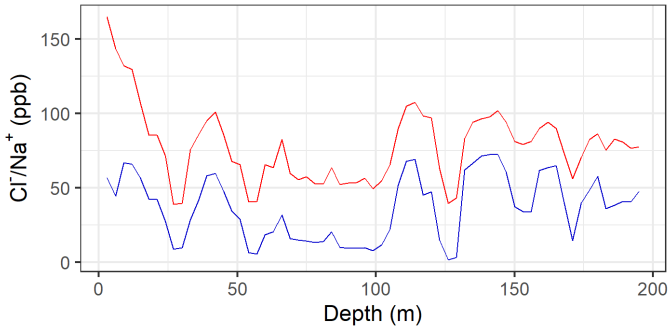

Figure 3.35 – Sodium (blue) and Chloride (red) concentration vs. depth profile for the Megadune Accumulation record

found. For both of the two datasets, a Na^+ and Mg^{2+} are strongly correlated in Factor 1 (factor loading > 0.8 after normalization), but when plotting the factor loadings, sea-salt ions were not grouped together as expected. Instead, as reported in Figure 3.41 and Table 3.13, Chloride, probably due to the post depositional processes and

the fact that the concentration in the first meters of snow is still subject to reactions with acidic species, is not strongly correlated with the other ions and for the surface snow it almost seems to correlate more with ions of crustal origin.

Table 3.12 – PCA analysis for the major ions found in the EAIIST Bulk samples, values marked with a * are over .6

	Factor 1	Factor 2
Na^+	0,959016*	0,157684
K^+	0,616099	0,507835
Mg^{2+}	0,925420*	0,020117
Ca^{2+}	0,481333	0,663589
Cl^-	0,591440	0,678004
NO_3^-	-0,239314	0,874939
SO_4^{2-}	-0,214129	-0,553248
Expl. Var.	2,840299	2,254806
Prp. Totl.	0,405757	0,322115

Table 3.13 – PCA analysis for the major ions found in the EAIIST Bulk samples, values marked with a * are over .6

	Factor 1	Factor 2
Na^+	0,944426*	0,1348151
K^+	0,850005*	0,313091
Mg^{2+}	0,705370*	-0,268112
Ca^{2+}	0,802701*	0,324723
Cl^-	0,374840	0,778328*
NO_3^-	0,179069	0,606878*
SO_4^{2-}	0,195631	-0,842620*
Expl. Var.	2,967167	1,977634
Prp. Totl.	0,423881	0,282519

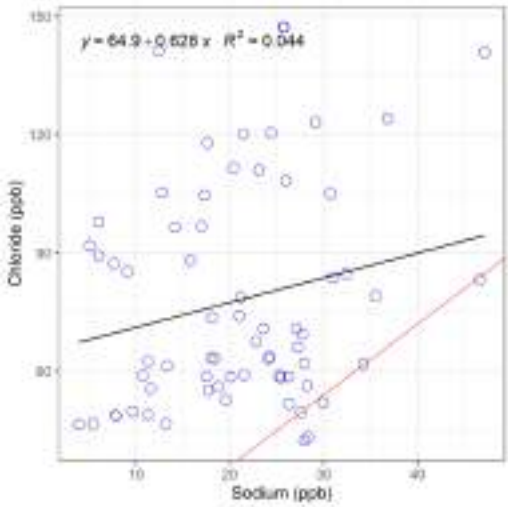

(a)

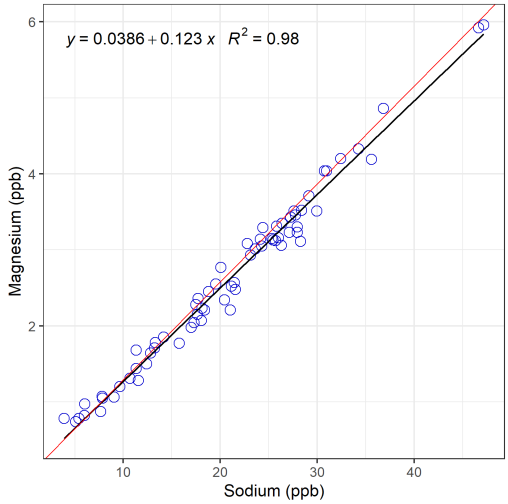

(b)

Figure 3.36 – Chloride/Sodium (a) and Magnesium/Sodium (b) ratio as found in the AGO5 snowpit

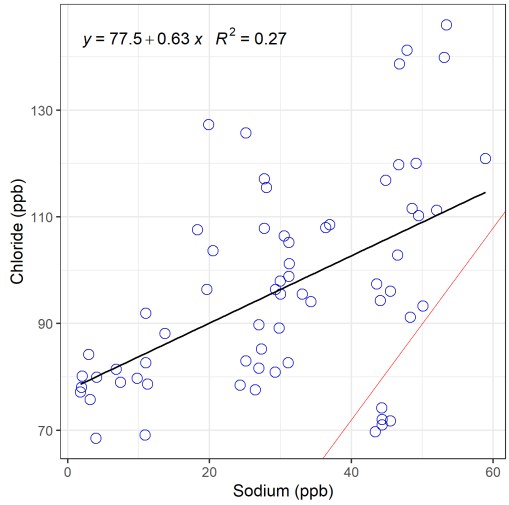

(a)

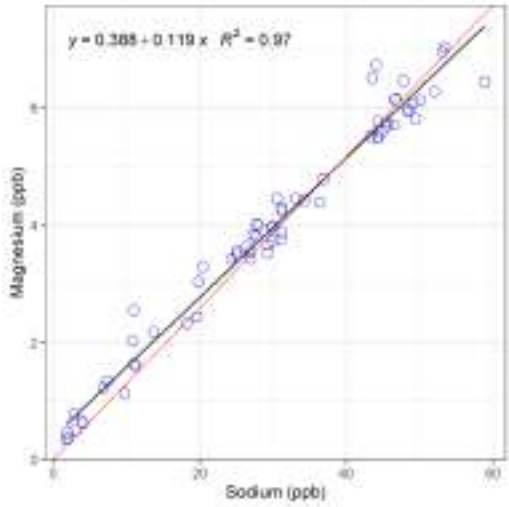

(b)

Figure 3.37 – Chloride/Sodium (a) and Magnesium/Sodium (b) ratio as found in the PALEO snowpit

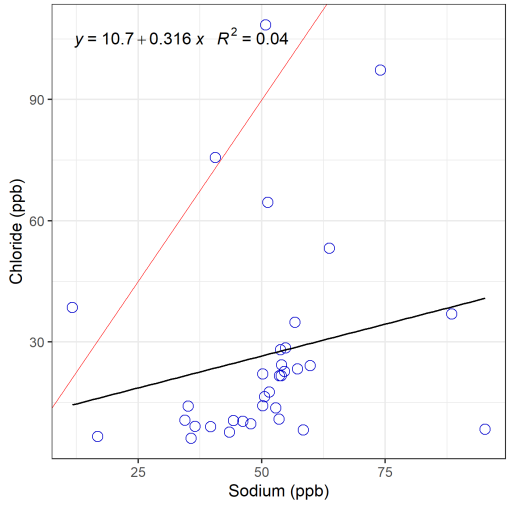

(a)

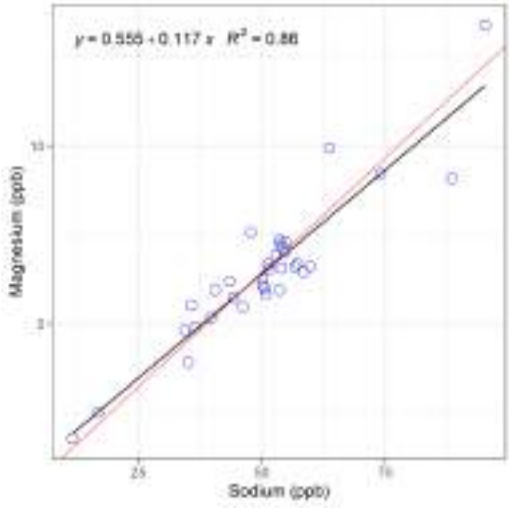

(b)

Figure 3.38 – Chloride/Sodium (a) and Magnesium/Sodium (b) ratio as found in the Wind Crust snowpit

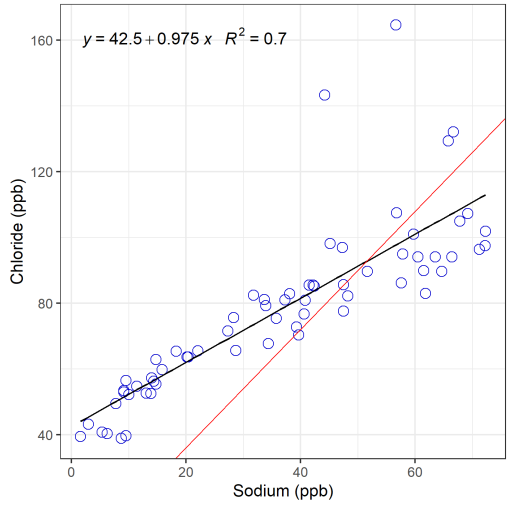

(a)

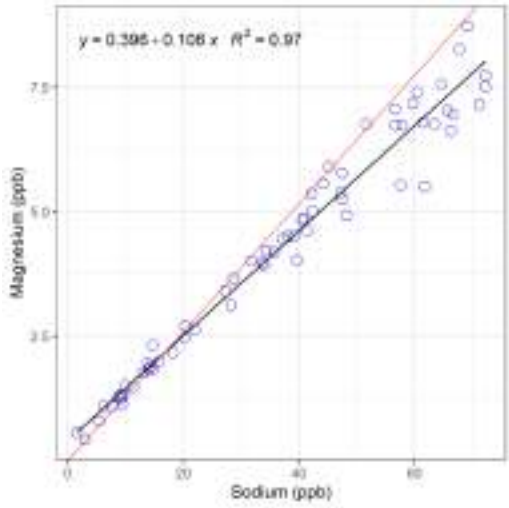

(b)

Figure 3.39 – Chloride/Sodium (a) and Magnesium/Sodium (b) ratio as found in the Megadune Accumulation snowpit

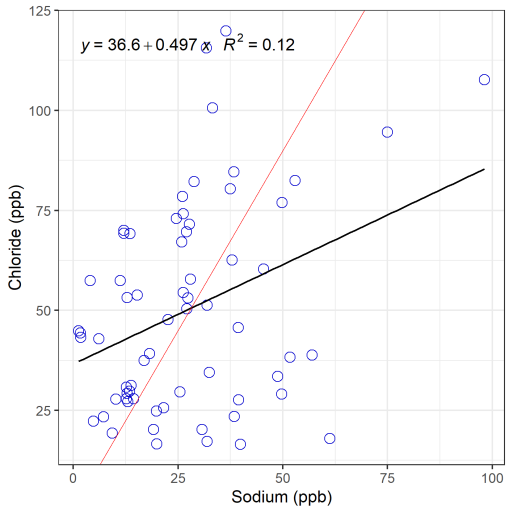

(a)

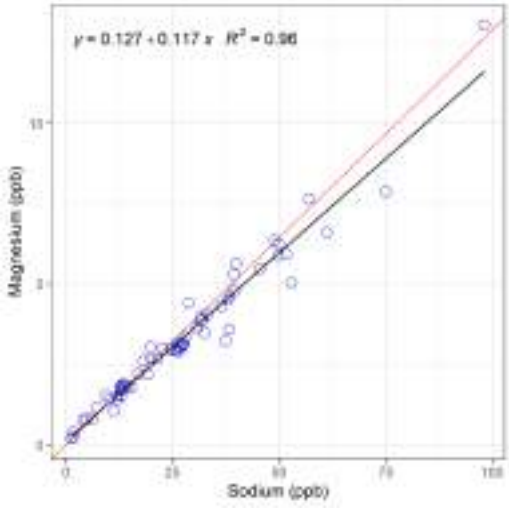

(b)

Figure 3.40 – Chloride/Sodium (a) and Magnesium/Sodium (b) ratio as found in the Megadune Erosion snowpit

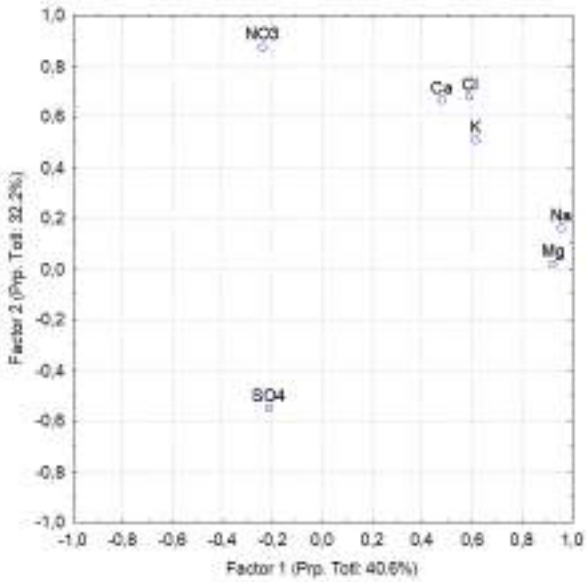

Figure 3.41 – PCA analysis for the major ions found in the EAIIST Surface samples plotting both Factor 1 and 2

3.6.2 Crustal ions

Since crustal aerosol is mostly constituted by non-soluble mineral dust, only a minority of its component can be analyzed by means of Ion Chromatography without pretreatment of the samples, mainly Ca^{2+}, K^{+} and Mg^{2+}. Magnesium records were already reported previously in Figure 3.30a and 3.30b, Calcium and Potassium levels throughout the traverse for both bulk and surface samples are reported in Figure from 3.43a to 3.44b. Alongside the dust records over Antarctica (Delmonte et al., 2002; Lambert et al., 2008) this makes possible to use calcium as a proxy for crustal sources of aerosol on the continent, especially in the innermost regions where the long-range transport is more prevalent (Morganti et al., 2007). Unlike Sodium, whose crustal component is statistically negligeable, for Calcium the

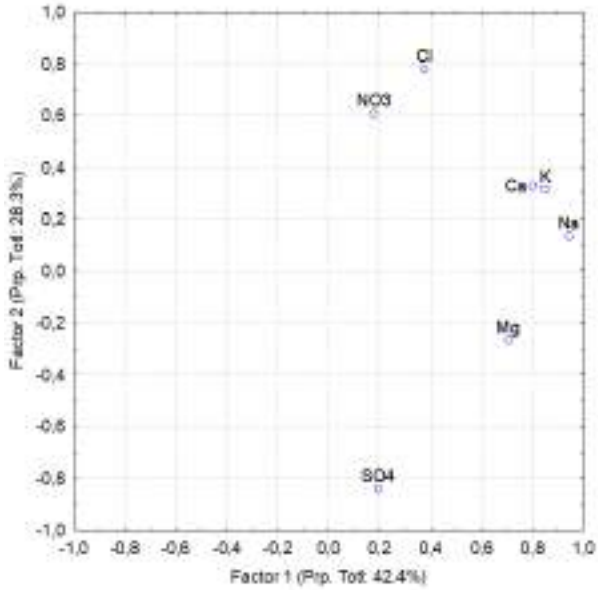

Figure 3.42 – PCA analysis for the major ions found in the EAIIST Bulk samples plotting both Factor 1 and 2

sea-salt component is not negligeable and can constitute up to the 25% of the soluble fraction of the ion found in the snow and ice cores. In fact, when considering the ratio between the two ions, it was found consistently higher than the one found in the sea water Figure from 3.45a to 3.46b, further confirming the presence of crustal sources for the ion in the records.

Concentration of both Calcium and Potassium seems to be lowered the furthest away from the Indian ocean, in par with what expected by the crustal origin, but for both ions (in the surface and bulk samples) the correlation is poor, and their profiles are characterized by a high degree of variability in concentration, making harder to find a clear cut, significant, relationship between the source of the aerosol and the concentration on the core. For Potassium in

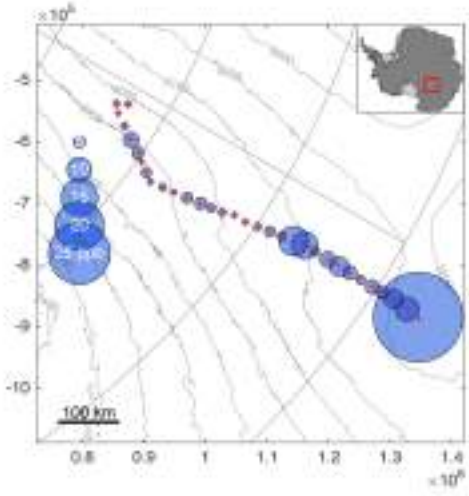

(a)

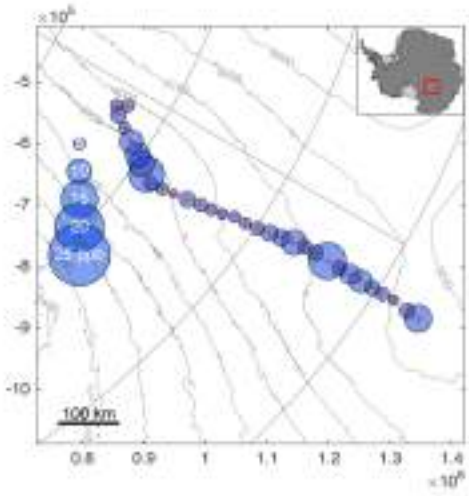

(b)

Figure 3.43 – Calcium concentration across the Antarctic plateau as found in the EAIIST surface (a) and bulk (b) traverse samples

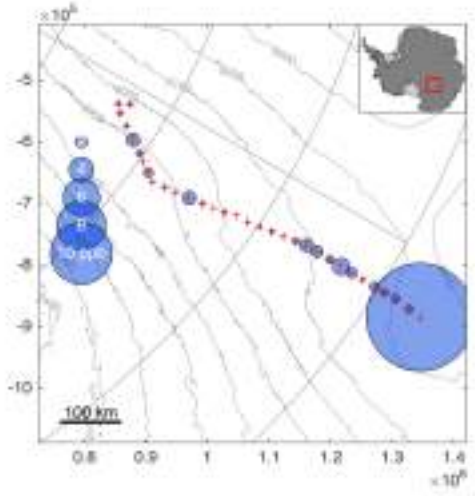

(a)

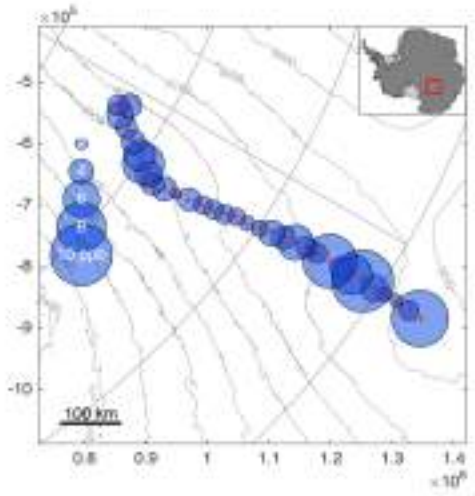

(b)

Figure 3.44 – Potassium concentration across the Antarctic plateau as found in the EAIIST surface (a) and bulk (b) traverse samples

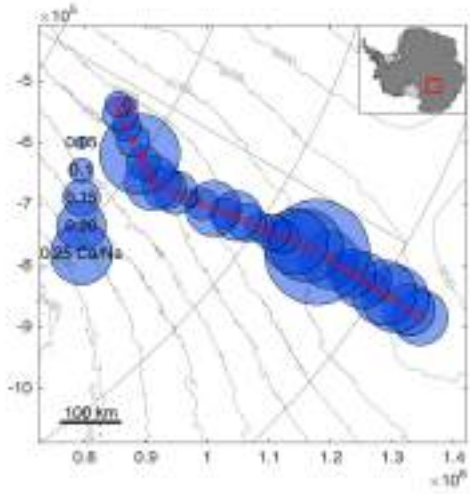

(a)

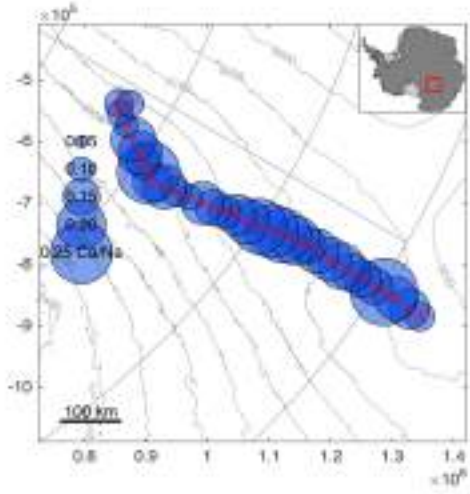

(b)

Figure 3.45 – Calcium/Sodium ratio across the Antacric plateau as found in the EAIIST surface (a) and bulk (b) traverse samples. Red circles show the ratio in the sea-water

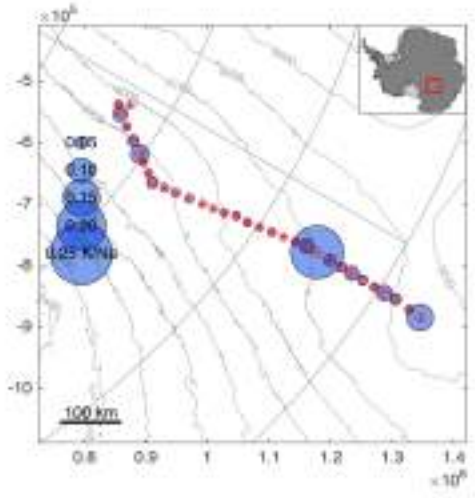

(a)

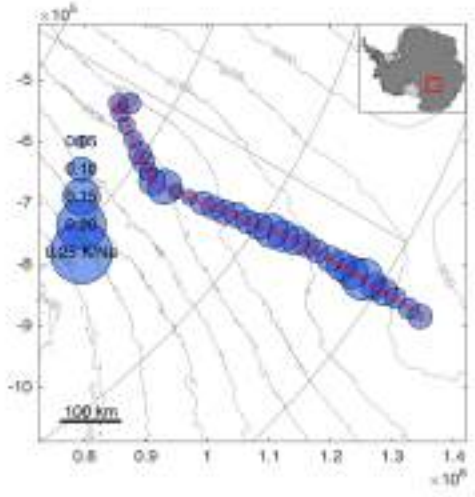

(b)

Figure 3.46 – Potassium/Sodium ratio across the Antarctic plateau as found in the EAIIST surface (a) and bulk (b) traverse samples. Red circles show the ratio in the sea-water

particular, due to the extremely low concentration in the snow (below 2 ppb on average) and the ease with which external contamination can be introduced, the apparent correlation seems to be ascribed more to the high variability of the data and the reduced dimensions of the dataset. This was particularly evident when analyzing the bulk samples, which display consistently higher concentration than the surface ones (twice on average) suggesting that the sampling procedure could have possibly introduced external contamination. In fact, despite the crustal origin of the Potassium, surface samples are characterized by an almost null concentration of non-sea salt Potassium (with 11 out of 32 samples displaying a negative concentration when using Sodium levels to evaluate the crustal fraction and as a result an average of 0.01 ppb of nssK). On the opposite, higher levels of non-sea salt (possibly crustal) Potassium were found in the bulk samples of the traverse (2.67 ppb on average, more than 63% of the total). This discrepancy is hard to explain, especially because sea-salt levels of Potassium are comparable when comparing the bulk and surface snow samples and this increase of concentration of Potassium on the lowest layer of snow was not found when considering the snow pits in the same area. In fact, with the exception of the Megadune Accumulation site, the average concentration of Potassium in the snow pits strongly resemble the one found in the surface snow ($<$2 ppb) and even for the Megadune A, the average concentration was still lower than the one found in the bulk samples. It has been noted that the procedure used to extract Bulk samples (i.e. sampling the first 1 meter of snow, mix it on the field and sub-sample the omogeneized snow) could have artificially risen the concentration of Potassium in the samples.

3.6.3 Nitrate

Nitrate's concentration in the surface and snow pit samples was investigated with the aim of getting a better understating of the post-depositional processes occurring across the continent. Both the spatial variability across the east Antarctic plateau and the concentration in the snow pits is considered in this section. Since the majority of the re-emission processes occurs in the uppermost layers of snow (Udisti et al., 2004) when considering the entirety of the EAIIST traverse and the bulk and surface samples were compared this tendency of the Nitrate was highlighted. Concentration in both datasets remained relatively constant in all the stop of the traverse as reported in Figure 3.47a and 3.47b, with minor, non-significant trends found when considering the distance from the sea. Indeed, concentration in the snow displayed a high variability across the traverse (average concentration in bulk samples 240.02 $\pm$ 70.61, bulk 52.21 $\pm$ 25.58 ppb), and even the apparent lower concentration of Nitrate in the surface snow of the last few stops of the traverse that could be potentially ascribed to the lower accumulation rate and therefore to the higher efficiency of the loss of Nitrate, could be a consequence of the higher dispersion of the data.

This was further highlighted when considering the Nitrate's concentration records from the snow pits. Indeed, here the tendency of the Nitrate of undergoing re-emission and post-depositional processes was made clear by the rapid decrease of its concentration as reported in Figure 3.48. In particular when considering the first sample as a reference of, it was found an average drop of 93% of the initial concentration in the first 10-15 cm of snow, a significantly higher and more pronounced drop that what found at Dome C (Traversi et al., 2009) where a similar loss was found in the first meter of snow. Due to the extreme profile and drop of concentration, no clear

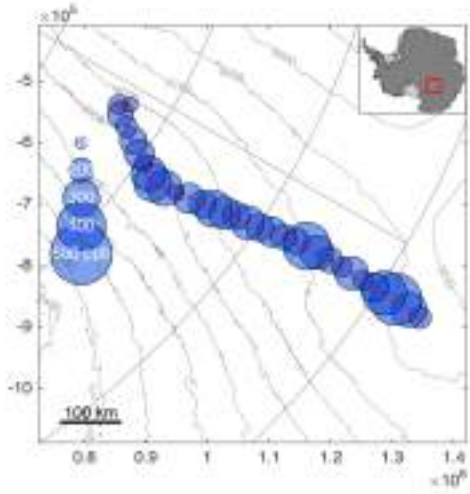

(a)

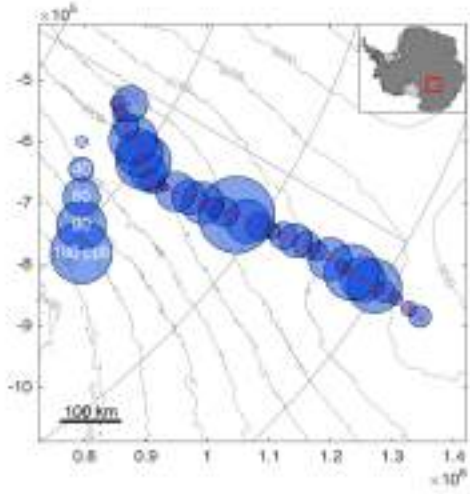

(b)

Figure 3.47 – Nitrate concentration across the Antarctic plateau as found in the EAIIST surface (a) and bulk (b) traverse samples. Note the difference in scale

fitting method was able to approximate the concentration of Nitrate in the snow. In order to evaluate the different loss rate on the sites, a break-point analysis was performed and the depth at which each break point was found for each site is reported in Table 3.14. As a reference, both the background (as in the average concentration of Nitrate under a 50 cm threshold) and the max concentration of Nitrate is also reported.

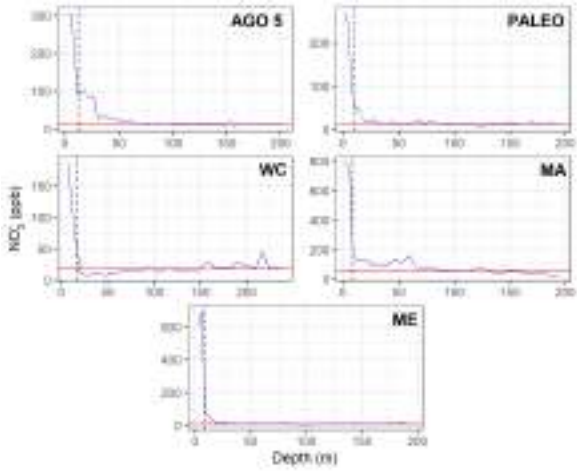

Figure 3.48 – Nitrate concentration for the five snow pits. Background concentration and break-point are also reported in red and grey respectively

Table 3.14 – Average background and maximum concentration of Nitrate found in the five shallow snow pit drilled during the EAIIST campaign

Site	Max (ppb)	Background (ppb)	Breakpoint (cm)
AGO-5	307.02	12.27 ± 3.59	12.4
Paleo	269.38	13.98 ± 2.39	9.1
Wind Crust	188.15	18.41 ± 7.16	16.9
Megadune A	793.00	60.34 ± 27.95	8.4
Megadune E	695.31	8.54 ± 1.90	7.9

Concentration of Nitrate in the cores are relatively low with most sites, with the exception of the Megadune Accumulation site, once taking in account for variability in the range of 10-20 ppb. Both Megadune A and Megadune E sites displayed the highest concentration of Nitrate in the uppermost layers of snow, which is somewhat unexpected for Megadune E, but their profile are extremely different. Despite showing a similar turning point in the concentration of Nitrate as reported in Table 3.14, the background concentration found in Megadune A is the highest found in the five snow pits, ascribed to the higher accumulation in this area (Megadune A is the downwind site, Megadune E displays similar concentration of Nitrate in the surface snow, but the katabatic winds action makes it a close-to-null accumulation site) and therefore a less disturbed process of deposition and fixing of the Nitrate in the snow. When comparing Megadune A site with the other three sites, despite the lower concentration found, the ratio between the Nitrate background and the maximum concentration was found to be close, suggesting a similarity between the four sites characterized by a normal snow accumulation rate.

3.7 Dome C 3D ionic records

Similar consideration can be made for the DC3D core, with the main difference that unlike snow pit records, the resolution here is lower (10 cm instead of 3 cm average for the snow pits) and the records cover the last millennia instead of the few decades. Principal Component Analysis was performed on the entire dataset, excluding the Ammonium records, due to the fact that more than half of the samples displayed a concentration under the detection limit possibly leading to non-relevant correlations. Results of PCA are reported in

Figure 3.49 and Table 3.15. Major sea-salt components (Magnesium and Sodium) are grouped together in Factor 2, but surprisingly Chloride does not seem to correlate with Sodium and instead is grouped together with non-sea salt cations (Calcium and Potassium) and Nitrate. Sulphate, instead, strongly correlated with Sodium, indicating how the majority of the sulphate reaching the site comes from sea spray, a marine secondary sources. It must be noted, for Sulphate in particular, that in the aerosol, Ammonium is one of the principal neutralizing ions for the acidic fraction and that the lack of ammonium records in PCA could have contributed to find a stronger association with Sodium than other markers here not considered.

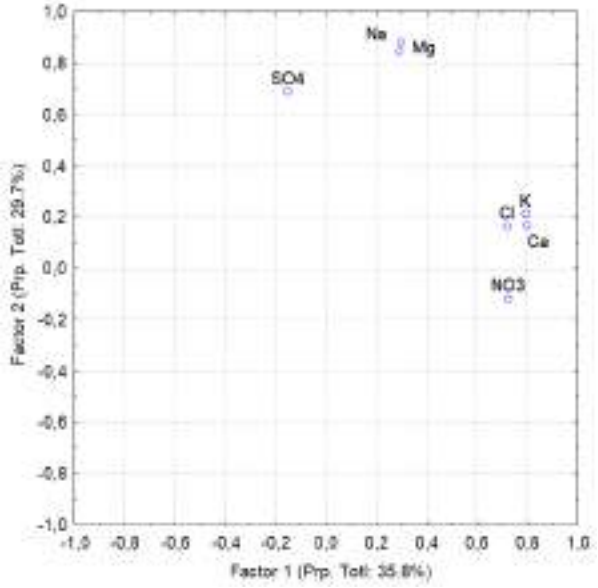

Figure 3.49 – PCA analysis for the major ions found in the DC3D ice core samples plotting both Factor 1 and 2

This lack of correlation between the principal components of the sea salt is further highlighted in Figure 3.50 where concentration

Table 3.15 – PCA analysis for the major ions found in the DC3D ice core samples, values marked with a * are over .6

	Factor 1	Factor 2
Na^+	0,292209	0,843188*
K^+	0,795425*	0,210979
Mg^{2+}	0,297272	0,882128*
Ca^{2+}	0,799262*	0,168287
Cl^-	0,720389*	0,164550
NO_3^-	0,722993*	-0,119313
SO_4^{2-}	-0,149967	0,688855*
Expl. Var	2,509446	2,077782
Prp. Totl	0,358492	0,296826

of Chloride is plotted against Sodium concentration. Indeed, only few sample points displayed a ratio of Cl/Na close or over 1.8 w/w (the one found in the sea water), with the majority of these samples concentrated in the first 5 meters of the core. Indeed, in this section an average of 1.42 ratio between the ions was found (compared to the rest of the core where only a value of 0.68 is present), but the downward pattern seems to suggest a loss of Chloride in the first meters of the core due to post-depositional processes and interaction with acidic species on the snow creating volatile HCl. The same tendency of having higher ratios between the two ions was also found in the snow pits previously discussed, but the records here discussed begins from a depth of over 2 from the snow mantle. Since the concentration of volatile compounds, as stated before, is only fixed in the snow and ice of Antarctica once a sufficiently high amount of precipitation fell on site (up to 4 m Udisti 2004), it is possible that this is the case.

In fact, unlike Sodium's levels, that stay relatively constant

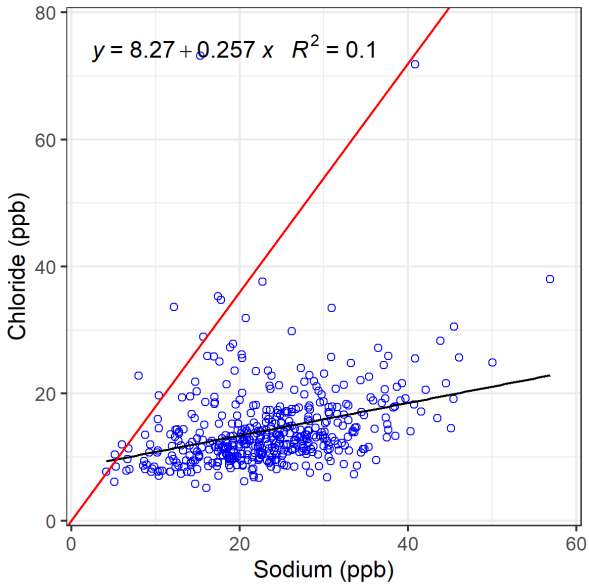

Figure 3.50 – Chloride/Sodium ratio as found in the DC3D ice core samples. The red line reports the ratio found in the sea water

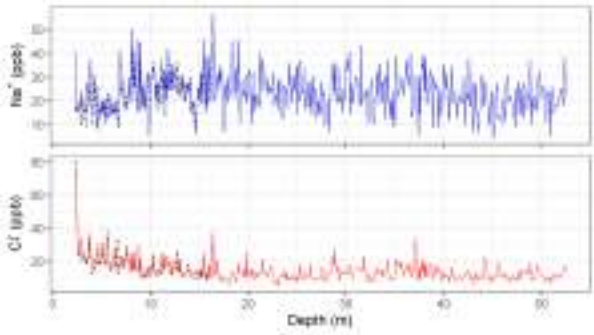

Figure 3.51 – Sodium and Chloride record as found in the DC3D core. Black dashed lines also report the samples analyzed with the different procedure described in this work.

throughout the core and are comparable with the one found in the snow pits, Chloride levels quickly decrease, as reported in Figure 3.51, further consolidating that this is the more likely explanation. Better correlation was found between Magnesium and Sodium levels as reported in Figure 3.52, further suggesting that the majority of the ion found in the core (and therefore the initial concentration of Chloride) comes from the sea. This is not the case for Potassium and Calcium, as reported in Figure 3.53 and Figure 3.54. The lack of correlation between the two crustal ions and Sodium is not unexpected, as many of the spikes in concentration are not found in the Sodium record. Most of the samples display a higher ratio that found in the sea water, and the non-null intercept is a clear indication of a secondary source of aerosol, possibly of crustal origin.

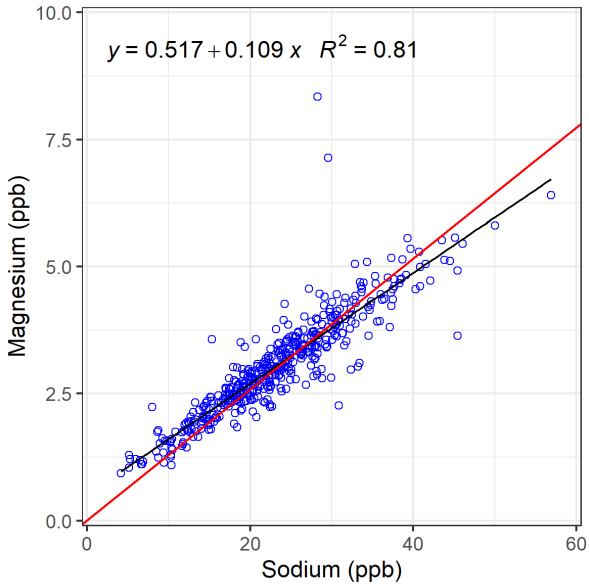

Figure 3.52 – Magnesium/Sodium ratio as found in the DC3D ice core samples. The red line reports the ratio found in the sea water

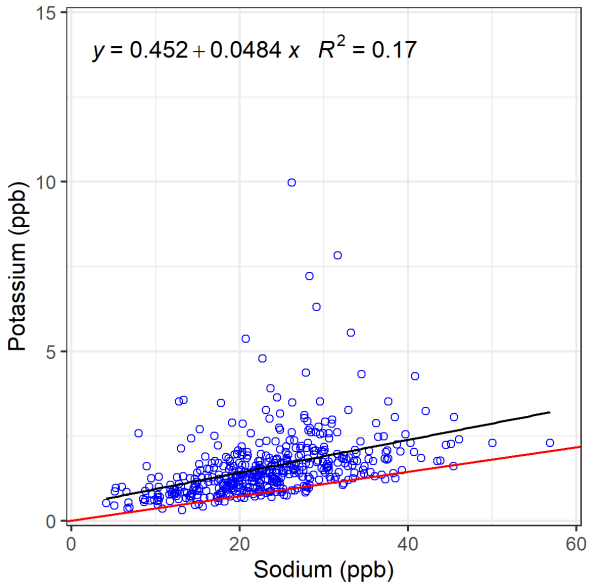

Figure 3.53 – Potassium/Sodium ratio as found in the DC3D ice core samples. The red line reports the ratio found in the sea water

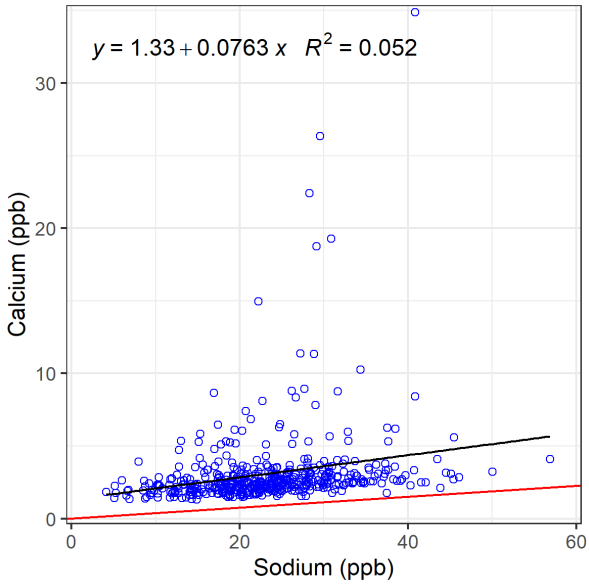

Figure 3.54 – Calcium/Sodium ratio as found in the DC3D ice core samples. The red line reports the ratio found in the sea water

3.8 Chemical markers found in GV7(B) ice core

For the GV7(B) core, the high resolution of the records made possible to study at a higher resolution, annual to sub annual, the ionic composition of the ice during the last millennia. Firstly, characteristic ratios for different ions were considered and the same approach used in the characterization of the snow pits and surface samples was here used not only to investigate the origin of the aerosol on the site but also to understand these processes at a higher resolution. For the latter, the dating procedure did not allow to achieve a real monthly resolution in the dating. Even for the uppermost sections of the core where a single year can be represented by over 12 samples, claiming monthly resolution is impossible with the method used. For this reason, when comparing different time periods, the choice of focusing on Summer and Winter time was made: the identification of Summer period was straightforward, as the dating was based on the identification of Summer maxima (minimum). For the winter periods, it was assumed that the local minimum in between each minimum was centered on the month of June. When possible, an interval of three months was chosen, but this was impossible for the lower section of the core, where the temporal resolution is low. Here just as it was done with the dating, each minimum was associated with the Winter period even when comprised by a single sample point and the possibility that this could have smoothed the signal kept into account when considering the profiles. As already stated, the majority of the Sodium in the core comes from marine sources (only 3% on average of the levels of Sodium were estimated to be from crustal origins and this figure is lower than the accuracy of the method used for the concentration interval of most samples)

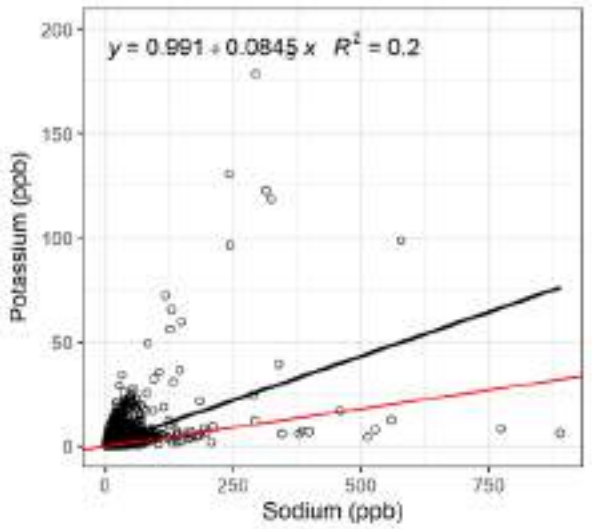

Figure 3.55 – Potassium/Sodium ratio as found in the GV7(B) ice core samples. The red line reports the ratio found in the sea water

and was therefore kept as a reference throughout this analysis. As already shown during the dating procedure, PCA results displayed a high correlation between all sea-salt ions (Na^+, Cl^-, Mg^{2+}) with Calcium seemingly not correlated at all with other crustal ions. It must be noted that Potassium levels were not considered in PC analysis when investigating different ions for the dating procedure, but as reported in Figure 3.55, correlation between Potassium and Sodium in the core is non-significant and the majority of the sample points are above the sea-water ratio suggesting a secondary source for this ion. Similar considerations were made with other sea-salt ions, most specifically Magnesium and Chloride as reported in Figure 3.56 and Figure 3.57 respectively. Two considerations are worth noting: extremely high spikes of concentration in Sodium or Chloride records, most likely to be ascribed to either one of the ions introduced in the sample as contamination rather than from significant sources

in the continent, were discarded since they would have forced the fitting to less-significant data, furthermore, in order to avoid artificial correlations, the concentration record of Sodium was entirely ascribed to marine sources assuming a null or negligeable crustal contribution. Both Magnesium and Chloride displayed an excellent correlation with Sodium as expected due to the close distance from the sea of the site, but for Magnesium, the ratio between the two ions seems lower than the one found in the sea water. This is probably due to few sample points characterized by a high concentration of Sodium forcing the fitting to lower values. Indeed, when considering the ratio's profile as reported in Figure 3.58 and 3.59 both displayed ratios display values extremely similar to what found in the sea water (0.128 ± 0.06 vs 0.129 for Magnesium and 1.97 ± 0.7 vs 1.8 for Chloride on average, the higher variability is due to the presence of higher spikes). For Chloride, despite the higher variability, the sea-salt contribution seems to be constant, on average, both at high and low contribution of sea spray on site, represented in Figure 3.60 as Sodium flux. This is not the case for Magnesium as reported in Figure 3.61, with sample points characterized by a high sea-spray contribution consistently displaying lower than expected ratios and most of the high ratio samples found on samples characterized by a low Sodium flux. The latter is most likely due to the different analytical performance for the two ions. Indeed, despite displaying an excellent reproducibility (under 2%) for higher concentration, higher degree of variability was found when investigating the reproducibility of the ion's determination at sub-ppb concentration. Here, the combination of the high background noise and the higher background line (most likely due to the presence of a small residue of Calcium in the Ultra-Pure water used when preparing the eluents solution) led to an artificial increase of the Magnesium signal too (the two

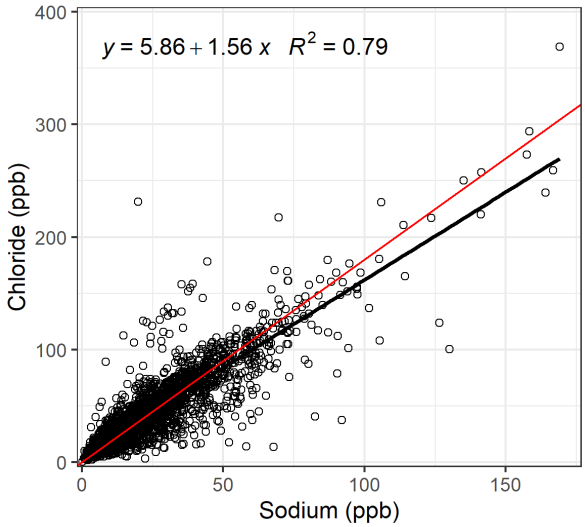

Figure 3.56 – Chloride/Sodium ratio as found in the GV7(B) ice core samples. The red line reports the ratio found in the sea water

peaks, despite being well resolved, at low concentration can affect each other).

When considering the two time periods investigated (winter and summer) no clear difference was found for the marine ions: during summer the Cl/Na ratio seems to be slightly lower than in winter (1.43 vs 1.63 ratio w/w as reported in Figure 3.62 and 3.63) but it's not a clear-cut difference and could be ascribed to the variability of the dataset rather than the higher temperatures and therefore a higher depletion of volatile HCl during the summer. Indeed, very few samples displayed high concentration of Sodium (only 5 in the winter period and 3 during summer respectively displayed a concentration over 100ppb) and the dispersion for these samples is higher. Similar considerations are true for Magnesium/Sodium ratio in the core, with the same negligeable difference between the two time periods as reported in Figure3.64 and 3.65.

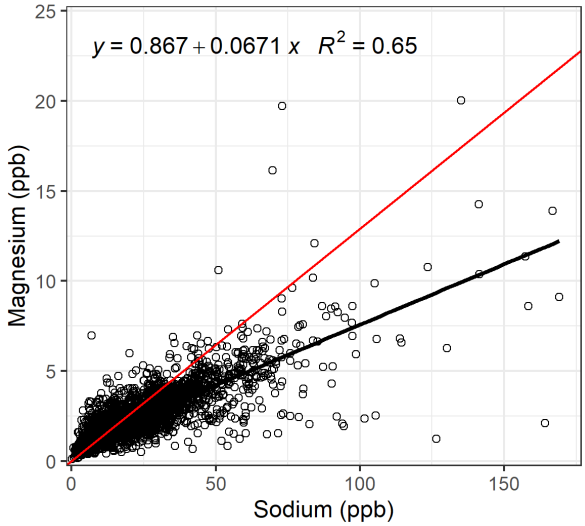

Figure 3.57 – Magnesium/Sodium ratio as found in the GV7(B) ice core samples. The red line reports the ratio found in the sea water

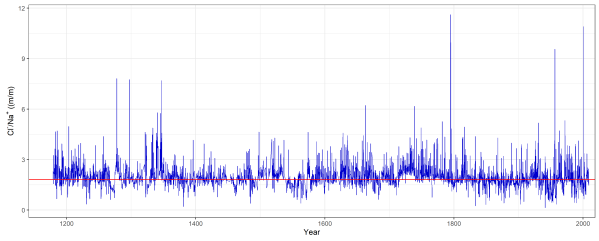

Figure 3.58 – Chloride/Sodium ratio across the 200m of GV7(B) analysed for this work. The red line reports the ratio found in the sea water

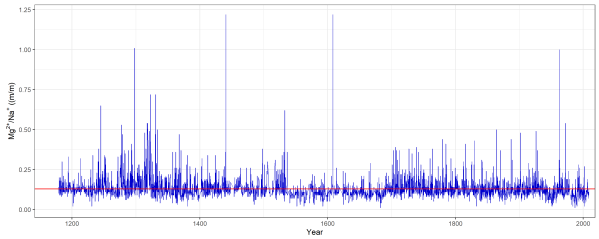

Figure 3.59 – Magnesium/Sodium ratio across the 200m of GV7(B) analysed for this work. The red line reports the ratio found in the sea water

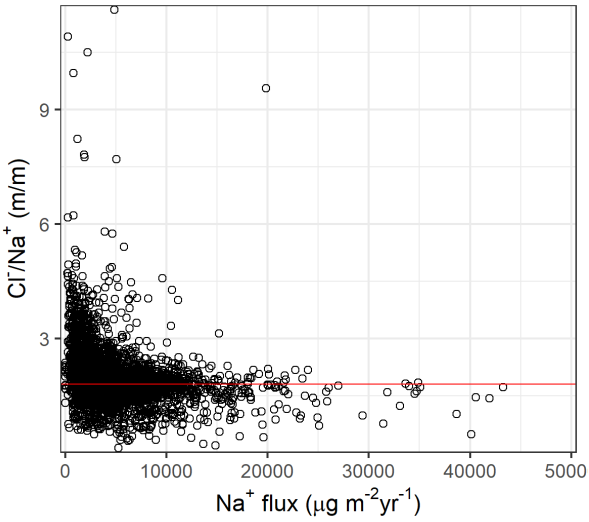

Figure 3.60 – Chloride/Sodium ratio as found in the GV7(B) ice core samples as a function of the Sodium contribution in the core. The red line reports the ratio found in the sea water

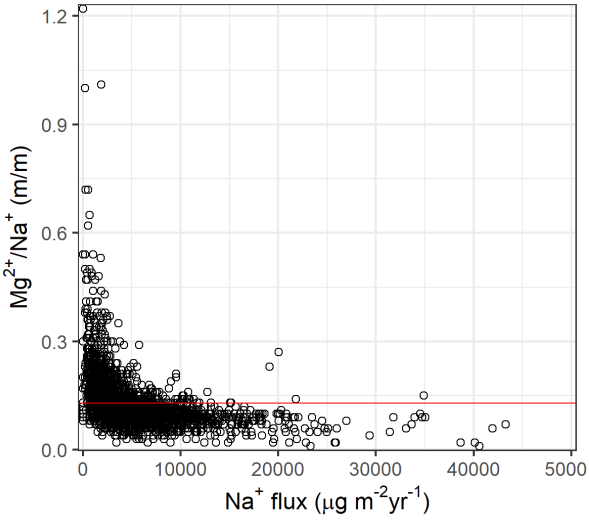

Figure 3.61 – Magnesium/Sodium ratio as found in the GV7(B)ice core samples as a function of the Sodium contribution in the core. The red line reports the ratio found in the sea water

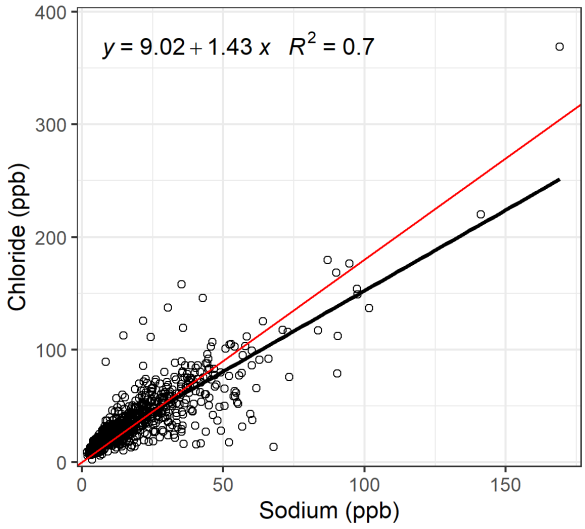

Figure 3.62 – Chloride/Sodium ratio as found in the GV7(B) ice core samples dated to the Austral summer. The red line reports the ratio found in the sea water

Indeed, as reported in Figure 3.66, when considering the average concentration of the two time period considered, each ion's concentration seems to remain somewhat constant throughout the year, with the exception of a few. This is made more clear in Table 3.16 where the average concentration found for each ion in both Summer and Winter is reported, together with the standard deviation here used as an evaluation of the erro. The latter is here used more as a way to evaluate the variability of the data instead of a statistical error (note that most of the standard deviation values are higher than the corresponding ion's concentration) and the absolute percentage difference between summer and winter. Of the Cations analyzed, Lithium and Ammonium will not receive an in-depth discussion; indeed a high degree of variability between Winter and Summer is found when considering Ammonium levels in the core, and since ammonium has

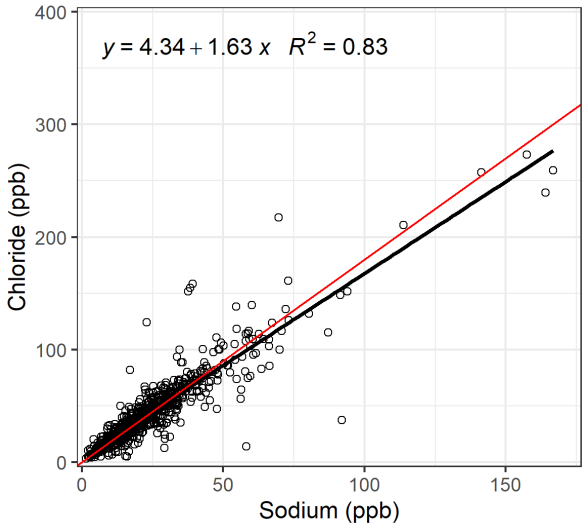

Figure 3.63 – Chloride/Sodium ratio as found in the GV7(B) ice core samples dated to the Austral winter. The red line reports the ratio found in the sea water

a role in the neutralization of the Sulphate in the aerosol (e.g. Yao et al. (2011)) the higher concentration in Summer could be ascribed to the rise of Sulphate. But it is worth noting that Ammonium is the cation who displays the higher number of samples (more than half) with concentration below detection limits. Furthermore, the Sodium and Ammonium chromatographic peaks are extremely close in the run, but the Ammonium levels are almost negligible when comparing to the Sodium ones in most samples, forcing the analysis to be done with a mathematical deconvolution of the peak using the software Chromeleon®that intrinsically introduced a higher degree of uncertainty in the analysis. Similarly, Fluoride and Formate levels in the core were found to be close to the detection limits in most of the samples and the difference in concentration, despite significant in percentage (>10%), is in the order of sub-ppb, close to the detection

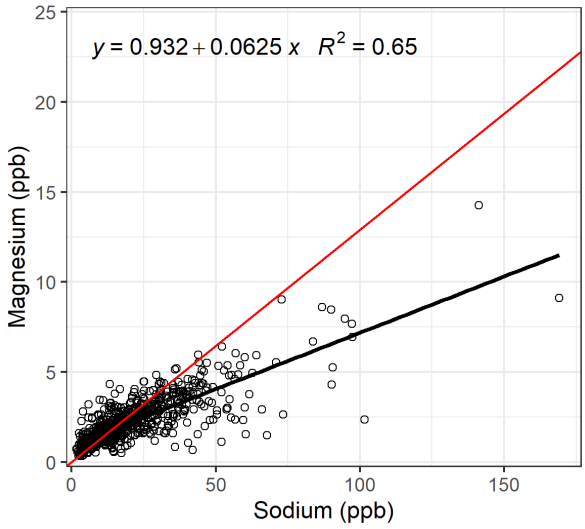

Figure 3.64 – Magnesium/Sodium ratio as found in the GV7(B) ice core samples dated to the Austral summer. The red line reports the ratio found in the sea water

limit as well. These four ions were considered for the ionic balance, but as displayed in Figure 3.66, their contribution to the ionic balance is almost negligible.

The other ions report a similar pattern as expected considering their seasonality, with seas salt ions displaying higher values in the winter months although the difference in concentration reported in Table 3.16 between the Summer minimum and winter maxima is less pronounced than the one noticed when investigating the seasonal variability with the aim of dating the core. This was expected, as only averaged values are here reported, and the window used to discriminate the Summer and Winter months is relatively big when compared to the tendency of each ions' concentration to rapidly increase during the seasonal maxima. Indeed, even when considering the ions used in the dating, only Sulphate displayed a higher vari-

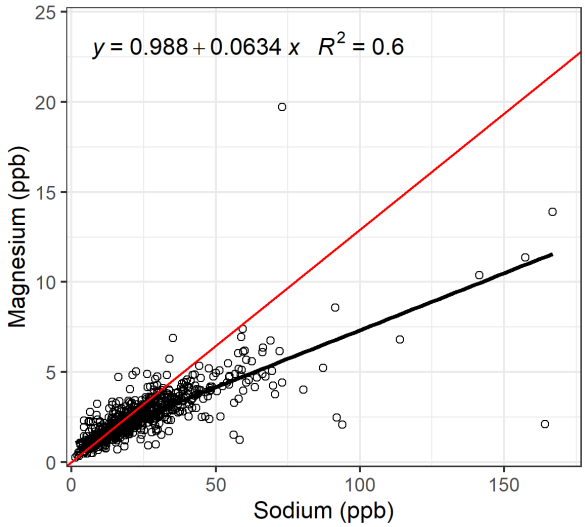

Figure 3.65 – Magnesium/Sodium ratio as found in the GV7(B) ice core samples dated to the Austral winter. The red line reports the ratio found in the sea water

ability between summer and winter ($>$ 50% difference), with Nitrate and MSA showing minimal to negligible difference respectively in the averages. This was expected, especially for MSA, whose variability will be further investigated further in the following sections, due to the low concentration displayed by the ion and the fact in the lower sections of the core the annual variation of the MSA was less clear compared to the Nitrate and Sulphate. Furthermore, the dating was accomplished using the nssSO_4^{2-} profile, which explains why the highest degree of variability between summer and winter is displayed by this ion, since the different seasonal maxima (or minima) do not always coincide. The difference in concentration of Sulphate reflects on the free acidity evaluated for the core in the two time periods. As reported in Figure 3.67, where the free acidity (in micro-equivalent per liter) is plotted against the Sulphate and Nitrate content of the

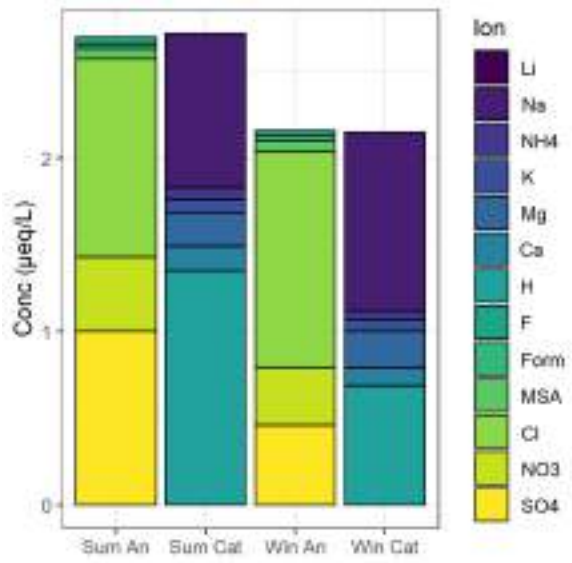

Figure 3.66 – Ionic balance for the GV7(B) ice core, both winter periods and summer periods are reported

core, the majority of the free acidity in the core comes from free Nitric and Sulfuric acid: correlation between the two records is low, but a clear pattern is present, and the lack of correlation seems to be due to a limited number of samples brining correlation down. This apparent correlation would easily explain the rise in acidity in the snow in summer months. When considering non-sea salt cations and crustal ones, Potassium levels were found to be relatively constant throughout the year (percentage difference, 10.23%), but this is not true for the Calcium levels, whose concentrations in Winter compared to the ones found in Summer differ more significantly (approx. 0.5 ppb, >25%). To investigate whether the difference in concentration was due to a difference in sources and or transport of the air masses, the concentration of Calcium was plotted against the Sodium one

Table 3.16 – Average winter and summer ionic concentration in the last millennia as found in the GV7(B) ice core

Ion	Concentration Avg. Summer	Avg. Winter	Difference (%)
Lithium	0.0172 ± 0.04	0.0163 ± 0.04	5.11
Sodium	20.4 ± 16.73	23.6 ± 17.6	13.88
Ammonium	1.17 ± 2.42	0.877 ± 1.52	25.19
Potassium	2.96 ± 4.99	2.65 ± 4.87	10.23
Magnesium	2.27 ± 1.95	2.49 ± 1.44	8.49
Calcium	2.76 ± 4.98	1.99 ± 2.51	27.74
Fluoride	0.750 ± 8.79	0.51 ± 2.03	30.78
Formate	1.55 ± 12.24	1.31 ± 2.00	15.13
MSA	5.84 ± 3.51	5.78 ± 3.59	1.06
Chloride	40.9 ± 39.8	44.3 ± 40.4	8.88
Nitrate	26.8 ± 14.1	20.1 ± 11.10	24.70
Sulphate	47.9 ±24.8	21.9 ± 13.06	54.29

and their ratio considered as reported in Figure 3.68 and 3.69. Correlation as expected was found to be low in both summer and winter due to the prevalent crustal sources for Calcium, but interestingly during Winter the ratio between the two seems lower than the one found in Summer. This could be explained both with the difference in long range transport during winter and summer (the Polar Vortex is stronger during the Winter) but also with the seasonal variability of Sodium. Calcium, unlike Sodium, also comes from secondary (crustal) sources and therefore should be more influenced by the Polar Vortex closing during the winter months than Sodium, which also arises from the sea, a more localized source. But it's worth noting that the variability in the ratio could be also ascribed to the fact that Calcium levels seems to be more constant throughout the core (reason why their record was not used in the dating of the

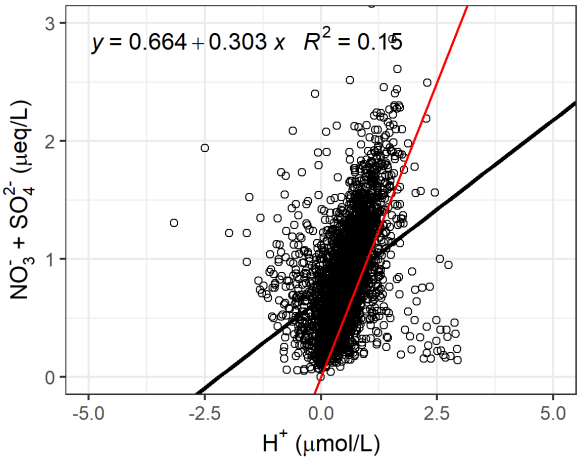

Figure 3.67 – Free acidity vs. Nitric and Sulphuric acid contribution as found in the GV7(B) core. The red line reports a 1:1 ratio between equivalent per liters

core) and the difference in the ratio could be ascribed solely on the variability of Sodium throughout the years.

3.9 Correlation with Environmental Parameters and Chemicals found in the GV7(B) core

In order to investigate the environmental variability in the last millennia, preliminary considerations were made on the first section (uppermost 95 m of the GV7(B) ice core) roughly corresponding to the time period 1700-2009 CE. This choice is somewhat arbitrary, but two major considerations were made when choosing the time interval i) the need of having a large enough dataset to be statistically relevant and at the same time a high enough resolution to be able to possibly investigate inter-annual cycles and ii) the lack of direct data

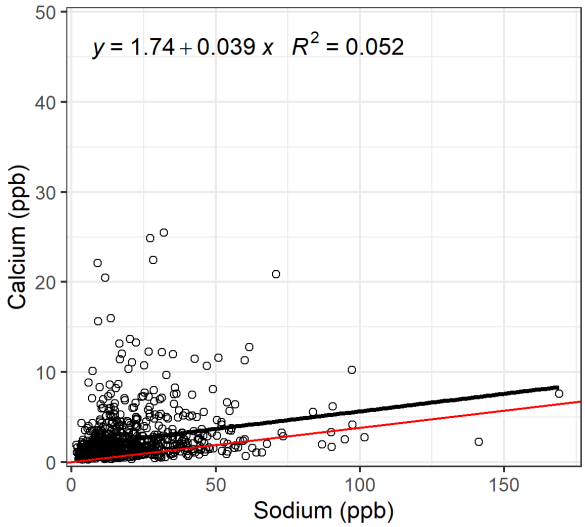

Figure 3.68 – Calcium/Sodium ratio as found in the GV7(B) ice core samples dated to the Austral summer. The red line reports the ratio found in the sea water

for most of the environmental parameters here considered. Indeed, most of the time series stopped around the year 1970 CE, after which satellite data are available. Since all the dataset here considered have a monthly resolution (in some case, daily) and due to the way the core was sectioned and the variation in accumulation rate, each dataset was reduced to make the comparison possible. Each year was therefore divided as previously done to investigate the inter-annual variability of each ion (three months period) and the average for each ion and environmental parameter was considered representative of each of these periods. This was done knowing that most years in the time period investigated contained at least 4 sample points (only two years were comprised of only three sample points, and in these cases the profile was reconstructed assuming constant levels throughout the missing years) and that a 3-month average was a sufficiently high

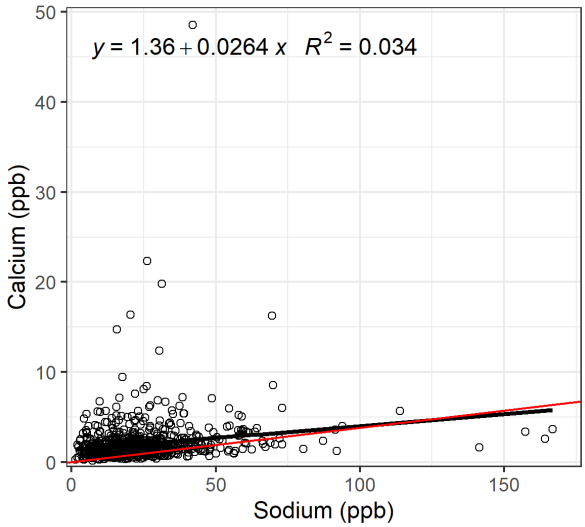

Figure 3.69 – Calcium/Sodium ratio as found in the GV7(B) ice core samples dated to the Austral winter. The red line reports the ratio found in the sea water

resolution to investigate inter-annual variability. Years characterized by a lower number of samples were considered to be characterized by an already averaged concentration of the ions. Monthly resolution was here not claimed, since the resolution of the core and the way it was analyzed doesn't allow to identify monthly patterns, but the choice of a 3-month average was found to be a good compromise between temporal resolution and the need to reduce the dataset. Furthermore, the wavelet analysis performed on the data used in the section below requires each time series to be characterized by a constant period which made mandatory reducing the time series.

3.9.1 Total Solar Irradiance

Since the amount of energy and the solar power over all wavelengths (per unit area) that reaches the upper atmosphere (Total Solar

Irradiance, TSI) has been successfully correlated with the Nitrate in polar snow (Traversi et al., 2009), for the GV7 site, high-resolution and low-resolution data were used to investigate this correlation. Data for TSI are available for satellite era (1970 CE - present) but also for previous years thanks to the ^{14}Be record that allows for reconstructing the solar irradiance records, but the resolution beyond the year 1700 CE quickly decreases (only 10-year average data are here considered). Figure 3.70 reports the three-months resolution data for the time period investigated for both Nitrate concentration found in the core and the TSI data. Figure 3.71 reports the same data, averaged in 10-years interval and plotted in the entirety of the time period here investigated. The 11-year cycle in the solar activity is clearly visible in the TSI profile, but such a clear pattern is not present in the Nitrate concentration profile, where only the annual summer maxima (already discussed previously) are visible. A number of Nitrate maximum seem to coincide with the local maxima of the solar activity, but linear correlation between the two series is low to non-existent ($r = -0.07$, $p = 0.01$). This was made even more clear when considered the 10-year averaged data, in particular in correspondence with local minimum of TSI, the concentration of Nitrate seems to be lower on average, but the correlation even when considering these two, is low and non-significant ($r = 0.15$, $p = 0.17$).

The apparent lack of correlation between the two series was further highlighted with wavelet analysis, as reported in Figure from 3.72 to 3.74. By decomposing a time series into time-frequency space using wavelets (e.g. Morlet wavelet, Spline wavelet) it is possible to identify the dominant modes and their time variability. Given two time series, and the corresponding wavelet transforms of the two, it is possible to define a cross-wavelet spectrum (a complex spectrum) as the product of the first time serie's wavelet transform and the

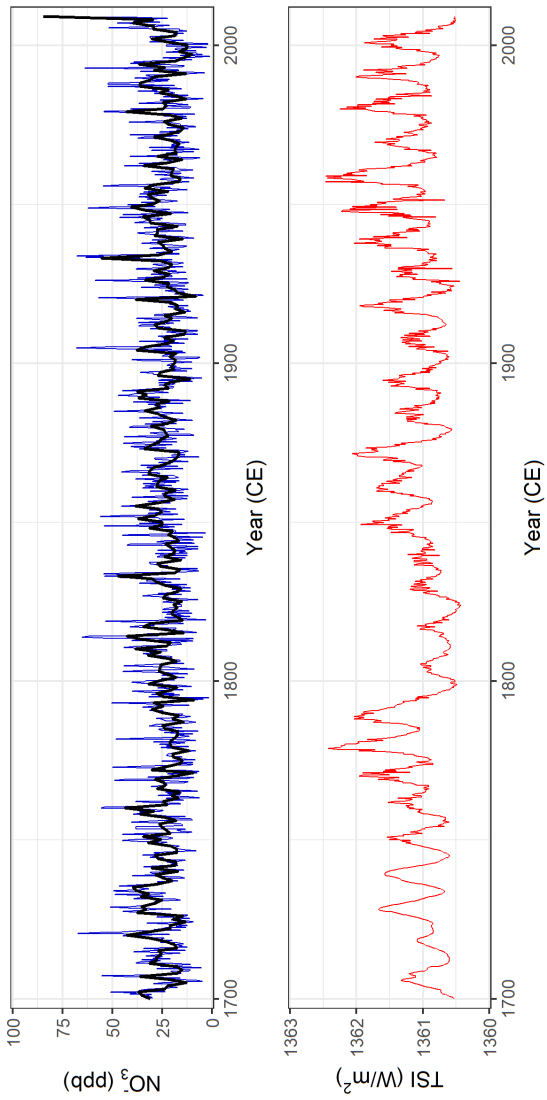

Figure 3.70 – Nitrate (blue, original data, black, three months average) and Total Solar Irradiance (red) records across the last three centuries

complex conjugate of the second. This is a measure of the correlation between the two signals in the time-frequency plane, which is useful

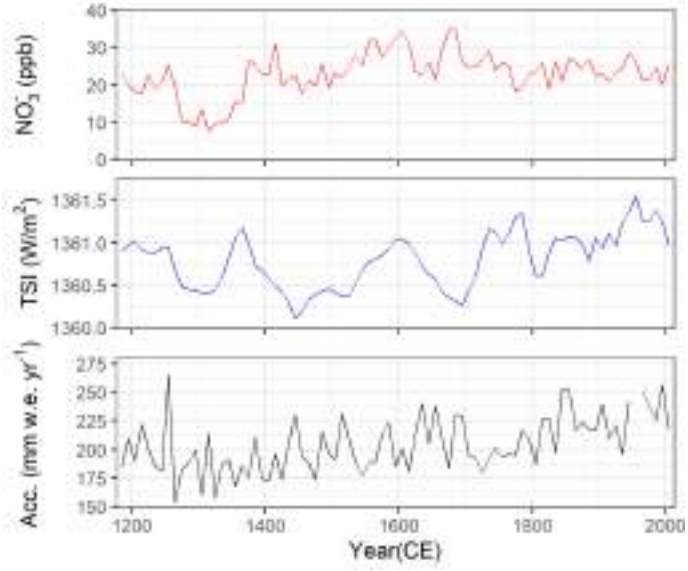

Figure 3.71 – Nitrate (solid blue), Total Solar Irradiance (solid red) and snow accumulation rate (solid black) records across the last millennia. 10 year average data.

when considering non-stationary signals. An in-depth description and analysis of the use of wavelets in the field of environmental science is beyond the scope of this work, and here they will simply be used with a semi-quantitative approach to investigate the periodicity of time series. MATLAB software wcoherence functions using the analytical Morlet wavelet was used to produce the images of wave coherence analysis. Both in the 3-months and the year average correlation showed a clear lack of correlation between Nitrate concentration and TSI in the 1700 - 2000CE time period, when focusing on the satellite time period (1979 - 2009 CE for the core, as reported in Figure 3.72) only a small section displayed a Magnitude-Squared Coherence over 0.7. The 1990 - 1995 CE time period displayed a strong out of phase correlation, both at 1- and 2- year periods but

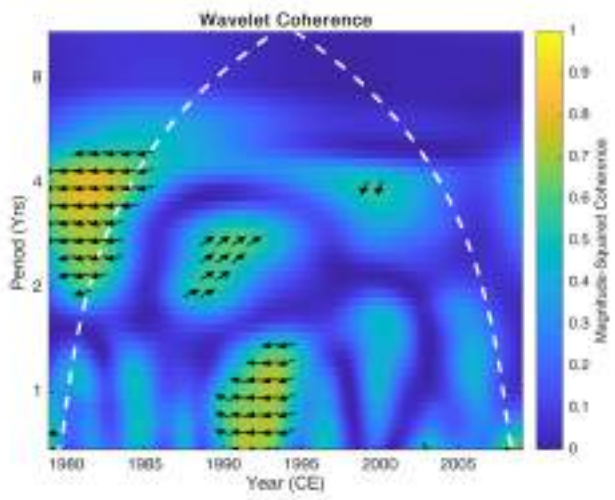

Figure 3.72 – Nitrate vs TSI wavelet coherence analysis (3-months resolution, satellite period: 1979 - 2009 CE)

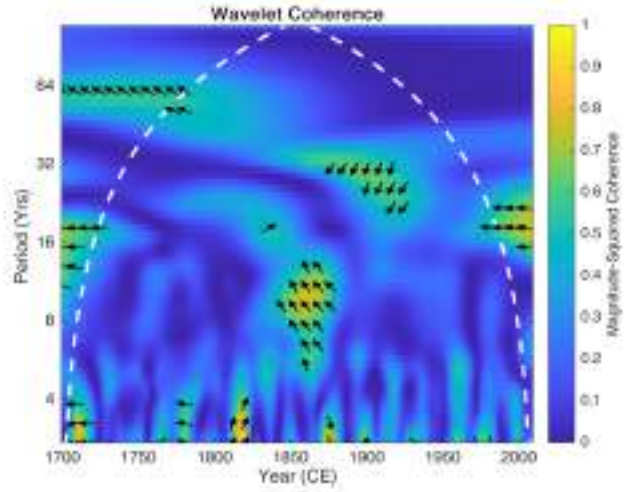

Figure 3.73 – Nitrate vs TSI wavelet coherence analysis (1-year resolution, time period 1700 - 2009 CE)

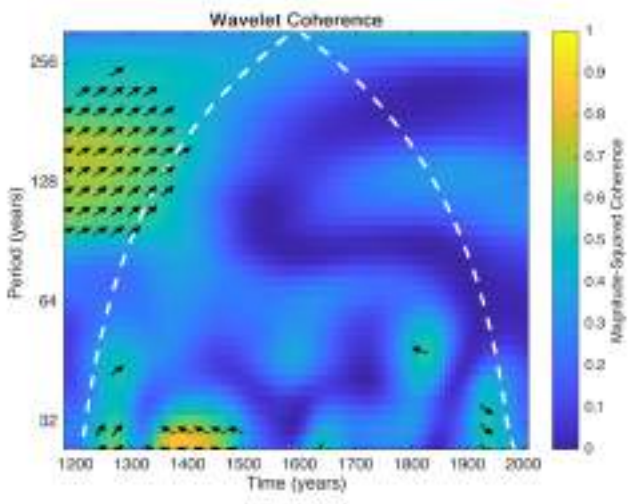

Figure 3.74 – Nitrate vs TSI wavelet coherence analysis (5-year resolution, time period: 1700 - 2000 CE)

no clear long-term pattern is visible when considering the Nitrate record and the TSI in the last few centuries as reported in Figure 3.73. Indeed, excluding the low-period section of the cross-wavelet spectrum, where high correlation zones can be identified (most likely present due to the high variability of the Nitrate concentration data and not because of a statistically significant correlation) only one time period (1980 - 1875 CE) diplayed a high cross-squared coherency. This is characterized by a somewhat high periodicity (8-10 years) and follows a local minimum in the TSI (Dalton Minimum ended in 1830 CE). A similar correlation, of lower coherency, is found in the same temporal range (1850 - 1910 CE) but it's found at low frequency (higher periods) and it's not repeated throughout the time period investigated, suggesting a lack of environmental significance and/or correlation in the long period. Similarly, no clear correlation was found when analyzing the two time series at a lower resolution

(10-years average) considering the entirety of the last millennia: the two local minimum in both the Nitrate concentration and the TSI is highlighted for the time period 1350 - 1450 CE, but the two series as already visible in Figure 3.74 quickly diverge and correlation seems to be non-significant on a longer time scale, since other minima in TSI did not displayed the same depletion in Nitrate in the core. Total Solar Irradiance, since the amount of radiation that reaches the planet is directly correlated with the temperature (Mendoza, 2005) was then tested and correlated with the snow accumulation rate evaluated on site in this work. Both yearly resolved data and 10-year average time series were tested and cross-wavelet spectrum produced. It must be noted that compared to the annually resolved TSI data, the snow accumulation rate data is characterized by an extremely high variability adue to the way it was evaluated in this work. By means of wavelet transform, this high variability should be smoothed, and the noise removed at least in parts especially when considering the cross-wavelet spectrum, where the goal was to investigate not the fine structure of the dataset as much as long-term patterns and periodicity in the signal. Regardless, the same 7-years running average smoothing function proposed by Frezzotti et al. (2007) was applied and the smoothed dataset compared by means of wavelet analysis to the TSI record of the 1700-2009CE time period. Figure 3.75 reports the temporal profile of TSI and snow accumulation rate in the time period investigated, Figures from 3.76 and 3.77 the cross-wavelet spectra, in both of which periods of correlation were highlighted.
These are short periods, far in between, characterized by a relatively high coherence and the relatively low period, but the short time period in which the two time series correlate seems to suggest that this is due to high concentration peaks occurring in the same time period. The statistical and environmental relevancy of these findings

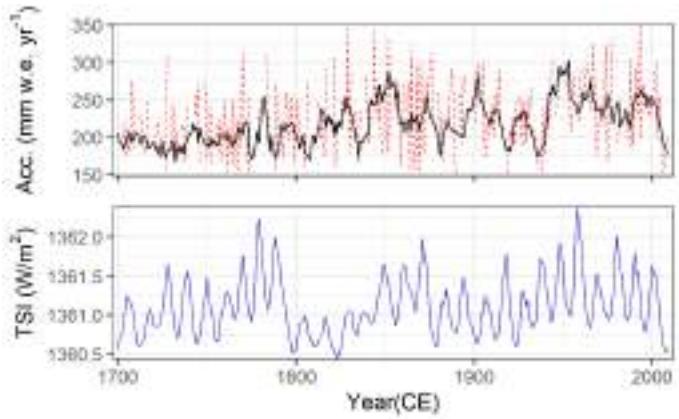

Figure 3.75 – Snow accumulation rate (dashed red, annually resolved, solid black, 10- years average) and TSI (solid blue, 10- years average)

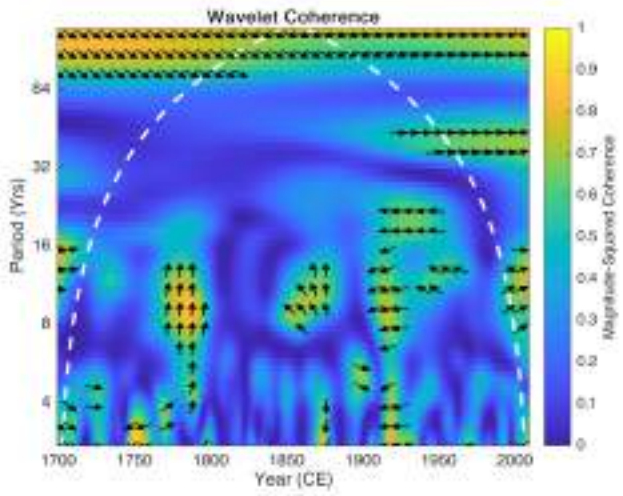

Figure 3.76 – Snow accumulation rate vs TSI wavelet coherence analysis (raw data, 1 - year resolution, time period 1700 -2009 CE)

is dubious: the high correlation in the 1750-1800 CE time period is characterized by an inverse phase of the two time series same with the one found in the 1900-1950CE time period, but the same is not

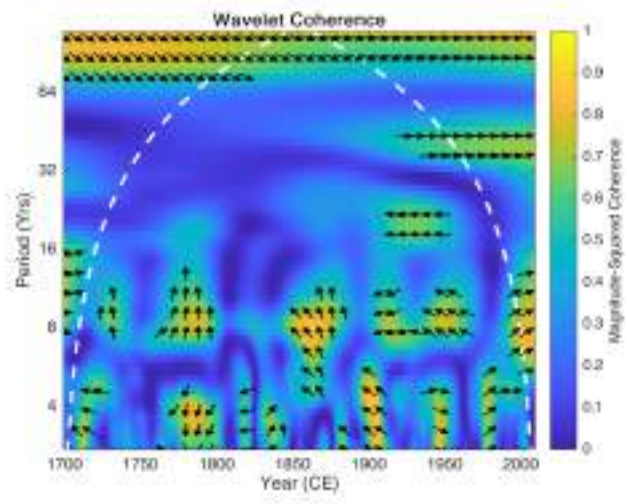

Figure 3.77 – Snow accumulation rate vs TSI wavelet coherence analysis (7 - year running average smooth, 1-year resolution, time period 1700 -2009 CE)

true for the high correlation found around the year 1850 CE, where high TSI values are associated with periods of high accumulation rate. This excludes the possibility of a long-term correlation in this temporal resolution characterized by a 9- to- 10- year periodicity. The two series seems to correlate when considering the high-period section of the cross-wavelet spectrum, but it must be considered that the majority of the data here are outside the cone of significancy. Here, the two series are in phase (0°to -30°of phase shift) with the Snow accumulation rate leading and the TSI record lagging behind. This in-phase correlation is also found in the 10- year averaged data as reported in Figure 3.78. The two complete records were already reported in Figure 3.71, where it's clear that a one-to-one correlation between the maxima is not present. Indeed, the two time series do not seem to linearly correlated even when considering longer time periods and lower temporal resolutions to smooth the signal ($r = 0.32$,

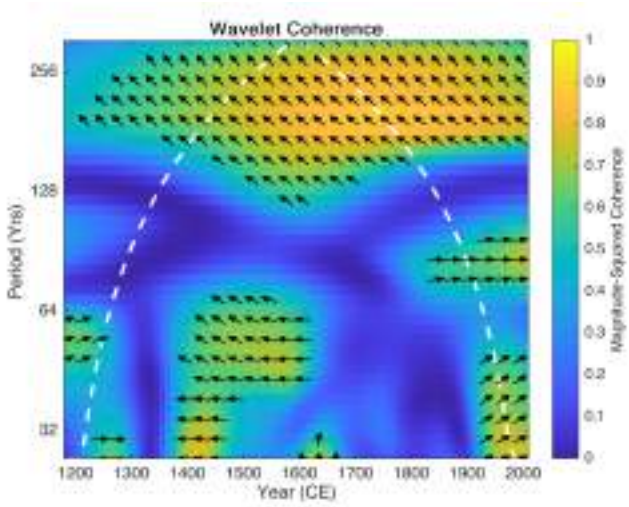

Figure 3.78 – Snow accumulation rate vs TSI wavelet coherence analysis (10 - year resolution, time period 1200 - 2000 CE)

$p < 0.01$) but high values of coherence were found when considering high periodicity of the two signals throughout the majority of the time period considered (1185 - 2005 CE). This is most likely due to the fact both records display a long-term rising, most noticeably in the time period 1700 - 2000 CE, but unlike TSI, the accumulation record does not display a clear oscillating pattern with such periodicity and the rising in accumulation was only statistically relevant in the last few centuries as previously discussed. When considering the long-term correlation, the two series do indeed correlate, but they're out of phase (75°), with the variation of TSI lagging behind the Accumulation record.

3.9.2 Sea Ice Extent

Sea ice influences and has a major role into modulating regional and global climate. It contributes to the amount of solar radiation

adsorbed by the planet since its presences increases Earth's albedo. The Sea Ice (TSI) also exerts a strong influence on the oceanic and biological system, making it a key parameter to investigate in environmental research. Sea Ice naturally shifts throughout the year, essentially doubling the extension of the continent during the Austral winter (Allen et al., 2011), but in the recent years global Sea Ice is undergoing major changes with a rapid decline in the Arctic, with expected consequences on the climate due to the ice-albedo feedbacks (Serreze and Meier, 2019). The opposite is somewhat true when considering the Antarctic continent, where the opposite trends of the Sea Ice around the Amundsen–Bellingshausen (decrease) and the Ross Sea (increase) (Turner et al., 2015; Comiso et al., 2017) contributed to a steady increase of sea ice as a whole for the continent (Parkinson and Cavalieri, 2012). Regardless of the trend, beyond the satellite era, only sporadic information and records about the sea ice coverage of the poles are present, and the only way to reliable investigate this key parameter of the planet's climate, is by using environmental proxies, since, as already stated, multiple chemical markers can be potentially affected by the growing sea ice around the coast of the Antarctic continent. In this section, major attention was given to find a possible correlation with the sea-salt markers recorded in the GV7(B) core, the levels of MSA and the sea ice extent together with other environmental markers. Sea Ice Extent time series for each regions of the Southern Ocean (Weddell Sea, Indian Ocean, Western-Pacific Ocean, Ross Sea and Bellingshausen and Amundsen Seas) were calculated from observations of Sea Ice concentrations from passive microwave satellite radiometers (Sea Ice Concentrations from Nimbus168 7 SMMR and DMSP SSM/I-SSMIS Passive Microwave Data) as reported by Parkinson and Cavalieri (2012). The complete dataset has a 25 km resolution updated daily.

The ice extent is calculated by summing the areas of the pixels within each region with ice concentrations of at least 15% and then averaged on a monthly basis. The five sectors the dataset uses are reported in Figure 3.79. As reported by Caiazzo et al. (2017), the air masses reaching the GV7 site are somewhat equally split in origin between the Antarctic plateau and the three closest free-water regions (Indian Ocean, Western Pacific Ocean and Ross Sea). Indeed, when considering three-days backtrajectories, 32% of the air masses arriving on site originate from Indian Ocean, and the second most prevalent origin (28%) from the Antarctic Plateau. Only 19% of the air masses originate from the Western Pacific Ocean, but these are associated with the most intense snowfall on the region. Therefore, when considering which dataset to use to correlate with the GV7(B) concentration records, the total Sea Ice Extent (the sum of the five sectors) and the ice coverage from the Indian Ocean, Western Pacific Ocean and Ross Sea were take into account. PC Analysis was considered in order to investigate with sector truly more strongly correlated with the chemical dataset, but the strong correlation of Sodium and Chloride (as well as the similar oscillating pattern in the extension of Sea Ice in all five sectors) masked the possible correlation in this kind of analysis. Since satellite data are available only in a small window of time, in this section only the 3-months average concentration record were considered. Figure 3.80 reports a preliminary comparison of the Sea Ice Extent (SIE, monthly resolved data and yearly average) and the MSA records found in the GV7(B) core (sample resolution). Since MSA concentration rise at the end of the year (Austral Summer) and the sea ice show a strong seasonal pattern, an apparent correlation is found when considering both the single sectors and the total SIE for the continent, but it must be noted that the latter dataset is characterized by a relatively

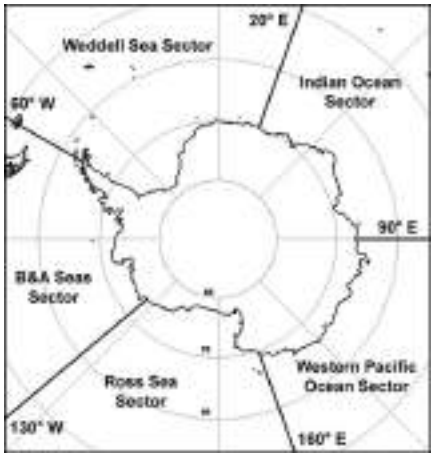

Figure 3.79 – Map of Antarctica and the five sector in which the souther ocean is divided as reported in Cavalieri and Parkinson (2008)

homogeneity (the data could be approximated by a sine function) while the MSA data display higher variability, with concentration as low as 0.30 ppb and as high as 20.0 ppb More importantly MSA concentration are characterized by long periods (up to decades) of relatively low concentration (avg. 5ppb) followed by spikes in concentration. These spikes in concentration don't seem to correlate with specific events in the SIE record. Similar consideration can be done with the Sodium and Chloride concentration profiles reported in Figure 3.80, where their seasonal pattern, already thoroughly explained in previous sections of this work, is indeed visible but does not seem to correspond with any particular events in the SIE record. In order to properly correlate the different sea markers, the same approach used for the Nitrate record was used here and each dataset of concentration and SIE data was reduced in resolution to a quarterly resolved dataset. Unlike TSI, only the first 30m of core were here considered therefore opening the possibility to further increase the temporal resolution (e.g. two-month resolution instead

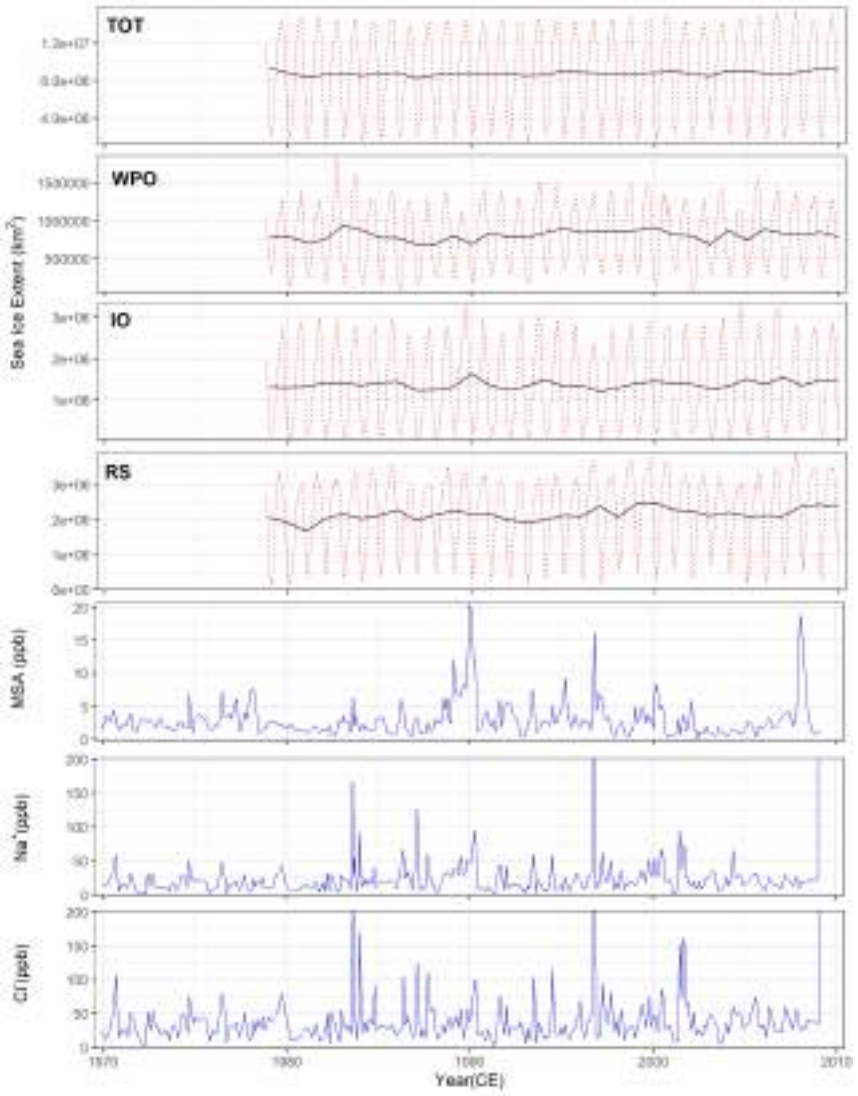

Figure 3.80 – Sea Ice Extent (solid black, annual average, dashed red, monthly resolved) data for the sectors here considered (TOT, entire of the continent, WPO, Western Pacific Ocean, IO, Indian Ocean, RS, Ross Sea) and chemical records (solid blue) found in the GV7(B) core.

of three-month) due to the larger number of sample point comprising each years, but ultimately this option was discarded. This was done both for consistency and ease of comparison of the different environmental results and more importantly because despite having a higher resolution in this section of the core, the number of samples per year quickly decreases. This approach would have forced to reconstruct the concentration for some of the period in which not enough samples were available, for example assuming constant the concentration of any given ion for a longer period of time. Table 3.17 reports the results of the linear fitting between each ion considered in this section and the SIE for the sectors considered (alongside the total SIE of the continent in the time period investigated). The fitting was performed using both the 3-month average previously described and on the smaller dataset of the 1-year average. The latter was used as a comparison, as it should not include any dating-based error since the assumption of a constant snow accumulation rate (that made possible the monthly resolved dating even if monthly resolution was never claimed) is removed.

As already stated, no clear linear correlation was found when considering the entirety of the time period considered, despite the presence of a clear seasonal pattern in each ion. This was expected, since as already stated, the SIE doesn't display the same wide variation in signal found in the ionic content of the core and a simple linear fitting models couldn't take into account for this. A better degree of correlation between all the chemical markers here considered is found with the Ross-Sea ice extent (as one could expect due to the position of the site), but correlation ($p > 0.1$) seems to be non-significant. Using higher degree of smoothing (3-year running average Curran (2003)) yielded similar results and non-significant correlations for the MSA records. Similarly, when considering the early winter maxima

Table 3.17 – Linear correlation between Sea Ice Extent and different chemicals found in the GV7(B) ice core

		Sodium	Chloride	MSA
Total Sea Ice Ext.	3-months Avg	r = 0.09 p = 0.344	r = 0.15 p = 0.098	r = -0.25 p = 0.006
	1-year Avg	r = 0.28 p = 0.115	r = 0.28 p = 0.115	r = 0.13 p = 0.492
WP Ocean Sea Ice Ext.	3-months Avg	r = 0.07 p = 0.417	r = 0.17 p = 0.071	r = -0.24 p = 0.008
	1-year Avg	r = -0.05 p = 0.788	r = -0.02 p = 0.920	r = -0.23 p = 0.013
Indian Ocean Sea Ice Ext.	3-months Avg	r = 0.10 p = 0.301	r = 0.16 p = 0.086	r = -0.23 p = 0.016
	1-year Avg	r = 0.14 p = 0.432	r = 0.10 p = 0.604	r = 0.21 p = 0.258
Ross Sea Sea Ice Ext.	3-months Avg	r = 0.11 p = 0.243	r = 0.16 p = 0.087	r = -0.23 p = 0.010
	1-year Avg	r = 0.25 p = 0.163	r = 0.29 p = 0.107	r = 0.21 p = 0.258

in the sea-ice extent and concentration (and flux) of sea-salt ions concentration (Severi et al., 2017). Low levels of correlation ($r < 0.2$) were also found when considering both the individual sectors, the total SIE of the continent and the composite record of SIE in the three sectors who were proven to be the most likely to affect the site. It is worth nothing that both positive and negative correlation were found between SIE and the chemical markers here considered (Abram et al., 2013) and, in particular for sea-salt markers (ssNa, ssCl), sea ice might not be the primary source for the massive influx on the continent. Indeed, both blowing snow (Yang et al., 2008) and changes in meteorology, e.g. wind speeds, air temperatures, humidity, (Levine

et al., 2014) have been proven to be a more substantial contribution to the sea-salt levels. It is worth noting that the model used to investigate the meteorology effect on the sea-salt concentration only covered a short period of time (1990 - 1998 CE) and was focused on investigating the interannual variability of ssNa. Both the way the chronology was obtained for the GV7(B) core and the resolution of the samples made impossible to investigate at such resolution the variation of ssNa, but these preliminary findings suggest that the effect of Sea Ice on both MSA and sea-salts concentration in ice cores. More interesting are the findings reported in Figure from 3.81 to 3.92 where, using the same procedure as used for the TSI and Nitrate correlation, cross-wavelet spectrums were used in order to investigate in the time-frequency spectrum where the different time series correlated and displayed coherence. Only 3-months averages were used. Low levels of correlation were found when considering the sea-salt ions, with both Sodium and chloride displaying low values of Magnitude-Squared coherence, especially when considering high periodicity. When considering the 1-year periodicity only the time period 1992-1995 CE display a strong, in phase (0°to -10°), correlation between each SIE record and sea-salt ion one. Indeed, in this section of the core, the seasonal chemical peaks seem to coincide exactly with the maxima in the SIE, but a lack of long-term correlation is evident. Similarly, only few time periods of higher correlation were found when considering higher periodicity (2- to 4- years periods) and only when considering two of the five sectors of Antarctica, Western Pacific Ocean and Ross Sea, but here the phase is not in line with what found at lower periods, with the two series out of phase (180°) in the 1985 - 1992 CE time period and slightly out of phase (70°-110°) in most recent years (1995 - 2005 CE with a higher period). The lack of correlation between sea-salt ions and the SIE, seems to

indicate that indeed despite the strong correlation between Sodium and Chloride and their ratio suggesting mostly a marine source (as expected due to the closeness of the site to the sea), the influence of marine ice is either negligible or not existent.

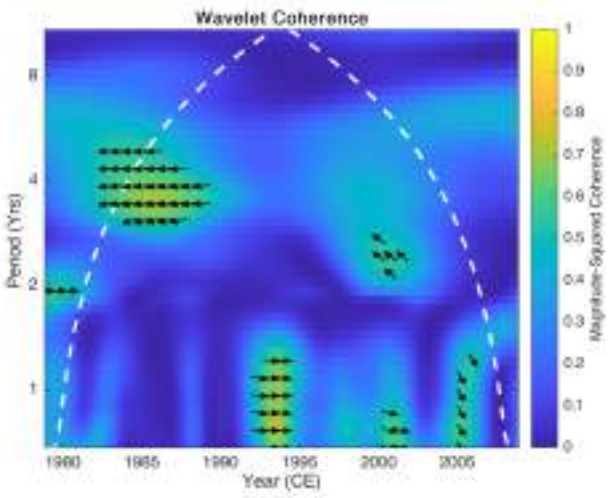

Figure 3.81 – Total SIE vs GV7(B) Chloride concentration record wavelet coherence analysis (3- months average values, 1979 - 2009 CE satellite age)

Regardless, in the few years in which a correlation was found, it is worth noting that the growing distance from the open water due to winter season does not seem to affect the ionic content in the core (the two signals are in phase). The presence of small sections of in-phase correlation might suggest that the influence of frost-flowers and or blowing snow from the growing sea ice in winter affects the concentration of sea-salt ions on the Antarctic plateau, but no long-term pattern was found to further corroborate their effect on the GV7 site. Better correlation was found considering the MSA and the different SIE records, both when considering the total variation of sea ice across the entirety of the continent and the three sectors

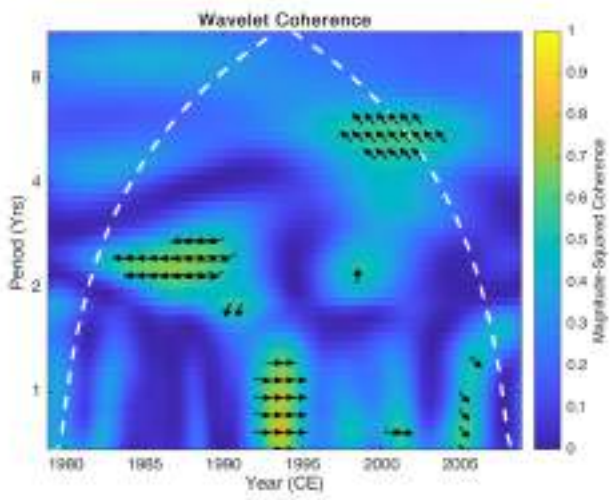

Figure 3.82 – West-Pacific Ocean SIE vs GV7(B) Chloride concentration record wavelet coherence analysis (3- months average values, 1979 - 2009 CE satellite age)

considered here. In particular, higher correlation was found in the 1985 - 2000 CE time period (1 year periodicity) where three sections of strong, out of phase (180°) correlation were present. The lack of correlation around the year 1991 - 1992 CE could be ascribed to the presence of a double peak in the MSA record in the winter of the year 1991 CE and the lack of a summer peak for the year 1993 CE which is not in line with the SIE record. This is hardly to be ascribed to a dating error, as this section of the core, characterized by the highest resolution, was also dated using $\delta^{18}O$ record which to this day is one of the most accurate way to date a core and the $nssSO_4^{2-}$ record is in line with the isotopic content of the core. MSA concentration in ice core has been proven to not be entirely fixed in the firn and snow samples Osman et al. (2017); Roberts et al. (2009) and indeed a volcanic peaks is found at these depts and the acidic layer associated to volcanic signal are known to cause diffusion of other chemical

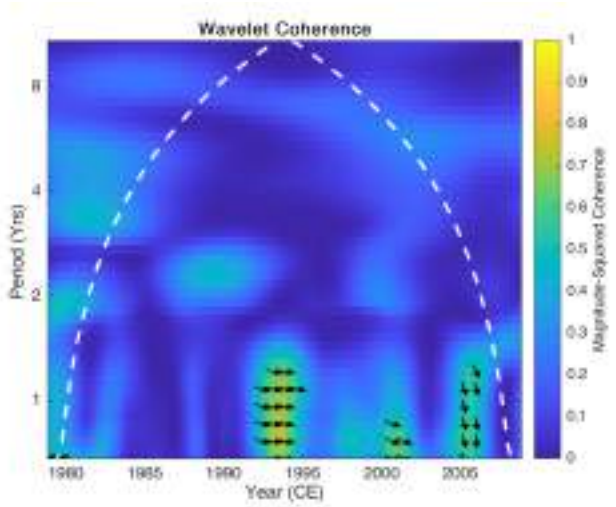

Figure 3.83 – Indian Ocean SIE vs GV7(B) Chloride concentration record wavelet coherence analysis (3- months average values, 1979 - 2009 CE satellite age)

in the core. Considering this, the 1- year periodicity should be the expected annual correlation (especially when considering the out of phase nature of the correlation) between MSA and sea ice. Indeed, MSA concentration during wintertime is lower (and such pattern is helpful in the dating of ice cores e.g., Abram et al. (2013)) than during summertime. This is ascribed to a number of factors, in part the limited marine production of DMS, precursor of MSA, during the austral night, but also due to the increased atmospheric transport distance due to the growing sea ice and the diminished OH radical concentration, which is a key oxidant of airborne DMS (Jourdain and Legrand, 2001). When considering higher periodicity, an in-phase correlation (0°to 30°) was found between MSA and the SIE record from the Ross Sea and the Indian Ocean (4 years periodicity) whilst the same correlation was not found when considering the Western Pacific Ocean, which is also the closest to the site and was thought

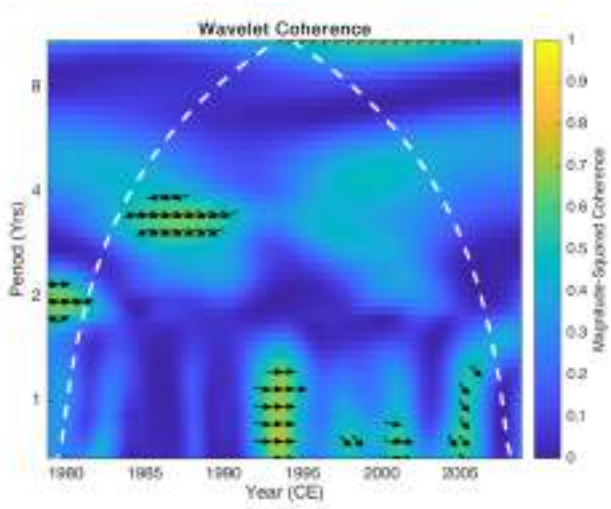

Figure 3.84 – Ross Sea SIEt vs GV7(B) Chloride concentration record wavelet coherence analysis (3- months average values, 1979 - 2009 CE satellite age)

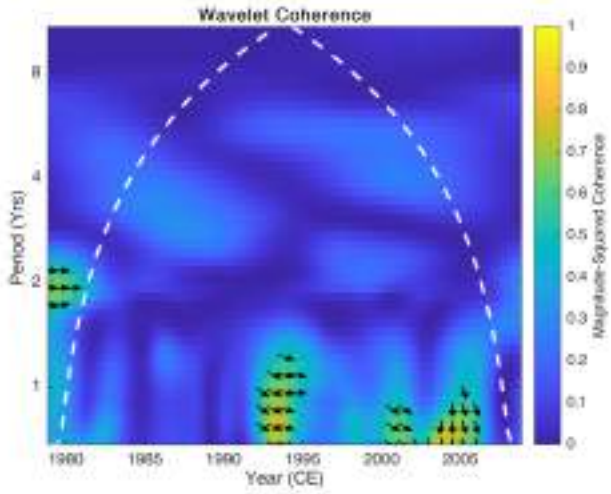

Figure 3.85 – Total SIE vs GV7(B) Sodium concentration record wavelet coherence analysis (3- months average values, 1979 - 2009 CE satellite age)

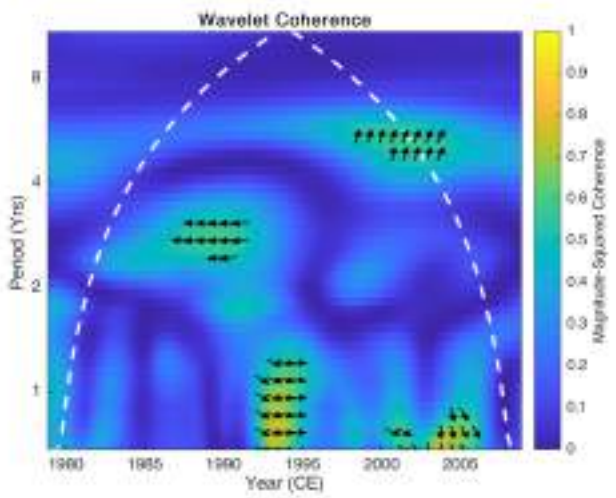

Figure 3.86 – West Pacific OceanSIE vs GV7(B) Sodium concentration record wavelet coherence analysis (3- months average values, 1979 - 2009 CE satellite age)

to influence the MSA concentration in the core. It is worth noting that despite some studies have found a correlation between sea ice extent and MSA (Welch et al., 1993) and they have successfully used these chemical marker as a proxy in the reconstruction of the SIE levels, concentration of MSA in the cores is not solely dependent on the amount of free ocean water available. Indeed, MSA levels in coastal cores (such the one here discussed) reflects not only the influence of the SIE, but also the atmospheric flows over the site that have a role on the SIE during winter as well (Turner, 2004). The direct effect of atmospheric and oceanic circulation and their correlation with the MSA and other environmental proxies in the core is discussed more in depth in the next section, here attention is given to the possibility that an indirect link between SIE and MSA could be a suitable explanation of the strong, in-phase correlation found with a period of 4-8 years. Since sea ice development and melting

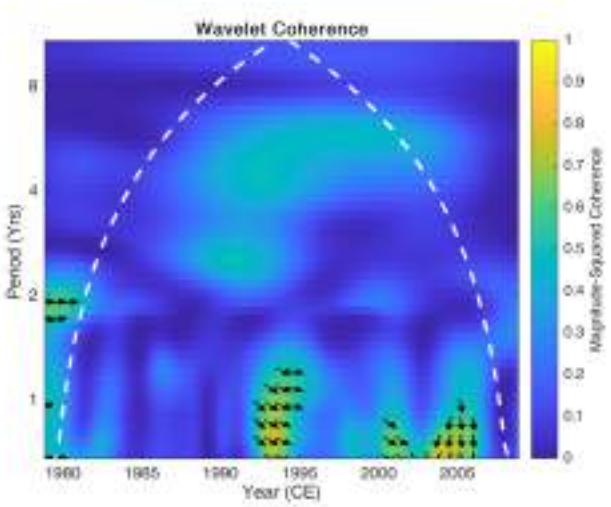

Figure 3.87 – Indian Ocean SIE vs GV7(B) Sodium concentration record wavelet coherence analysis (3- months average values, 1979 - 2009 CE satellite age)

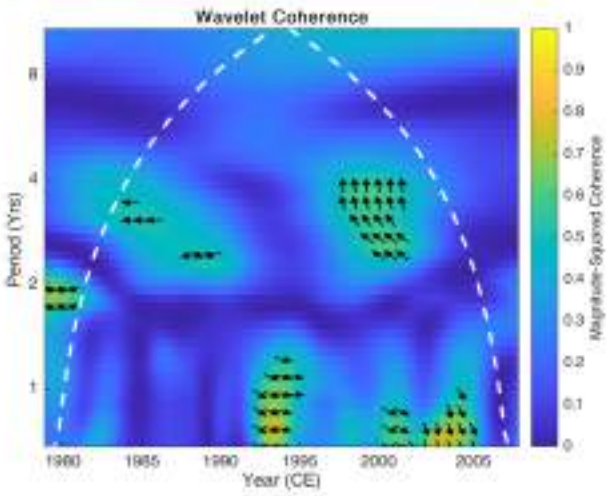

Figure 3.88 – Ross Sea SIE vs GV7(B) Sodium concentration record wavelet coherence analysis (3- months average values, 1979 - 2009 CE satellite age)

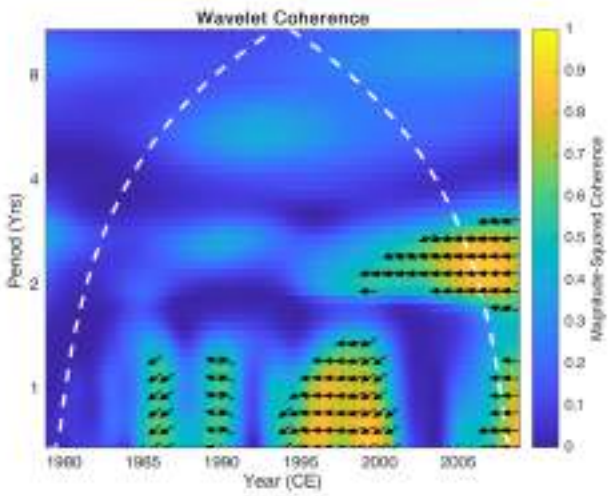

Figure 3.89 – Total SIE vs GV7(B) MSA concentration record wavelet coherence analysis (3- months average values, 1979 - 2009 CE satellite age)

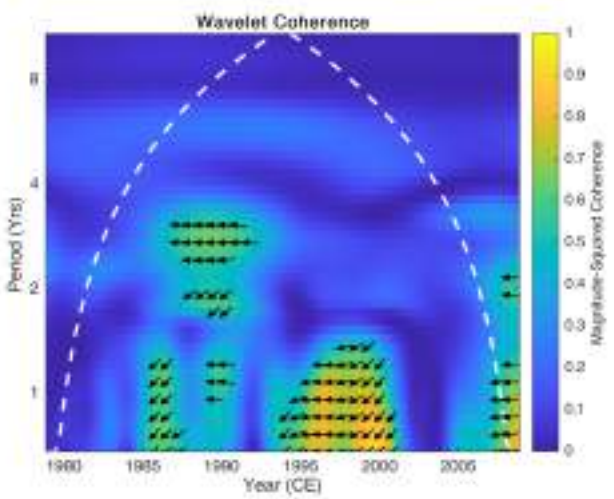

Figure 3.90 – West Pacific Ocean SIE vs GV7(B) MSA concentration record wavelet coherence analysis (3- months average values, 1979 - 2009 CE satellite age)

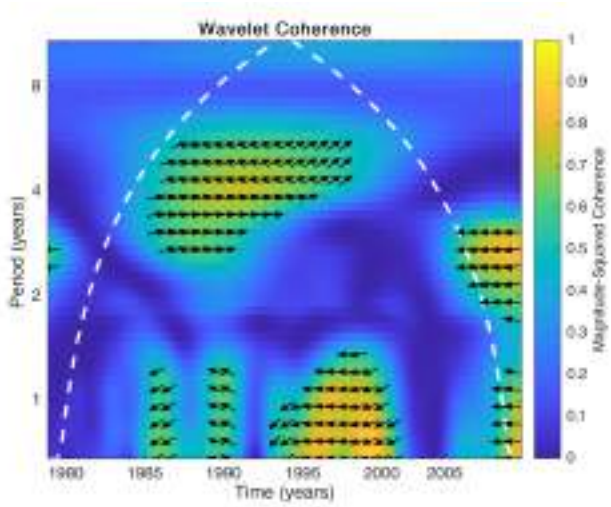

Figure 3.91 – Indian Ocean SIE vs GV7(B) MSA concentration record wavelet coherence analysis (3- months average values, 1979 - 2009 CE satellite age)

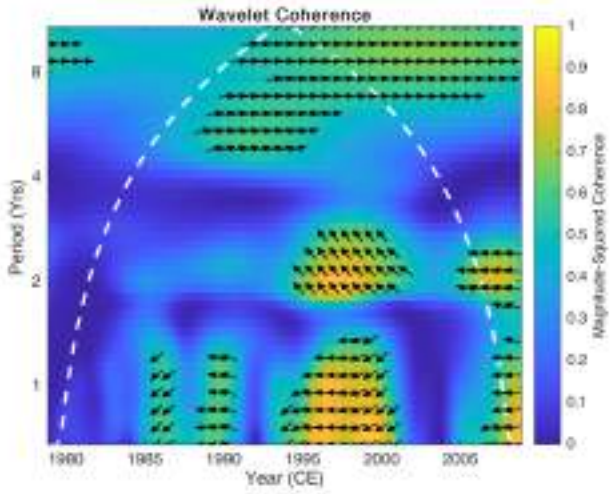

Figure 3.92 – Ross Sea SIE vs GV7(B) MSA concentration record wavelet coherence analysis (3- months average values, 1979 - 2009 CE satellite age)

throughout the different seasons is dependent on the atmospheric circulation and oceanic, multiple studies have investigated the SIE and El Nino Southern Oscillation (ENSO; the most prominent climate phenomenon of the Pacific Ocean with repercussions not only on the tropical but also the sub-tropical region of both hemispheres) correlation (Karoly, 1993; Kiladis and Diaz, 1989). The nature of the connection is complex and still explored to this day, but the best evidence suggests that the ENSO causes anomalies in the sea ice in the following years (Simmonds and Jacka, 1995). Furthermore, variation in the West Pacific oceanic circulation and ENSO have been associated with a variation of the atmospheric pattern on the Ross Sea (Bertler et al., 2006). This area, despite not bringing heavy snowfalls on site (Caiazzo et al., 2017) compared to other sectors of Antarctica, is still associated with a large nember of back trajectories that arrive on site. The number of back trajectories increases during the Austral Summer, reaching their maximum during the September-November period, which is also associated with the highest MSA concentration throughout the year. This alone is not enough to justify the 4- to 8- years period correlation, but as reported by Bertler et al. (2006) ENSO events (characterized by an average periodicity of 3 to 7 years) are able not only to affect the amount of heat that reaches the continent (with a difference of approximately 1K in the Ross Sea's temperature between Niña and Niño events) but also on the long distance atmospheric transport. The ENSO has been proven to influence the strength and position of the Amundsen Sea Low (Meyerson et al., 2002; Bertler, 2004; Turner, 2004), a semi-permanent low-pressure system that governs the direction and magnitude of the meridional moisture flux in the area. During el Niño events, this low-pressure system can shift east, whilst during el Niña (SOI $>$ 1, colder events) it is centered on the Ross Sea basin. This enhances the

low-level easterly jet and promotes the katabatic flow from inland but at the same time promotes the advection of air masses from the sea to the area object of study in this work, increasing transport processes. On the basis of the positive relationship between the SIE and SOI in the area (Kwok and Comiso, 2002), the correlation between MSA and SIE can be therefore explained by the strong influence of the Pacific circulation on both.

3.9.3 Atmospheric circulation over Antarctica

Unlike chemical markers, which can provide information on the centuries to millennia time scale, SIE data despite the high resolution, only cover a small window of time, which as already stated could explain the lack of long-term correlation and the lack of correlation found in the previous section of this work. Since the influence of the Oceanic circulation on both primary production and long-term transport and SIE was proposed to be a plausible explanation for some of the high period cross wavelet correlation found when analyzing SIE, attention was given to the direct correlation between MSA (and other chemical markers) and indexes that could provide information of the circulation over the Pacific. As already stated, one of the largest climatic cycles that effects the Pacific area, with repercussions not only on the area where it originates but also in the area surrounding the Pacific basin and far regions (Kiladis and Diaz, 1989) is ENSO. This is a recurring climate pattern involving changes in pressure and the strength of the westerlies with repercussions on the temperatures of the water in the central and eastern tropical Pacific Ocean. This has some obvious consequences on the weather of some mid-latitude regions (e.g. North America, New Zealand) but also on more remote areas. Indeed, evidences of the transmission of the ENSO signal to higher latitude (teleconnection) have been found since the 1970s (e.g.

Trenberth 1975) but the expression of this correlation both on the oceanic circulation and the meteorological conditions around and on the Antarctic continent is still investigated (Turner, 2004). During the el-Niño (warm) phase of the ENSO, a shift towards east of the Walker Circulation can be identified over the Pacific Ocean. The weakening (or reversal) of the Easterly winds make so that warm water moves eastward bringing precipitation over South America, but it also has consequences on the sea. During the warm phase of the ENSO, the upwelling on the east side of the pacific is reduced (the opposite is true during la-Niña, the cold phase of the ENSO), with repercussion on the heat distribution through the ocean. This cycle of cold and warm phase of ENSO can be represented by a number of indices, here, the Southern Oscillation Index (Trenberth and for Atmospheric Research Staff , Eds) (SOI, the twice normalized difference in surface pressure between Darwin, Australia and Tahiti) is used, together with the Southern Annular Mode index (SAM) (Marshall et al., 2018). The latter is not a true expression of the ENSO as much as a component of one of the principal modes of atmospheric variability of the extra-tropical regions of the South Hemispheres (Turner, 2004) and can be observed as a contraction/expansion of the polar vortex around the continent. This brings a shift of the mid-latitude jets and affects the surface pressures and westerly winds in the Antarctic regions. The correlations between ENSO and SAM are still debated, and it's clear that a clear-cut, linear correlation between the two is not present, but it's just as clear that changes in the SAM will affect the weather (e.g. in recent years SAM has entered a positive phase, with a decrease in surface pressure and an increase in the strength of the winds) and that the ENSO affects the SAM. Here, correlation between the two indexes is not considered, but SAM is used to gain insights on the transport processes and the origin of the

aerosol components (and in turn, the snow) found in the continent. The two indexes were already used in previous work (Becagli et al., 2009) as a way to extent the knowledge of the SIE on the assumption that the teleconnection between SIE and these circulation modes (Kwok and Comiso, 2002; Lefebvre, 2004) is present. Indeed, when considering the positive anomalies in the Ross Sea's SIE these seems to coincide with positive values of SOI (Becagli et al., 2009), and several studies (Legrand et al., 1991; Meyerson et al., 2002; Fundel et al., 2006) have recorded a correlation between MSA and SOI but the understanding of the influence of the atmospheric circulation around the continent on the concentration of chemicals in the snow is still low. Figure 3.93 reports the two circulation indexes and the chemical markers previously described. As reported by the authors of the SOI and SAM indexes, the monthly resolved data display a high degree of variability and were, therefore, smoothed. Both annual averages and 3- months averages were used. A number of key peaks in the chemical profiles (most noticeably in around the year 1950 CE) seems to coincide with positive anomalies in the SOI index, suggesting a possible correlation which was investigated in this section. This is even more noticeable when considering the MSA/nssSO_4^{2-} ratio (Legrand et al., 1991) as reported in Figure 3.94, although it is worth noting that a number of "spikes" were found in the record mostly because of the way nssSO_4^{2-} was evaluated. Despite the best efforts in removing externals contaminants and avoiding sample contamination, Sodium remains one of the most abundant element and contamination of this ions were found in some of the samples. These led to extremely low (or negative) levels of calculated nssSO_4^{2-} and artificially high levels of the ratio reported. A number of spikes could be identified in the ratio between the two markers, but when using similar approaches described in the dating

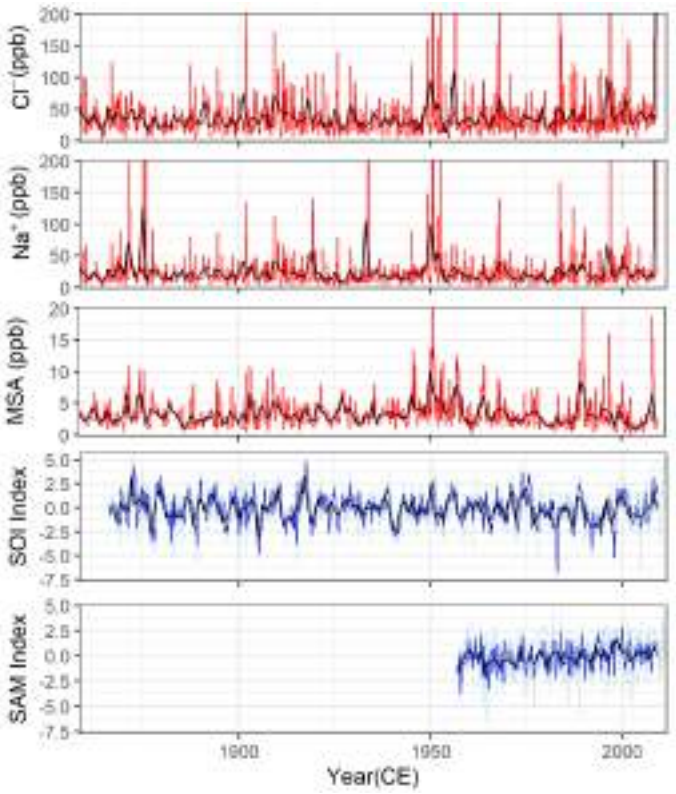

Figure 3.93 – Southern Oscillation Index and Southern Annular Mode (dashed blue, raw data, solid blue, 3-months average, solid black, yearly average) compared to the chemical signatures found in the GV7(B) ice core (solid red, 3-months average, solid black, annual averages).

procedure to discriminate real rise in the ratio from the background, only a few numbers of peaks were found, and these did not align with the Nino and/or Nina events [Turner 2004]. This was most likely due to the presence of the aforementioned spikes and negative values, making this approach less reliable and less useful for the purpose of investigating the past climate, at least from this record. For the cross-wavelet spectrum analysis, this record was discarded in favor of raw MSA data. The same approach in the data manipulation

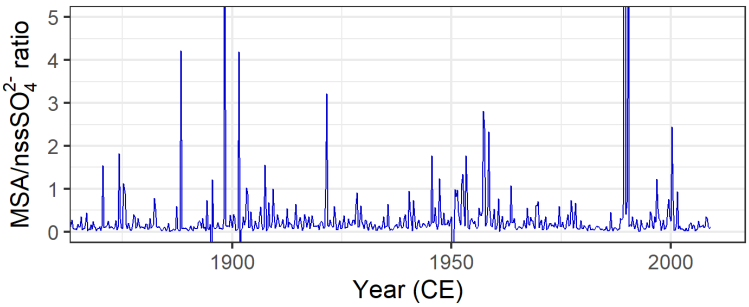

Figure 3.94 – MSA/nssSO_4^{2-} ratio as found in the GV7(B) core investigating anomalies in the Southern Circulation

and procedure to investigate the coherence of the different temporal series before was used for this section. Table 3.18 reports the results of linear correlation between the different ions and the SAM and SOI indexes. Both 3-months and yearly average were used to evaluate the possible correlation.

Table 3.18 – Linear correlation between Sothern Oscillation Index, Southern Annular Mode and different chemicals found in the GV7(B) ice core

		Sodium	Chloride	MSA
SOI	3-months Avg	r = 0.01 p = 0.733	r = 0.01 p = 0.879	r = 0.10 p = 0.018
	1-year Avg	r = 0.10 p = 0.239	r = 0.18 p = 0.026	r = 0.21 p = 0.013
SAM	3-months Avg	r = 0.02 p = 0.574	r = 0.05 p = 0.235	r = -0.01 p = 0.856
	1-year Avg	r = -0.01 p = 0.950	r = 0.05 p = 0.711	r = -0.21 p = 0.138

Correlation was found to be low ($r < 0.2$ in most cases) and non-significant in both cases as initially expected, due to the extreme variability in the chemical concentration when compared to the

average. Indeed, the majority of the ionic content throughout the year seems to be focused on few samples characterized by extremely high concentration and these too display a higher degree of variability that is not found in the SAM nor SOI record. The same procedure applied at the SIE was therefore applied here, and wavelet coherence plots were produced, as reported in Figure from 3.95 to 3.100. Here, a better degree of correlation was found, not when considering low periodicity, but for high periods. In particular, when considering the SOI-MSA correlation (Figure 3.95) a 4 to 8- years period correlation was found (0°– 90°phase shift, meaning the two series are in synch with each other) in the last 60 years. The same is not true when considering the SAM index as reported in Figure 3.96. Here, is clear how correlation between the two series is low, and indeed, with the exception of the time period 1960 - 1975 CE where a strong, out of phase correlation is found (period 8 years, 180°phase shift), a magnitude squared coherence below 0.4 if found in the majority of the period investigated and even the coherence previously noted, despite its high value of squared magnitude coherence, it's out of the cone of influence and therefore, possibly non-significant. The opposite was found to be somewhat true for the other two markers here considered as reported in Figure 3.97 and Figure 3.99. In particular high magnitude of correlation was found for Chloride and SAM throughout the period investigated (4- years period, 180°- 90°of phase shift), whilst no clear correlation was found when considering the SOI index and the same marker. Indeed, only two time periods displayed a significantly high correlation (1950 – 1970 CE, 4- to 8- years period and 1900 - 1920 CE, 8- to 10- years period). The correlation here is in phase (approx. 45°phase shift), which would be imply that significant changes in the SOI are then followed by a similar change in the marine aerosol that reaches the site, but on

the decadal resolution and only for few selected years, which makes difficult to extrapolate a long term correlation. Since unlike SOI, SAM is an expression of the circulation over Antarctica, the results displayed on Figure 3.98 and Figure 3.100 could potentially confirm the lack of influence of the Sea Ice (i.e. frost flowers) on the marine aerosol contribution for the site, and the stronger contribution of the local meteorology on Sodium and Chloride levels found in the continent.

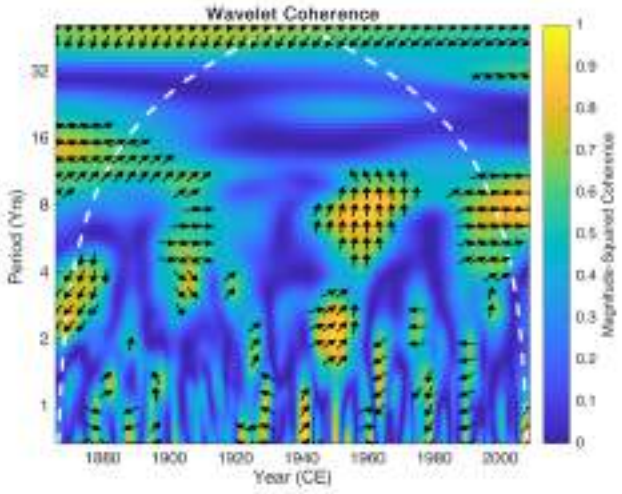

Figure 3.95 – SOI vs GV7(B) MSA concentration record wavelet coherence analysis (1866 - 2009 CE time period, 3-months resolution)

Environmental studies of the Southern Hemisphere circulation normally investigate only the zonally symmetric components of the SAM (or SOI), however, a significant asymmetric component is superimposed over the zonal flow. Here, the Zonal Wave 3 (ZW3) and its correlation with sea-salt ions concentration in the core and MSA is investigated. ZW3 is a major, asymmetrical and quasi-stationary part of a larger atmospheric circulation associated with the meridional

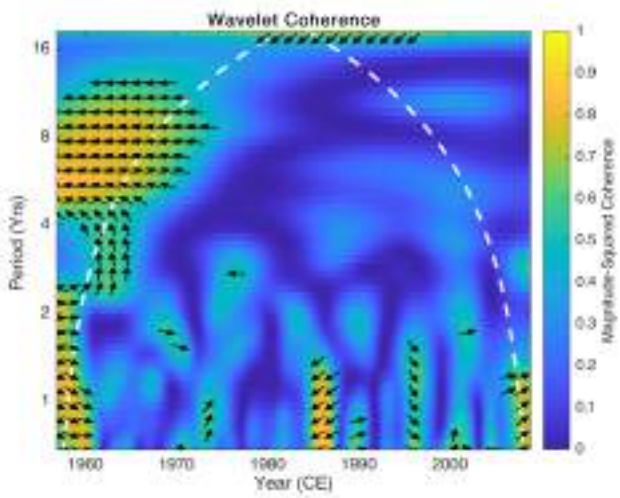

Figure 3.96 – SAM vs GV7(B) MSA concentration record wavelet coherence analysis (1957 - 2009 CE time period, 3-months resolution)

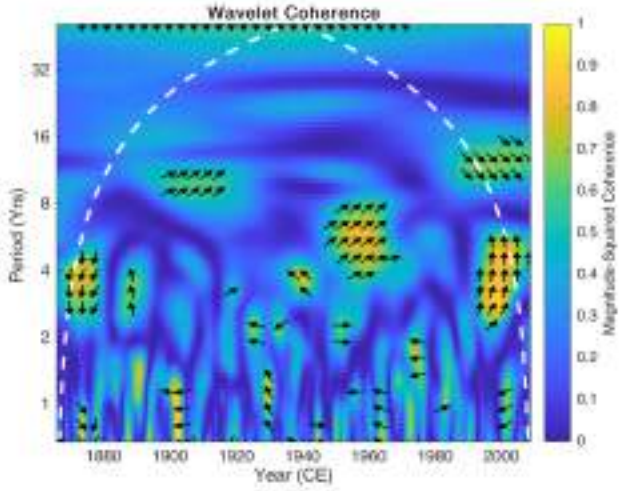

Figure 3.97 – SOI vs GV7(B) Chloride concentration record wavelet coherence analysis (1866 - 2009 CE time period, 3-months resolution)

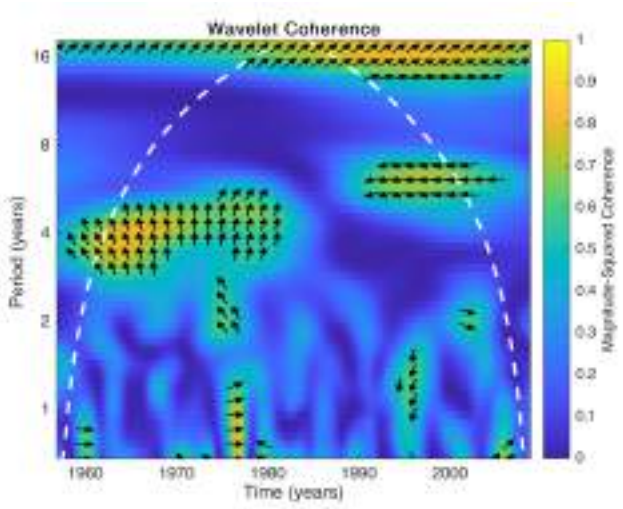

Figure 3.98 – SAM vs GV7(B) Chloride concentration record wavelet coherence analysis (1957 - 2009 CE time period, 3-months resolution)

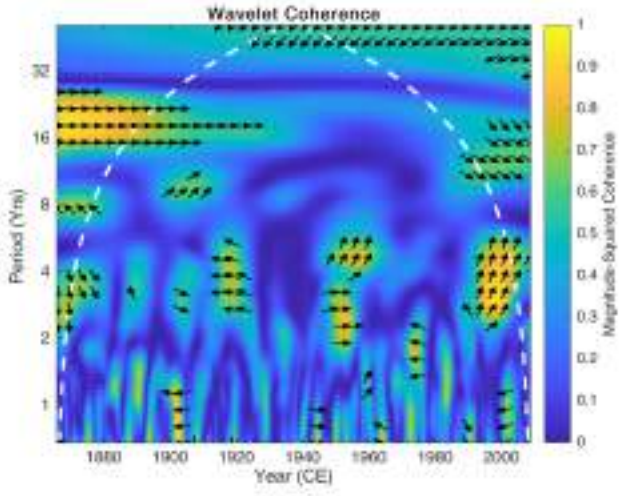

Figure 3.99 – SOI vs GV7(B) Sodium concentration record wavelet coherence analysis (1866 - 2009 CE time period, 3-months resolution)

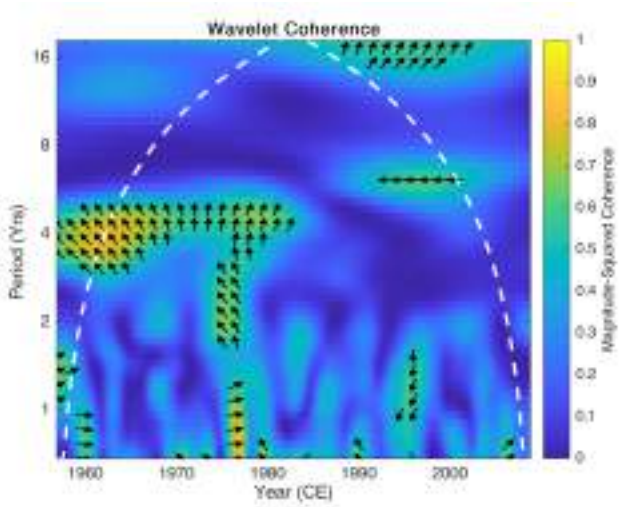

Figure 3.100 – SAM vs GV7(B) Sodium concentration record wavelet coherence analysis (1957 - 2009 CE time period, 3-months resolution)

flow in the extratropical Southern Hemisphere characterized by three high and three low-pressure centers. This has been shown to have a substantial impact on the heat transport and on the SIE (Raphael, 2004, 2007; Raphael and Hobbs, 2014) and it was, indeed, correlated with the decrease in sea ice in the most recent years (Raphael, 2007). It is a critical part in the monthly to inter-annual circulation (Trenberth, 1980) and the multidecadal variability evident in the SH was suggested to be related to variability in the strength and location of the ridges and troughs of ZW3 (Reason, 2000). Investigating the mechanism that bring the formation of the ZW3 is beyond the scope of this work, but it has been shown to be driven by zonally asymmetric deep convection in the tropics, and that extratropical orography and landmasses distribution have little influence over the ZW3 (Goyal et al., 2021). When comparing the ZW3 index with the MSA levels as reported in Figure 3.101, low levels of correlation were

found in general, especially considering high periods in the cross-wavelet spectrum. Minor correlation was found in the 1-year period section, but only for short periods of time (at most, three years) and only in the 1985 - 1995 CE range. Higher degree of agreement between the two series seems to be present when considering higher periods ($>$ 8 years), but the lack of a bigger dataset made impossible to investigate the possibility of a correlation with this periodicity. Once again, when considering the same approach with Sodium and Chloride as reported n Figure 3.102 and Figure 3.103, better degrees of correlation were found on the multi-annual periodicity (4- to 8-years), further consolidating the hypothesis of a reduced or at least not as prevalent influence of the distance to the sea (i.e. the SIE) in the final concentration of marine aerosol on site, and the importance of local circulation paths and metereology.

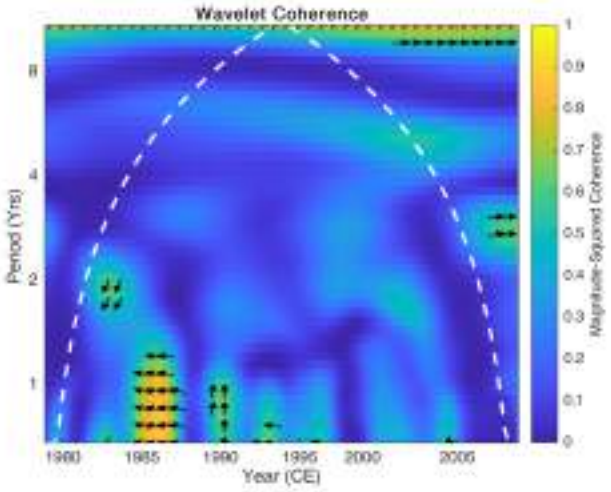

Figure 3.101 – ZW3 index vs GV7(B) MSA concentration record wavelet coherence analysis (1979 - 2009 CE time period, 3-months resolution)

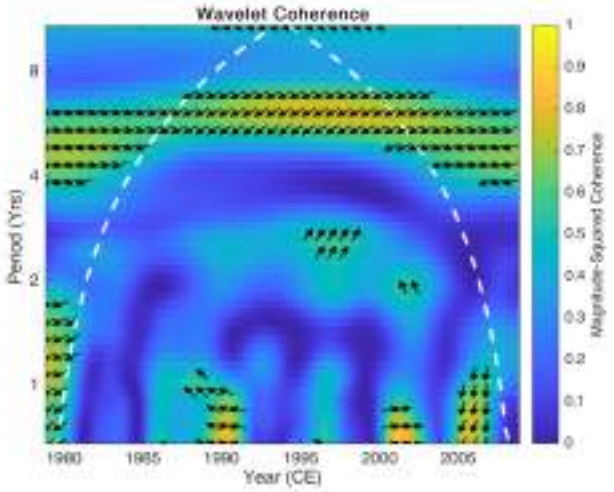

Figure 3.102 – ZW3 index vs GV7(B) Chloride concentration record wavelet coherence analysis (1979 - 2009 CE time period, 3-months resolution)

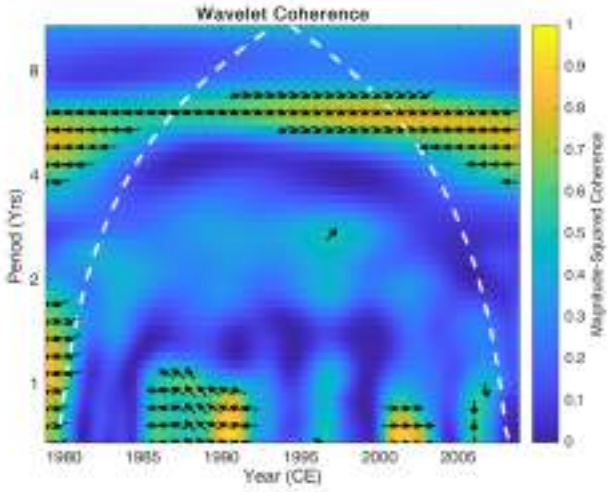

Figure 3.103 – ZW3 index vs GV7(B) Sodium concentration record wavelet coherence analysis (1979 - 2009 CE time period, 3-months resolution)

Chapter 4

Conclusions

Ice and firn cores, especially those drilled in the polar regions, have been proven throughout the years to be a key tool in understanding the past climate. The continuous and non-disturbed snow accumulation over the Antarctic ice sheet preserves the history of past atmospheric composition; by means of dry and wet deposition, chemicals and compounds are scavenged from the atmosphere and are locked in the ice of antarctica. By analyzing the chemical signal left in the ice, reconstructions of long-term records of temperature and atmospheric composition is possible, but in order to do so, an accurate dating is needed. In this work, a number of firn and ice samples drilled throughout the East Antarctic plateau were analyzed for ionic, metal content and other trace elements in order to investigate the spatial and temporal variability across this section of the continent and the last millennium. Both deep cores, shallow snow pits and surface snow samples were considered, with the drilling sites chosen both on the coast (GV7) and across the Antarctic plateau (Dome C and samples taken during the traverse that ended in the SP) in order to investigate different time scale and different resolutions.

Two steps are critical when it comes to using these kinds of samples for paleoclimatic studies: the first one is the need to obtain reliable, uncontaminated information (sometimes in the sub-ppb levels of concentration), the other is strictly related to the interpretation of the chemical signal, which is the need of having a reliable depth vs. age correlation (i.e. each ice layers has to be put in a temporal scale). Great care was therefore given during this work to optimize both steps. The DC3D ice cores' samples provided a unique opportunity to investigate the effect of external contamination introduced with different decontamination procedures: unlike other core, either too small in diameter or shared between different research group, the large amount of firn/ice made possible to split the sample in multiple parts and investigate which decontamination procedure was better suited for this samples in anticipation for future campaigns on the same site. At the same time, the volume of sample allowed for multiple analysis to be performed in the same lab in the context of this work with the purpose of dating. In particular, both ionic content, total conductivity and trace elements were used both for the DC3D and the GV7(B) core to ensure the most accurate dating. This was accomplished for the majority of the samples by relying on well know past volcanic eruptions, a well-established method in paleoclimatology to assign an accurate date to an ice layer. The presence of high levels of sulfuric acid due to the large amount of SO_2 emitted during an eruption makes possible to reliably identify in these records (signal vs. depth) and to date the core. But the GV7(B) ice core, due to the high snow accumulation on the site provided for a unique opportunity in itself to test different dating procedures (annual to sub-annual resolution) found in literature and optimize a dating for this core. In particular, both isotopic records, volcanic signatures (in both ionic and trace elements records), dust and tephra

levels and chemical records of seasonal markers (e.g. Sodium, MSA) were considered an used together to date the entirety of the 200m of core. Isotopic records are probably the most reliable ways of date ice cores at sub-annual resolution, but data for the GV7(B) core are scarce and isotopic analysis despite not requiring decontaminating the samples is more expensive and involved than ionic chromatography, making finding an alternative mandatory. Here the combination of $nssSO_4^{2-}$ and Na^+ records was used to date each layer in between know past volcanic eruptions. Dating of the different snow and ice samples did not only provide the opportunity to place each sample in a temporal scale, but also made possible to produce accurate records of the snow accumulation rate across the east Antarctic plateau. In particular it was possible to obtain annually resolved records of the snow accumulation on the GV7 site spanning most of the last millennium. Despite the number of projects across the continent, not many records cover this period, and the information of the snow accumulation, and therefore the surface mass balance of Antarctica, is still lacking. Here considerations on both the long term trend found in the accumulation on site and the one found in the last few decades were made, providing more insights on the variability of the continent in this key time period (the last two millennia) to understand its impact on the climate. Once this first step was accomplished, focus was shift on the interpretation of the chemical signals found in the deep cores and the other snow samples. The area spanning from Dome C and the south pole is still relatively unexplored and the EAIIST traverse's samples (both in the form of shallow snow pits and surface snow samples) represented a first opportunity to investigate the spatial variability of the ionic content in the Antarctic plateau. Particular interest was given to volatile acidic compounds, mainly in the form of HCl and HNO_3. Their concentration quickly diminishes

in the snow due to evaporation and re-emission processes and in this work these processes have been investigated in sites with different characteristic. The same general trend has been found throughout the plateau, with the estimated snow accumulation on site seemingly influencing the speed at which these volatile compounds are removed from the snow, but when compared to other records, concentration during the EAIIST traverse dropped faster than expecting. Lastly, attention was given to the interpretation of the chemical signals found in the GV7(B) ice core. Despite what's find in literature, no clear linear correlation was found between MSA records and the SIE, indicating that the relationship between primary phytoplanktonic production and the coverage of the sea during winter months is not as simple as thought. Indeed, a correlation seems present, and this was investigating using wavelet analysis in the context of finding a way of reconstructing the climate from chemical markers, at the same time, the same was done with atmospheric circulation indexes finding possible correlation between the ENSO phenomena and MSA levels in Antarctica.

Bibliography

N. J. Abram, E. W. Wolff, and M. A. Curran. A review of sea ice proxy information from polar ice cores. *Quaternary Science Reviews*, 79:168–183, 11 2013. ISSN 02773791. doi: 10.1016/j.quascirev.2013.01.011.

C. S. Allen, J. Pike, and C. J. Pudsey. Last glacial–interglacial sea-ice cover in the SW Atlantic and its potential role in global deglaciation. *Quaternary Science Reviews*, 30, 9 2011.

R. B. Alley, C. A. Shuman, D. A. Meese, A. J. Gow, K. C. Taylor, K. M, Cuffey, J. J. Fitzpatrick, P. M. Grootes, G. A. Zielinski, M. Ram, G. Spinelli, and B. Elder. Visual-stratigraphic dating of the GISP2 ice core: Basis, reproducibility, and application. *Journal of Geophysical Research: Oceans*, 102:26367–26381, 11 1997. ISSN 21699291. doi: 10.1029/96JC03837.

O. C. Allkofer and J. M. Fox. New Conceptions on the Meteorology of Stratospheric Fallout from Nuclear Weapon Tests. *Archiv fur Meteorologie, Geophysik und Bioklimatologie, Serie A*, 15:299–317, 1966.

J. A. C. Alvarado, P. Steinmann, S. Estier, F. Bochud, M. Haldimann, and P. Froidevaux. Anthropogenic radionuclides in atmospheric

air over Switzerland during the last few decades. *Nature Communications*, 5, 5 2014.

M. M. Arienzo, J. R. McConnell, N. Chellman, A. S. Criscitiello, M. Curran, D. Fritzsche, S. Kipfstuhl, R. Mulvaney, M. Nolan, T. Opel, M. Sigl, and J. Steffensen. A method for Continuous 239Pu Determinations in Arctic and Antarctic Ice Cores. *Environmental Science & Technology*, 50:7066–7073, 7 2016.

K. R. Arrigo, G. van Dijken, and S. Pabi. Impact of a shrinking Arctic ice cover on marine primary production. *Geophysical Research Letters*, 35, 10 2008.

L. Augustin, C. Barbante, P. Barnes, J. Barnola, M. Bigler, E. Castellano, O. Cattani, J. Chappellaz, D. DahlJensen, B. Delmonte, G. Dreyfus, G. Durand, S. Falourd, H. Fischer, J. Fluckiger, M. Hansson, P. Huybrechts, R. Jugie, S. Hohnsen, J. Jouzel, P. Kaufmann, J. Kipdstuhl, F. Lambert, V. Lipenkov, G. Littot, A. Longinelli, R. Lorrain, V. Maggi, V. Masson-Delmotte, H. Miller, R. Mulvaney, J. Oerlemans, H. Oerter, G. Orombellu, F. Parrenin, D. Peel, J. Petit, D. Raynaud, C. Ritz, U. Ruth, J. Schwander, U. Siegenthaler, R. Souchez, B. Stauffer, J. Steffensen, B. Stenni, T. Stocker, I. Tabacco, R. Udisti, R. van de Wal, M. van den Broeke, J. Weiss, F. Wilhelms, J. Winther, E. Wolff, M. Zucchelli, and E. Members. Eight glacial cycles from an Antarctic ice core. *Nature*, 429, 6 2004.

N. Baglan, C. Cossonnet, P. Pitet, D. Cavadore, L. Exmelin, and P. Berard. On the use of ICP-MS for measuring plutonium in urine. *Journal of Radioanalytical and Nuclear Chemistry*, 243:397–401, 2000. ISSN 02365731. doi: 10.1023/A:1016013811974.

S. Becagli, M. Proposito, S. Benassai, O. Flora, L. Genoni, R. Gragnani, O. Largiuni, S. L. Pili, M. Severi, B. Stenni, R. Traversi, R. Udisti, and M. Frezzotti. Chemical and isotopic snow variability in East Antarctica along the 2001/02 ITASE traverse. *Annals of Glaciology*, 39:473–482, 9 2004.

S. Becagli, E. Castellano, O. Cerri, M. Curran, M. Frezzotti, F. Marino, A. Morganti, M. Proposito, M. Severi, R. Traversi, and R. Udisti. Methanesulphonic acid (MSA) stratigraphy from a Talos Dome ice core as a tool in depicting sea ice changes and southern atmospheric circulation over the previous 140 years. *Atmospheric Environment*, 43:1051–1058, 2 2009.

S. Becagli, C. Scarchilli, R. Traversi, U. Dayan, M. Severi, D. Frosini, V. Vitale, M. Mazzola, A. Lupi, S. Nava, and R. Udisti. Study of present-day sources and transport processes affecting oxidised sulphur compounds in atmospheric aerosols at Dome C (Antarctica) from year-round sampling campaigns. *Atmospheric Environment*, 52:98–108, 6 2012. ISSN 13522310. doi: 10.1016/j.atmosenv.2011.07.053.

S. Becagli, L. Lazzara, C. Marchese, U. Dayan, S. E. Ascanius, M. Cacciani, L. Caiazzo, C. D. Biagio, T. D. Iorio, A. di Sarra, P. Eriksen, F. Fani, F. Giardi, D. Meloni, G. Muscari, G. Pace, M. Severi, R. Traversi, and R. Udisti. Relationships linking primary production, sea ice melting, and biogenic aerosol in the Arctic. *Atmospheric Environment*, 136:1–15, 7 2016. ISSN 18732844. doi: 10.1016/j.atmosenv.2016.04.002.

S. Benassai, S. Becagli, R. Gragnani, O. Magand, M. Proposito, I. Fattori, R. Traversi, and R. Udisti. Sea-spray deposition in

Antarctic coastal and plateau areas from ITASE traverses. *Annals of Glaciology*, 41:32–40, 9 2005.

M. H. Bergin, E. A. Meyerson, J. E. Dibb, and P. A. Mayewski. Relationship between continuous aerosol measurements and firn core chemistry over a 10-year period at the South Pole. *Geophysical Research Letters*, 25:1189–1192, 4 1998.

T. A. Berhanu, C. Meusinger, J. Erbland, R. Jost, S. K. Bhattacharya, M. S. Johnson, and J. Savarino. Laboratory study of nitrate photolysis in Antarctic snow. II. Isotopic effects and wavelength dependence. *The Journal of Chemical Physics*, 140, 6 2014.

T. A. Berhanu, J. Savarino, J. Erbland, W. C. Vicars, S. Preunkert, J. F. Martins, and M. S. Johnson. Isotopic effects of nitrate photochemistry in snow: a field study at Dome C, Antarctica. *Atmospheric Chemistry and Physics*, 15, 10 2015.

S. Bertinetti, F. Ardini, M. A. Vecchio, L. Caiazzo, and M. Grotti. Isotopic analysis of snow from Dome C indicates changes in the source of atmospheric lead over the last fifty years in East Antarctica. *Chemosphere*, 255:126858, 9 2020.

N. A. N. Bertler. El nino suppresses Antarctic warming. *Geophysical Research Letters*, 31:L15207, 2004.

N. A. N. Bertler, T. R. Naish, P. A. Mayewski, and P. J. Barrett. Opposing oceanic and atmospheric ENSO influences on the Ross Sea Region, Antarctica. *Advances in Geosciences*, 6:83–86, 1 2006.

H. J. M. Bowen. *Environmental chemistry of the elements*. Academic Press, 1979.

E. J. Brook. Ice Core Methods | Overview. *Encyclopedia of Quaternary Science*, pages 1145–1156, 2007.

L. Caiazzo, S. Becagli, D. Frosini, F. Giardi, M. Severi, R. Traversi, and R. Udisti. Spatial and temporal variability of snow chemical composition and accumulation rate at Talos Dome site (East Antarctica). *Science of the Total Environment*, 550:418–430, 4 2016. ISSN 18791026. doi: 10.1016/j.scitotenv.2016.01.087.

L. Caiazzo, G. Baccolo, C. Barbante, S. Becagli, M. Bertò, V. Ciardini, I. Crotti, B. Delmonte, G. Dreossi, M. Frezzotti, J. Gabrieli, F. Giardi, Y. Han, S.-B. Hong, S. Hur, H. Hwang, J.-H. Kang, B. Narcisi, M. Proposito, C. Scarchilli, E. Selmo, M. Severi, A. Spolaor, B. Stenni, R. Traversi, and R. Udisti. Prominent features in isotopic, chemical and dust stratigraphies from coastal East Antarctic ice sheet (Eastern Wilkes Land). *Chemosphere*, 176: 273–287, 6 2017.

J.-P. Candelone, M. A. Bolshov, S. N. Rudniev, S. Hong, and C. F. Boutron. Bismuth in recent snow from Central Greenland: Preliminary results. *Atmospheric Environment*, 29, 8 1995.

A. M. Caruana and G. Malin. The variability in DMSP content and DMSP lyase activity in marine dinoflagellates. *Progress in Oceanography*, 120, 1 2014.

E. Castellano, S. Becagli, J. Jouzel, A. Migliori, M. Severi, J. P. Steffensen, R. Traversi, and R. Udisti. Volcanic eruption frequency over the last 45 ky as recorded in EPICA-Dome C ice core (East Antarctica) and its relationship with climatic changes. *Global and Planetary Change*, 42:195–205, 7 2004. ISSN 09218181. doi: 10.1016/j.gloplacha.2003.11.007.

E. Castellano, S. Becagli, M. Hansson, M. Hutterli, J. R. Petit, M. R. Rampino, M. Severi, J. P. Steffensen, R. Traversi, and R. Udisti. Holocene volcanic history as recorded in the sulfate stratigraphy of

the European Project for Ice Coring in Antarctica Dome C (EDC96) ice core. *Journal of Geophysical Research D: Atmospheres*, 110: 1–12, 3 2005. ISSN 01480227. doi: 10.1029/2004JD005259.

D. J. Cavalieri and C. L. Parkinson. Antarctic sea ice variability and trends, 1979 - 2006. *Journal of Geophysical Research: Oceans*, 113: C07004, 2008.

W. Chisholm, K. Rosman, C. Boutron, J. Candelone, and S. Hong. Determination of lead isotopic ratios in Greenland and Antarctic snow and ice at picogram per gram concentrations. *Analytica Chimica Acta*, 311:141–151, 7 1995.

J. Cole-Dai and E. Mosley-Thompson. The Pinatubo eruption in South Pole snow and its potential value to ice-core paleovolcanic records. *Annals of Glaciology*, 29:99–105, 1999. doi: https://doi.org/10.3189/172756499781821319.

J. Cole-Dai, E. Mosley-Thompson, and L. G. Thompson. Annually resolved southern hemisphere volcanic history from two Antarctic ice cores. *Journal of Geophysical Research Atmospheres*, 102:16761–16771, 7 1997. ISSN 01480227. doi: 10.1029/97jd01394.

J. C. Comiso, R. A. Gersten, L. V. Stock, J. Turner, G. J. Perez, and K. Cho. Positive Trend in the Antarctic Sea Ice Cover and Associated Changes in Surface Temperature. *Journal of Climate*, 30:2251–2267, 3 2017.

K. M. Cuffey and S. J. Eric. Isotopic diffusion in polar firn: itnplications for interpretation of seasonal clitnate paratneters in ice-core records, with etnphasis on central Greenland. *Journal of Glaciology*, 44:273–284, 1998.

M. A. J. Curran. Ice Core Evidence for Antarctic Sea Ice decline since the 1950s. *Science*, 302, 11 2003.

G. A. Cutter, K. W. Bruland, and R. W. Risebrough. Deposition and accumulation of plutonium isotopes in Antarctica. *Nature*, 5714:628 – 629, 1979.

J. Dai, E. Mosley-Thompson, and L. G. Thompson. *Journal of Geophysical Research.*

W. Dansgaard. Stable isotopes in precipitation. *Tellus*, 16:436–468, 11 1964. ISSN 00402826. doi: 10.1111/j.2153-3490.1964.tb00181.x.

G. de Leeuw, E. L. Andreas, M. D. Anguelova, C. W. Fairall, E. R. Lewis, C. O'Dowd, M. Schulz, and S. E. Schwartz. Production flux of sea spray aerosol. *Reviews of Geophysics*, 49, 5 2011.

R. M. DeConto and D. Pollard. Contribution of Antarctica to past and future sea-level rise. *Nature*, 531, 3 2016.

L. Deleebeeck, J. Avnskjold, and A. Snedden. Short- and long-term stability of electrolytic conductivity certified reference materials. *Accreditation and Quality Assurance*, 25, 4 2020.

R. J. Delmas, M. Legrand, A. J. Aristarain, and F. Zanolini. Volcanic deposits in Antarctic snow and ice. *Journal of Geophysical Research*, 90:12901, 1985.

R. J. Delmas, S. Kirchner, J. M. Palais, and J.-R. Petit. 1000 years of explosive volcanism recorded at the South Pole. *Tellus B: Chemical and Physical Meteorology*, 44:335–350, 1 1992.

B. Delmonte, J. Petit, and V. Maggi. Glacial to Holocene implications of the new 27000-year dust record from the EPICA Dome C (East Antarctica) ice core. *Climate Dynamics*, 18:647–660, 2002.

B. Delmonte, B. Giovanni, M. Fausto, Y. Iizuka, and M. Valter. Dust flux in peripheral East Antarctica: preliminary results from GV7 ice core and extension of the TALDICE dust record to the sub-micron range. *Geophysical Research Abstracts*, 17:2015–2375, 2015.

J. E. Dibb and S. I. Whitlow. Recent climate anomalies and their impact on snow chemistry at south pole, 1987-1994. *Geophysical Research Letters*, 23, 5 1996.

J. E. Dibb, R. W. Talbot, J. W. Munger, D. J. Jacob, and S. M. Fan. Air-snow exchange of HNO3 and NOy at Summit, Greenland. *Journal of Geophysical Research Atmospheres*, 103:3475–3486, 2 1998. ISSN 01480227. doi: 10.1029/97JD03132.

G. Dreschhoff and E. J. Zeller. Ultra-High Resolution Nitrate in Polar Ice as Indicator of Past Solar Activity. *Solar Electromagnetic Radiation Study for Solar Cycle*, 22:365–374, 1998.

J. A. Eddy. The Maunder Minimum. *Science*, 192:1189–1202, 1976.

M. Eisenbud and T. Gesell. *Environmental Radioactivity*. Academic Press, 4th edition, 1997.

A. A. Ekaykin, D. O. Vladimirova, V. Y. Lipenkov, and V. Masson-Delmotte. Climatic variability in Princess Elizabeth Land (East Antarctica) over the last 350 years. *Climate of the Past*, 13, 1 2017.

S. Epstein and T. Mayeda. Variation of o18 content of waters from natural sources. *Geochimica et Cosmochimica Acta*, 4, 11 1953.

J. Erbland, W. C. Vicars, J. Savarino, S. Morin, M. M. Frey, D. Frosini, E. Vince, and J. M. Martins. Air-snow transfer of

nitrate on the East Antarctic Plateau - Part 1: Isotopic evidence for a photolytically driven dynamic equilibrium in summer. *Atmospheric Chemistry and Physics*, 13:6403–6419, 2013. ISSN 16807316. doi: 10.5194/acp-13-6403-2013.

T. Extier, A. Landais, C. Bréant, F. Prie, L. Bazin, G. Dreyfus, D. M. Roche, and M. Leuenberger. On the use of δ18oatm for ice core dating. *Quaternary Science Reviews*, 185:244–257, 4 2018.

J. T. Fasullo, R. Tomas, S. Stevenson, B. Otto-Bliesner, E. Brady, and E. Wahl. The amplifying influence of increased ocean stratification on a future year without a summer. *Nature Communications*, 8: 1236, 12 2017.

D. G. Ferris, J. Cole-Dai, A. R. Reyes, and D. M. Budner. South pole ice core record of explosive volcanic eruptions in the first and second millennia A.D. and evidence of a large eruption in the tropics around 535 A.D. *Journal of Geophysical Research*, 116: D17308, 9 2011.

H. Fischer, F. Fundel, U. Ruth, B. Twarloh, A. Wegner, R. Udisti, S. Becagli, E. Castellano, A. Morganti, M. Severi, E. Wolff, G. Littot, R. Röthlisberger, R. Mulvaney, M. A. Hutterli, P. Kaufmann, U. Federer, F. Lambert, M. Bigler, M. Hansson, U. Jonsell, M. de Angelis, C. Boutron, M. L. Siggaard-Andersen, J. P. Steffensen, C. Barbante, V. Gaspari, P. Gabrielli, and D. Wagenbach. Reconstruction of millennial changes in dust emission, transport and regional sea ice coverage using the deep EPICA ice cores from the Atlantic and Indian Ocean sector of Antarctica. *Earth and Planetary Science Letters*, 260:340–354, 8 2007.

A. F. Foster, M. A. Curran, B. T. Smith, T. D. V. Ommen, and V. I. Morgan. Covariation of Sea Ice and methanesulphonic acid

in Wilhelm II Land, East Antarctica. *Annals of Glaciology*, 44, 9 2006.

P. Fretwell, H. D. Pritchard, D. G. Vaughan, J. L. Bamber, N. E. Barrand, R. Bell, C. Bianchi, R. G. Bingham, D. D. Blankenship, G. Casassa, G. Catania, D. Callens, H. Conway, A. J. Cook, H. F. J. Corr, D. Damaske, V. Damm, F. Ferraccioli, R. Forsberg, S. Fujita, Y. Gim, P. Gogineni, J. A. Griggs, R. C. A. Hindmarsh, P. Holmlund, J. W. Holt, R. W. Jacobel, A. Jenkins, W. Jokat, T. Jordan, E. C. King, J. Kohler, W. Krabill, M. Riger-Kusk, K. A. Langley, G. Leitchenkov, C. Leuschen, B. P. Luyendyk, K. Matsuoka, J. Mouginot, F. O. Nitsche, Y. Nogi, O. A. Nost, S. V. Popov, E. Rignot, D. M. Rippin, A. Rivera, J. Roberts, N. Ross, M. J. Siegert, A. M. Smith, D. Steinhage, M. Studinger, B. Sun, B. K. Tinto, B. C. Welch, D. Wilson, D. A. Young, C. Xiangbin, and A. Zirizzotti. Bedmap2: improved ice bed, surface and thickness datasets for Antarctica. *The Cryosphere*, 7, 2 2013.

M. Frezzotti, S. Urbini, M. Proposito, C. Scarchilli, and S. Gandolfi. Spatial and temporal variability of surface mass balance near Talos Dome, East Antarctica. *Journal of Geophysical Research: Earth Surface*, 112, 6 2007.

M. Frezzotti, C. Scarchilli, S. Becagli, M. Proposito, and S. Urbini. A synthesis of the Antarctic surface mass balance during the last 800 yr. *The Cryosphere*, 7, 2 2013.

F. Fundel, H. Fischer, R. Weller, F. Traufetter, H. Oerter, and H. Miller. Influence of large-scale teleconnection patterns on methane sulfonate ice core records in Dronning Maud Land. *Journal of Geophysical Research*, 111, 2006.

J. Gabrieli, G. Cozzi, P. Vallelonga, M. Schwikowski, M. Sigl, C. Boutron, and C. Barbante. Historical reconstruction of Plutonium contamination in the Swiss-Italian Alps. *E3S Web of Conferences*, 1:14001, 4 2013.

P. Gabrielli, C. Barbante, C. Turetta, A. Marteel, C. Boutron, G. Cozzi, W. Cairns, C. Ferrari, and P. Cescon. Direct Determination of Rare Earth Elements at the Subpicogram per Gram Level in Antarctic Ice by ICP-SFMS Using a Desolvation System. *Analytical Chemistry*, 78:1883–1889, 3 2006.

A. Galuszka and Z. Migaszewski. *Chemical Signals of the Anthropocene*. 2017.

M. Galí and R. Simó. Occurrence and cycling of dimethylated sulfur compounds in the Arctic during summer receding of the ice edge. *Marine Chemistry*, 122, 10 2010.

C. Gao, A. Robock, S. Self, J. B. Witter, J. P. Steffenson, H. B. Clausen, M.-L. Siggaard-Andersen, S. Johnsen, P. A. Mayewski, and C. Ammann. The 1452 or 1453 A.D. Kuwae eruption signal derived from multiple ice core records: Greatest volcanic sulfate event of the past 700 years. *Journal of Geophysical Research*, 111: D12107, 2006.

C. Gao, L. Oman, A. Robock, and G. L. Stenchikov. Atmospheric volcanic loading derived from bipolar ice cores: Accounting for the spatial distribution of volcanic deposition. *Journal of Geophysical Research*, 112:D09109, 5 2007.

R. Goyal, M. Jucker, A. S. Gupta, H. H. Hendon, and M. H. England. Zonal wave 3 pattern in the Southern Hemisphere generated by tropical convection. *Nature Geoscience*, 14:732–738, 10 2021.

A. M. Grannas, A. E. Jones, J. Dibb, M. Ammann, C. Anastasio, H. J. Beine, M. Bergin, J. Bottenheim, C. S. Boxe, G. Carver, G. Chen, J. H. Crawford, F. Dominé, M. M. Frey, M. I. Guzmán, D. E. Heard, D. Helmig, M. R. Hoffmann, R. E. Honrath, L. G. Huey, M. Hutterli, H. W. Jacobi, P. Klán, B. Lefer, J. Mcconnell, J. Plane, R. Sander, J. Savarino, P. B. Shepson, W. R. Simpson, J. R. Sodeau, R. V. Glasow, R. Weller, E. W. Wolff, and T. Zhu. An overview of snow photochemistry: evidence, mechanisms and impacts. *European Geosciences Union*, 7:4329–4373, 2007.

C. U. Hammer. Acidity of Polar Ice Cores in Relation to Absolute Dating, Past Volcanism, and Radio–Echoes. *Journal of Glaciology*, 25:359–372, 1980.

C. U. Hammer. Initial Direct Current in the Buildup of Space Charges and the Acidity of Ice Cores. *Journal of Physical Chemistry*, 87: 4099–4103, 1983.

C. U. Hammer, H. B. Clausen, and W. Dansgaard. Greenland ice sheet evidence of post-glacial volcanism and its climatic impact. *Nature*, 288:230–235, 1980.

E. P. Hardy, P. W. Krey, and H. L. Volchok. Global Inventory and Distribution of Fallout Plutonium. *Nature*, 241, 2 1973.

L. H. Hartman, A. V. Kurbatov, D. A. Winski, A. M. Cruz-Uribe, S. M. Davies, N. W. Dunbar, N. A. Iverson, M. Aydin, J. M. Fegyveresi, D. G. Ferris, T. J. Fudge, E. C. Osterberg, G. M. Hargreaves, and M. G. Yates. Volcanic glass properties from 1459 C.E. volcanic event in South Pole ice core dismiss Kuwae caldera as a potential source. *Scientific Reports*, 9:14437, 12 2019.

M. M. Herron and C. C. Langway. Dating of Ross Ice Shelf Core by chemical analysis. *Journal of Glaciology*, 24, 1979.

C. Holme, V. Gkinis, M. Lanzky, V. Morris, M. Olesen, A. Thayer, B. H. Vaughn, and B. M. Vinther. Varying regional d18o–temperature relationship in high-resolution stable water isotopes from east Greenland. *Climate of the Past*, 15, 5 2019.

R. W. Hurst, T. E. Davis, and B. D. Chinn. Lead fingerprints of gasoline contamination. pages 304A – 307A, 1996.

H. Hwang, S. D. Hur, J. Lee, Y. Han, S. Hong, and H. Motoyama. Plutonium fallout reconstructed from an Antarctic Plateau snowpack using inductively coupled plasma sector field mass spectrometry. *Science of the Total Environment*, 669:505–511, 6 2019.

M. Igarashi, Y. Nakai, Y. Motizuki, K. Takahashi, H. Motoyama, and K. Makishima. Dating of the Dome Fuji shallow ice core based on a record of volcanic eruptions from AD 1260 to AD 2001. *Polar Science*, 5:411–420, 12 2011.

E. Isaksson, W. Karlén, P. Mayewski, M. Twickler, and S. Whitlow. A high-altitude snow chemistry record from Amundsenisen, Dronning Maud Land, Antarctica. *Journal of Glaciology*, 47, 9 2001.

E. Isaksson, T. Kekonen, J. Moore, and R. Mulvaney. The methanesulfonic acid (MSA) record in a Svalbard ice core. *Annals of Glaciology*, 42:345–351, 9 2005.

S. Jiang, G. Shi, J. Cole-Dai, L. Geng, D. G. Ferris, C. An, and Y. Li. Nitrate preservation in snow at Dome A, East Antarctica from ice core concentration and isotope records. *Atmospheric Environment*, 213:405–412, 9 2019.

A. E. Jones, R. Weller, A. Minikin, E. W. Wolff, W. T. Sturges, H. P. McIntyre, S. R. Leonard, O. Schrems, and S. Bauguitte. Oxidized nitrogen chemistry and speciation in the Antarctic troposphere. *Journal of Geophysical Research: Atmospheres*, 104, 9 1999.

B. Jourdain and M. Legrand. Seasonal variations of atmospheric dimethylsulfide, dimethylsulfoxide, sulfur dioxide, methanesulfonate, and non-sea-salt sulfate aerosols at Dumont d'Urville (coastal Antarctica) (December 1998 to July 1999). *Journal of Geophysical Research: Atmospheres*, 106:14391–14408, 7 2001.

J. Jouzel and V. Masson-Delmotte. Deep ice cores: the need for going back in time. *Quaternary Science Reviews*, 29, 12 2010.

J. Jouzel and L. Merlivat. Deuterium and Oxygen 18 in precipitation: Modeling of the isotopic effects during snow formation. *Journal of Geophysical Research*, 89, 1984.

D. Karoly. El nino — historical and paleoclimatic aspects of the southern oscillation edited by henry f. diaz and vera markgraf cambridge university press (1992). *Antarctic Science*, 5(4):411–411, 1993. doi: 10.1017/S0954102093210550.

M. D. Keller, W. K. Bellows, and R. R. L. Guillard. *Dimethyl Sulfide Production in Marine Phytoplankton*, pages 167–182. 1989. doi: 10.1021/bk-1989-0393.ch011.

T. Kellerhals, L. Tobler, S. Brütsch, M. Sigl, L. Wacker, H. W. Gäggeler, and M. Schwikowski. Thallium as a Tracer for Preindustrial Volcanic Eruptions in an Ice Core Record from Illimani, Bolivia. *Environmental Science & Technology*, 44, 2 2010.

A. J. Kettle and M. O. Andreae. Flux of dimethylsulfide from

the oceans: A comparison of updated data sets and flux models. *Journal of Geophysical Research: Atmospheres*, 105, 11 2000.

G. N. Kiladis and H. F. Diaz. Global Climatic Anomalies Associated with Extremes in the Southern Oscillation. *Journal of Climate*, 2: 1069–1090, 9 1989.

G. E. Kocharov, I. V. Kudryavtsev, M. G. Ogurtsov, E. Sonninen, and H. Jungner. The nitrate content of Greenland ice and solar activity. *Astronomy Reports*, 44, 12 2000.

B. G. Koffman, E. G. Dowd, E. C. Osterberg, D. G. Ferris, L. H. Hartman, S. D. Wheatley, A. V. Kurbatov, G. J. Wong, B. R. Markle, N. W. Dunbar, K. J. Kreutz, and M. Yates. Rapid transport of ash and sulfate from the 2011 Puyehue-Cordon Caulle (Chile) eruption to West Antarctica. *Journal of Geophysical Research: Atmospheres*, 122:8908–8920, 8 2017.

S. Kremser, L. W. Thomason, M. von Hobe, M. Hermann, T. Deshler, C. Timmreck, M. Toohey, A. Stenke, J. P. Schwarz, R. Weigel, S. Fueglistaler, F. J. Prata, J.-P. Vernier, H. Schlager, J. E. Barnes, J.-C. A. na Marrero, D. Fairlie, M. Palm, E. Mahieu, J. Notholt, M. Rex, C. Bingen, F. Vanhellemont, A. Bourassa, J. M. C. Plane, D. Klocke, S. A. Carn, L. Clarisse, T. Trickl, R. Neely, A. D. James, L. Rieger, J. C. Wilson, and B. Meland. Stratospheric aerosol-Observations, processes, and impact on climate. *Reviews of Geophysics*, 54, 6 2016.

G. Krinner, O. Magand, I. Simmonds, C. Genthon, and J. L. Dufresne. Simulated Antarctic precipitation and surface mass balance at the end of the twentieth and twenty-first centuries. *Climate Dynamics*, 28:215–230, 2 2007.

R. Kwok and J. C. Comiso. Southern ocean climate and sea ice anomalies associated with the southern oscillation. *Journal of Climate*, 15:487–501, 2002. URL `https://ntrs.nasa.gov/search.jsp?R=20010028707`.

H. H. Lamb. Volcanic Dust in the atmosphere; with a chronology and assessment of its meteorological. *Philosophical Transactions of the Royal Society of London. Series A, Mathematical and Physical Sciences*, 266:425–533, 1970.

F. Lambert, B. Delmonte, J. R. Petit, M. Bigler, P. R. Kaufmann, M. A. Hutterli, T. F. Stocker, U. Ruth, J. P. Steffensen, and V. Maggi. Dust-climate coupling over the past 800 000 years from the EPICA Dome C ice core. *Nature*, 452:616–619, 2008.

G. Lambert, B. Ardouin, and Mesbah-Bendezu. *Atmosphere to snow transfers in Antarctica*. United States: Elsevier Science Publishing Co, Inc., 1983.

C. C. Langway, K. Osada, H. B. Clausen, C. U. Hammer, and H. Shoji. A 10-century comparison of prominent bipolar volcanic events in ice cores. *Journal of Geophysical Research*, 100:16241, 1995.

C. Leck and C. Persson. Seasonal and short-term variability in dimethyl sulfide, sulfur dioxide and biogenic sulfur and sea salt aerosol particles in the arctic marine boundary layer during summer and autumn. *Tellus B: Chemical and Physical Meteorology*, 48, 1 1996.

W. Lefebvre. Influence of the Southern Annular Mode on the sea ice–ocean system. *Journal of Geophysical Research*, 109, 2004.

M. Legrand and P. Mayewski. Glaciochemistry of polar ice cores: A review. *Reviews of Geophysics*, 35:219–243, 1997. ISSN 87551209. doi: 10.1029/96RG03527.

M. Legrand, C. Feniet-Saigne, E. S. Sattzman, C. Germain, N. I. Barkov, and V. N. Petrov. Ice-core record of oceanic emissions of dimethylsulphide during the last climate cycle. *Nature*, 350, 3 1991.

M. Legrand, E. Wolff, and D. Wagenbach. Antarctic aerosol and snowfall chemistry: implications for deep Antarctic ice-core chemistry. *Annals of Glaciology*, 29:66–72, 1999.

M. R. Legrand and R. J. Delmas. The ionic balance of Antarctic snow: A 10-year detailed record. *Atmospheric Environment*, 18: 1867–1874, 1984.

M. R. Legrand and R. J. Delmas. Relative contributions of tropospheric and stratospheric sources to nitrate in Antarctic snow. *Tellus B*, 38 B:236–249, 1986. ISSN 16000889. doi: 10.1111/j.1600-0889.1986.tb00190.x.

M. R. Legrand and S. Kirchner. Origins and variations of Nitrate in South Polar precipitation. *Journal of Geophysical Research*, 95, 1990.

M. Levasseur, M. Gosselin, and S. Michaud. A new source of dimethylsulfide (DMS) for the arctic atmosphere: ice diatoms. *Marine Biology*, 121, 12 1994.

J. G. Levine, X. Yang, A. E. Jones, and E. W. Wolff. Sea salt as an ice core proxy for past sea ice extent: A process-based model study. *Journal of Geophysical Research: Atmospheres*, 119, 5 2014.

J. Löndahl. Physical and Biological properties of Bioaerosols. *Bioaerosol Detection Technologies*, pages 33–48, 2014.

O. Magand, M. Frezzotti, M. Pourchet, B. Stenni, L. Genoni, and M. Fily. Climate variability along latitudinal and longitudinal transects in East Antarctica. *Annals of Glaciology*, 39:351–358, 2004.

L. Marshall, A. Schmidt, M. Toohey, K. S. Carslaw, G. W. Mann, M. Sigl, M. Khodri, C. Timmreck, D. Zanchettin, W. T. Ball, S. Bekki, J. Brooke, S. Dhomse, C. Johnson, J. F. Lamarque, A. N. Legrande, M. J. Mills, U. Niemeier, J. O. Pope, V. Poulain, A. Robock, E. Rozanov, A. Stenke, T. Sukhodolov, S. Tilmes, K. Tsigaridis, and F. Tummon. Multi-model comparison of the volcanic sulfate deposition from the 1815 eruption of Mt. Tambora. *Atmospheric Chemistry and Physics*, 18:2307–2328, 2 2018.

E. A. Martell. The size distribution and interaction of radioactive and natural aerosols in the stratosphere. *Tellus*, 18:486–498, 8 1966.

J. Masarik and J. Beer. An updated simulation of particle fluxes and cosmogenic nuclide production in the Earth's atmosphere. *Journal of Geophysical Research*, 114, 6 2009.

F. Maupetit and R. J. Delmas. Chemical composition of Falling Snow at Dumont D'Urville, Antarctica. *Journal of Atmospheric Chemistry*, 14:31–42, 1992.

J. R. McConnell, O. J. Maselli, M. Sigl, P. Vallelonga, T. Neumann, H. Anschütz, R. C. Bales, M. A. J. Curran, S. B. Das, R. Edwards, S. Kipfstuhl, L. Layman, and E. R. Thomas. Antarctic-wide array

of high-resolution ice core records reveals pervasive lead pollution began in 1889 and persists today. *Scientific reports*, page 5848.

L. M. McInnes, D. S. Covert, P. K. Quinn, and M. S. Germani. Measurements of chloride depletion and sulfur enrichment in individual sea-salt particles collected from the remote marine boundary layer. *Journal of Geophysical Research*, 99:8257, 1994.

B. Mendoza. Total solar irradiance and climate. *Advances in Space Research*, 35:882–890, 1 2005.

C. Meusinger, T. A. Berhanu, J. Erbland, J. Savarino, and M. S. Johnson. Laboratory study of nitrate photolysis in Antarctic snow. i. observed quantum yield, domain of photolysis, and secondary chemistry. *The Journal of Chemical Physics*, 140, 6 2014.

E. A. Meyerson, P. A. Mayewski, K. J. Kreutz, L. D. Meeker, S. I. Whitlow, and M. S. Twickler. The polar expression of ENSO and sea-ice variability as recorded in a South Pole ice core. *Annals of Glaciology*, 35, 9 2002.

J. C. Moore, H. Nar1ta, and N. Maeno. A continuous 770-year record of Volcanic Activity from East Antarctica. *JOURNAL OF GEOPHYSICAL RESEARCH*, 96:353–370, 1991.

A. Morganti, S. Becagli, E. Castellano, M. Severi, R. Traversi, and R. Udisti. An improved flow analysis-ion chromatography method for determination of cationic and anionic species at trace levels in Antarctic ice cores. *Analytica Chimica Acta*, 603:190–198, 11 2007.

R. Mulvaney and E. W. Wolff. Spatial variability of the major chemistry of the Antarctic ice sheet. *Annals of Glaciology*, 20: 440–447, 1994.

R. Mulvaney, D. Wagenbach, and E. W. Wolff. Postdepositional change in snowpack nitrate from observation of year-round near-surface snow in coastal Antarctica. *Journal of Geophysical Research: Atmospheres*, 103, 5 1998.

B. Narcisi and J.-R. Petit. *Volcanism in Antarctica: 200 Million Years of Subduction, Rifting and Continental Break-Up*. Geological Society, 2021.

B. Narcisi, M. Proposito, and M. Frezzotti. Ice record of a 13th century explosive volcanic eruption in northern Victoria Land, East Antarctica. *Antarctic Science*, 13:174–181, 6 2001.

B. Narcisi, J. R. Petit, B. Delmonte, C. Scarchilli, and B. Stenni. A 16,000-yr tephra framework for the Antarctic ice sheet: A contribution from the new Talos Dome Core. *Quaternary Science Reviews*, 49:52–63, 8 2012.

B. Narcisi, J. R. Petit, B. Delmonte, V. Batanova, and J. Savarino. Multiple sources for tephra from AD 1259 volcanic signal in Antarctic ice cores. *Quaternary Science Reviews*, 210:164–174, 2019.

R. Nardin, A. Amore, S. Becagli, L. Caiazzo, M. Frezzotti, M. Severi, B. Stenni, and R. Traversi. Volcanic Fluxes Over the Last Millennium as Recorded in the Gv7 Ice Core (Northern Victoria Land, Antarctica). *Geosciences*, 10:38, 1 2020.

R. Nardin, M. Severi, A. Amore, S. Becagli, F. Burgay, L. Caiazzo, V. Ciardini, G. Dreossi, M. Frezzotti, S.-B. Hong, I. Khan, B. M. Narcisi, M. Proposito, C. Scarchilli, E. Selmo, A. Spolaor, B. Stenni, and R. Traversi. Dating of the GV7 East Antarctic ice core by high-resolution chemical records and focus on the accumulation

rate variability in the last millennium. *Climate of the Past*, pages 2073–2089, 2021.

A. Neftel, J. Beer, H. Oeschger, F. Zürcher, and R. C. Finkel. Sulphate and nitrate concentrations in snow from South Greenland 1895–1978. *Nature*, 314:611–613, 4 1985.

C. G. Newhall and S. Self. The volcanic explosivity index (VEI): an estimate of explosive magnitude for historical volcanism. *Journal of Geophysical Research*, 87:123–1238, 1982. ISSN 01480227. doi: 10.1029/jc087ic02p01231.

D. Noone and S. Ian. Sea ice control of water isotope transport to Antarctica and implications for ice core interpretation. *Journal of Geophysical Research*, 109, 2004.

K. Noro and N. Takenaka. Post-depositional loss of nitrate and chloride in Antarctic snow by photolysis and sublimation: a field investigation. *Polar Research*, 39, 12 2020.

Y. Nozaki. A fresh look at element distribution in the North Pacific Ocean. *Eos*, 78:221, 1997.

Y. Nyamgerel, Y. Han, S. Kim, S.-B. Hong, J. Lee, and S. D. Hur. Chronological characteristics for snow accumulation on Styx Glacier in northern Victoria Land, Antarctica. *Journal of Glaciology*, pages 1–11, 8 2020.

M. K. Obryk, A. G. Fountain, P. T. Doran, W. B. Lyons, and R. Eastman. Drivers of solar radiation variability in the McMurdo Dry Valleys, Antarctica. *Scientific Reports*, 8, 12 2018.

J. O'Dwyer, E. Isaksson, T. Vinje, T. Jauhiainen, J. Moore, V. Pohjola, R. Vaikmäe, and R. S. W. van de Wal. Methanesulfonic acid

in a Svalbard Ice Core as an indicator of ocean climate. *Geophysical Research Letters*, 27, 4 2000.

C. Oppenheimer. Climatic, environmental and human con sequences of the largest known historic eruption: Tambora volcano (Indonesia) 1815. *Progress in Physical Geography*, 27:230–259, 6 2003.

M. Osman, S. B. Das, O. Marchal, and M. J. Evans. Methanesulfonic acid (MSA) migration in polar ice: data synthesis and theory. *The Cryosphere*, 11:2439–2462, 11 2017.

C. L. Parkinson and D. J. Cavalieri. Antarctic sea ice variability and trends, 1979–2010. *The Cryosphere*, 6:871–880, 8 2012.

F. Parrenin, J. Jouzel, C. Waelbroeck, C. Ritz, and J.-M. Barnola. Dating the Vostok ice core by an inverse method. *Journal of Geophysical Research: Atmospheres*, 106, 12 2001.

F. Parrenin, F. Rèmy, C. Ritz, M. J. Siegert, and J. Jouzel. New modeling of the Vostok ice flow line and implication for the glaciological chronology of the Vostok ice core. *Journal of Geophysical Research*, 109:D20102–undefined, 2004.

E. C. Pasteur, R. Mulvaney, D. A. Peel, E. S. Saltzman, and P.-Y. Whung. A 340 year record of biogenic sulphur from the Weddell Sea area, Antarctica. *Annals of Glaciology*, 21, 1 1995.

M. Pourchet, F. Pinglot, and C. Lorius. Some meteorological applications of radioactive fallout measurements in Antarctic snows. *Journal of Geophysical Research*, 88:6013, 1983.

S. Preunkert, B. Jourdain, M. Legrand, R. Udisti, S. Becagli, and O. Cerri. Seasonality of sulfur species (dimethyl sulfide, sulfate, and methanesulfonate) in Antarctica: Inland versus coastal regions. *Journal of Geophysical Research Atmospheres*, 113, 2008.

M. Proposito and M. Frezzotti. Preliminary glacio-chemical analysis of GV5 and GV7 firn cores collected along the Oates Coast-Talos Dome Transect. *Terra Antartica Reports*, 14:111–116, 2008.

M. R. Rampino. Stratospheric Aerosols, and Climatic Impact. *QUATERNARY RESEARCH*, 18:127–143, 1982.

A. M. Rankin, V. Auld, and E. W. Wolff. Frost flowers as a source of fractionated sea salt aerosol in the polar regions. *Geophysical Research Letters*, 27, 11 2000.

A. M. Rankin, E. W. Wolff, and S. Martin. Frost flowers: Implications for tropospheric chemistry and ice core interpretation. *Journal of Geophysical Research: Atmospheres*, 107, 12 2002.

A. M. Rankin, E. W. Wolff, and R. Mulvaney. A reinterpretation of sea-salt records in greenland and Antarctic ice cores? *Annals of Glaciology*, 39:276–282, 2004.

M. N. Raphael. A zonal wave 3 index for the Southern Hemisphere. *Geophysical Research Letters*, 31, 12 2004.

M. N. Raphael. The influence of atmospheric zonal wave three on Antarctic sea ice variability. *Journal of Geophysical Research*, 112: D12112, 6 2007.

M. N. Raphael and W. Hobbs. The influence of the large-scale atmospheric circulation on Antarctic sea ice during ice advance and retreat seasons. *Geophysical Research Letters*, 41:5037–5045, 7 2014.

S. O. Rasmussen, K. K. Andersen, A. M. Svensson, J. P. Steffensen, B. M. Vinther, H. B. Clausen, M. L. Siggaard-Andersen, S. J. Johnsen, L. B. Larsen, D. Dahl-Jensen, M. Bigler, R. Röthlisberger,

H. Fischer, K. Goto-Azuma, M. E. Hansson, and U. Ruth. A new Greenland ice core chronology for the last glacial termination. *Journal of Geophysical Research Atmospheres*, 111, 3 2006.

C. Reason. Multidecadal climate variability in the subtropics/mid-latitudes of the Southern Hemisphere oceans. *Tellus A: Dynamic Meteorology and Oceanography*, 52:203–223, 1 2000.

F. Remy and I. E. Tabacco. Bedrock features and ice flow near the EPICA Ice Core Site (Dome C, Antarctica). *Geophysical Research Letters*, 27:405–408, 2 2000.

J. Roberts, C. Plummer, T. Vance, T. V. Ommen, A. Moy, S. Poynter, A. Treverrow, M. Curran, and S. George. A 2000-year annual record of snow accumulation rates for Law Dome, East Antarctica. *Climate of the Past*, 11:697–707, 5 2015.

J. L. Roberts, T. D. V. Ommen, M. A. Curran, and T. R. Vance. Methanesulphonic acid loss during ice-core storage: recommendations based on a new diffusion coefficient. *Journal of Glaciology*, 55:784–788, 9 2009.

A. Robock. Volcanic Eruptions and Climate. *Reviews of Geophysics*, 38:191–2019, 2000.

R. Röthlisberger, M. A. Hutterli, S. Sommer, E. W. Wolff, and R. Mulvaney. Factors controlling nitrate in ice cores: Evidence from the Dome C deep ice core. *Journal of Geophysical Research Atmospheres*, 105:20565–20572, 8 2000a.

R. Röthlisberger, M. A. Hutterli, S. Sommer, E. W. Wolff, and R. Mulvaney. Factors controlling nitrate in ice cores: Evidence from the Dome C deep ice core. *Journal of Geophysical Research: Atmospheres*, 105, 8 2000b.

R. Röthlisberger, M. A. Hutterli, E. W. Wolff, R. Mulvaney, H. Fischer, M. Bigler, K. Goto-Azuma, M. E. Hansson, U. Ruth, M.-L. Siggaard-Andersen, and J. P. Steffensen. Nitrate in Greenland and Antarctic ice cores: a detailed description of post-depositional processes. *Annals of Glaciology*, 35:209–216, 2002. URL `http://nsidc.org`.

R. Röthlisberger, R. Mulvaney, E. W. Wolff, M. A. Hutterli, M. Bifler, M. de Angelis, M. Hansson, J. P. Steffensen, and U. Roberto. Limited dechlorination of sea-salt aerosol during the last glacial period: Evidence from the European Project for Ice Coring in Antarctica (EPICA) Dome C ice core. *Journal of Geophysical Research*, 108, 2003.

J. Savarino, J. Kaiser, S. Morin, D. M. Sigman, and M. H. Thiemens. Nitrogen and oxygen isotopic constraints on the origin of atmospheric nitrate in coastal Antarctica. *Atmospheric Chemistry and Physics*, 7, 4 2007.

C. Scarchilli, M. Frezzotti, and P. M. Ruti. Snow precipitation at four ice core sites in East Antarctica: provenance, seasonality and blocking factors. *Climate Dynamics*, 37:2107–2125, 11 2011.

S. Self, M. R. Rampino, and M. J. Carr. A reappraisal of the 1835 eruption of Cosiguina and its atmospheric impact. *Bulletin of Volcanology*, 52:57–65, 10 1989. ISSN 0258-8900. doi: 10.1007/BF00641387.

M. C. Serreze and W. N. Meier. The Arctic's sea ice cover: trends, variability, predictability, and comparisons to the Antarctic. *Annals of the New York Academy of Sciences*, 1436:36–53, 1 2019.

M. Severi, S. Becagli, E. Castellano, A. Morganti, R. Traversi, R. Ud-

isti, U. Ruth, H. Fischer, P. Huybrechts, E. Wolff, F. Parrenin, P. Kaufmann, F. Lambert, and J. P. Steffensen. Synchronisation of the EDML and EDC ice cores for the last 52 kyr by volcanic signature matching. *Climate of the Past*, 3:367–374, 7 2007. URL `https://cp.copernicus.org/articles/3/367/2007/`.

M. Severi, R. Udisti, S. Becagli, B. Stenni, and R. Traversi. Volcanic synchronisation of the EPICA-DC and TALDICE ice cores for the last 42 kyr BP. *Climate of the Past*, 8:509–517, 2012. ISSN 18149324. doi: 10.5194/cp-8-509-2012.

M. Severi, S. Becagli, D. Frosini, M. Marconi, R. Traversi, and R. Udisti. A novel Fast Ion Chromatographic Method for the Analysis of Fluoride in Antarctic Snow and Ice. *Environmental Science & Technology*, 48, 2 2014.

M. Severi, S. Becagli, L. Caiazzo, V. Ciardini, E. Colizza, F. Giardi, K. Mezgec, C. Scarchilli, B. Stenni, E. R. Thomas, R. Traversi, and R. Udisti. Sea salt sodium record from Talos Dome (East Antarctica) as a potential proxy of the Antarctic past sea ice extent. *Chemosphere*, 177:266–274, 2017.

G. Shi, A. M. Buffen, M. G. Hastings, C. Li, H. Ma, Y. Li, B. Sun, C. An, and S. Jiang. Investigation of post-depositional processing of nitrate in East Antarctic snow: isotopic constraints on photolytic loss, re-oxidation, and source inputs. *Atmospheric Chemistry and Physics*, 15:9435–9453, 8 2015.

M. Sigl, J. R. McConnell, L. Layman, O. Maselli, K. McGwire, D. Pasteris, D. Dahl-Jensen, J. P. Steffensen, B. Vinther, R. Edwards, R. Mulvaney, and S. Kipfstuhl. A new bipolar ice core record of volcanism from WAIS Divide and NEEM and implications for

climate forcing of the last 2000 years. *Journal of Geophysical Research Atmospheres*, 118:1151–1169, 2 2013.

M. Sigl, J. R. McConnell, M. Toohey, M. Curran, S. B. Das, R. Edwards, E. Isaksson, K. Kawamura, S. Kipfstuhl, K. Krüger, L. Layman, O. J. Maselli, Y. Motizuki, H. Motoyama, D. R. Pasteris, and M. Severi. Insights from Antarctica on Volcanic forcing during the common era. *Nature Climate Change*, 4:693–697, 2014.

M. Sigl, M. Winstrup, J. R. McConnell, K. C. Welten, G. Plunkett, F. Ludlow, U. Büntgen, M. Caffee, N. Chellman, D. Dahl-Jensen, H. Fischer, S. Kipfstuhl, C. Kostick, O. J. Maselli, F. Mekhaldi, R. Mulvaney, R. Muscheler, D. R. Pasteris, J. R. Pilcher, M. Salzer, S. Schüpbach, J. P. Steffensen, B. M. Vinther, and T. E. Woodruff. Timing and climate forcing of volcanic eruptions for the past 2,500 years. *Nature*, 523:543–549, 7 2015.

M. Sigl, T. J. Fudge, M. Winstrup, J. Cole-Dai, D. Ferris, J. R. McConnell, K. C. Taylor, K. C. Welten, T. E. Woodruff, F. Adolphi, M. Bisiaux, E. J. Brook, C. Buizert, M. W. Caffee, N. W. Dunbar, R. Edwards, L. Geng, N. Iverson, B. Koffman, L. Layman, O. J. Maselli, K. McGwire, R. Muscheler, K. Nishiizumi, D. R. Pasteris, R. H. Rhodes, and T. A. Sowers. The WAIS Divide deep ice core WD2014 chronology - Part 2: Annual-layer counting (0-31 ka BP). *Climate of the Past*, 12:769–786, 3 2016.

H. Sigurdsson. Evidence of volcanic loading of the atmosphere and climate response. *Global and Planetary Change*, 3:277–289, 1990.

T. Simkin and L. Siebert. *Volcanoes of the World*. Geoscience Press, 2nd edition, 1994. doi: 10.1017/S001675689730613X.

I. Simmonds and T. H. Jacka. Relationships between the Interan-

nual Variability of Antarctic Sea Ice and the Southern Oscillation. *Journal of Climate*, 8:637–647, 3 1995.

H. Sodemann and A. Stohl. Asymmetries in the moisture origin of antarctic precipitation. *Geophysical Research Letters*, 36, 11 2009.

J. Stefels, M. Steinke, S. Turner, G. Malin, and S. Belviso. Environmental constraints on the production and removal of the climatically active gas dimethylsulphide (DMS) and implications for ecosystem modelling. *Biogeochemistry*, 83:245–275, 3 2007. ISSN 01682563. doi: 10.1007/s10533-007-9091-5.

E. J. Steig, P. J. Polissar, M. Stuiver, P. M. Grootes, and R. C. Finkel. Large amplitude solar modulation cycles of 10Be in Antarctica: Implications for atmospheric mixing processes and interpretation of the ice core record. *Geophysical Research Letters*, 23, 3 1996.

E. J. Steig, Q. Ding, J. W. C. White, M. Küttel, S. B. Rupper, T. A. Neumann, P. D. Neff, A. J. E. Gallant, P. A. Mayewski, K. C. Taylor, G. Hoffmann, D. A. Dixon, S. W. Schoenemann, B. R. Markle, T. J. Fudge, D. P. Schneider, A. J. Schauer, R. P. Teel, B. H. Vaughn, L. Burgener, J. Williams, and E. Korotkikh. Recent climate and ice-sheet changes in West Antarctica compared with the past 2,000 years. *Nature Geoscience*, 6:372–375, 2013.

B. Stenni, M. Proposito, R. Gragnani, O. Flora, J. Jouzel, S. Falourd, and M. Frezzotti. Eight centuries of volcanic signal and climate change at Talos Dome (East Antarctica). *Journal of Geophysical Research D: Atmospheres*, 107:3–1, 5 2002. ISSN 01480227. doi: 10.1029/2000jd000317.

B. Stenni, J. Jouzel, V. Masson-Delmotte, R. Röthlisberger, E. Castellano, O. Cattani, S. Falourd, S. Johnsen, A. Longinelli, and J. Sachs.

A late-glacial high-resolution site and source temperature record derived from the EPICA Dome C isotope records (East Antarctica). *Earth and Planetary Science Letters*, 217, 1 2004.

W. Sunda, D. J. Kieber, R. P. Kiene, and S. Huntsman. An antioxidant function for DMSP and DMS in marine algae. *Nature*, 418, 7 2002.

G. Tao, R. Yamada, Y. Fujikawa, A. Kudo, J. Zheng, D. A. Fisher, and R. M. Koerner. Determination of trace amounts of heavy metals in Arctic ice core samples using inductively coupled plasma mass spectrometry. *Talanta*, 55:765–772, 2001. URL `www.elsevier.com/locate/talanta`.

L. I. M. A. team LIMA. Transantarctic Mountains, West Antarctica, East Antarctica, 2019. URL `http://lima.nasa.gov/pdf/A3_overview.pdf`. Accessed: 11-06-2021).

K. Teinilä, V.-M. Kerminen, and R. Hillamo. A study of size-segregated aerosol chemistry in the Antarctic atmosphere. *Journal of Geophysical Research: Atmospheres*, 105:3893–3904, 2 2000.

E. R. Thomas, J. M. V. Wessem, J. Roberts, E. Isaksson, E. Schlosser, T. J. Fudge, P. Vallelonga, B. Medley, J. Lenaerts, N. Bertler, M. R. V. D. Broeke, D. A. Dixon, M. Frezzotti, B. Stenni, M. Curran, and A. A. Ekaykin. Regional Antarctic snow accumulation over the past 1000 years. *Climate of the Past*, 13:1491–1513, 11 2017.

S. A. Thorpe. Bubble clouds and the dynamics of the upper ocean. *Quarterly Journal of the Royal Meteorological Society*, 118, 1 1992.

A. R. Tome and P. M. A. Miranda. Piecewise linear fitting and trend changing points of climate parameters. *Geophysical Research Letters*, 31, 1 2004.

D. A. Toole and D. A. Siegel. Light-driven cycling of dimethylsulfide (DMS) in the Sargasso Sea: Closing the loop. *Geophysical Research Letters*, 31, 5 2004.

F. Traufetter, H. Oerter, H. Fischer, R. Weller, and H. Miller. Spatio-temporal variability in volcanic sulphate deposition over the past 2 kyr in snow pits and firn cores from amundsensen, antarctica. *Journal of Glaciology*, 50:137–146, 2004.

R. Traversi, S. Becagli, E. Castellano, A. Migliori, M. Severi, and R. Udisti. High-resolution fast ion chromatography (FIC) measurements of chloride, nitrate and sulphate along the EPICA Dome C ice core. *Annals of Glaciology*, 35, 9 2002.

R. Traversi, S. Becagli, E. Castellano, O. Largiuni, A. Migliori, M. Severi, M. Frezzotti, and R. Udisti. Spatial and temporal distribution of environmental markers from coastal to plateau areas in Antarctica by firn core chemical analysis. *International Journal of Environmental Analytical Chemistry*, 84:457–470, 5 2004.

R. Traversi, S. Becagli, E. Castellano, O. Cerri, A. Morganti, M. Severi, and R. Udisti. Study of Dome C site (East Antartica) variability by comparing chemical stratigraphies. *Microchemical Journal*, 92: 7–14, 5 2009.

R. Traversi, I. G. Usoskin, S. K. Solanki, S. Becagli, M. Frezzotti, M. Severi, B. Stenni, and R. Udisti. Nitrate in Polar Ice: A New Tracer of Solar Variability. *Solar Physics*, 280:237–254, 9 2012.

R. Traversi, R. Udisti, D. Frosini, S. Becagli, V. Ciardini, B. Funke, C. Lanconelli, B. Petkov, C. Scarchilli, M. Severi, and V. Vitale. Insights on nitrate sources at Dome C (East Antarctic Plateau)

from multi-year aerosol and snow records. *Tellus, Series B: Chemical and Physical Meteorology*, 66, 2014. ISSN 16000889. doi: 10.3402/tellusb.v66.22550.

K. Trenberth and N. C. for Atmospheric Research Staff (Eds). The Climate Data Guide: Southern Oscillation Indices: Signal, Noise and Tahiti/Darwin SLP (SOI), 2 2020. URL `fromhttps://climatedataguide.ucar.edu/climate-data/southern-oscillation-indices-signal-noise-and-tahitidarwin-slp-soi`. Accessed: 11-06-2021).

K. E. Trenberth. A quasi-biennial standing wave in the Southern Hemisphere and interrelations with sea surface temperature. *Quarterly Journal of the Royal Meteorological Society*, 101:55–74, 1 1975.

K. E. Trenberth. Planetary waves at 500 mb in the Southern Hemisphere. *Monthly Weather Review*, 108:1378–1389, 9 1980.

C. R. Trepte and M. H. Hitchman. Tropical stratospheric circulation deduced from satellite aerosol data. *Nature*, 355:626–628, 2 1992.

J. Turner. The El Niño-southern oscillation and Antarctica. *International Journal of Climatology*, 24:1–31, 1 2004.

J. Turner, J. S. Hosking, T. J. Bracegirdle, G. J. Marshall, and T. Phillips. Recent changes in Antarctic Sea Ice. *Philosophical Transactions of the Royal Society A: Mathematical, Physical and Engineering Sciences*, 373:20140163, 7 2015. doi: 10.1098/rsta.2014.0163.

J. Turner, G. J. Marshall, K. Clem, S. Colwell, T. Phillips, H. Lu, C. J. Turner, and B. A. Survey. Antarctic temperature variability

and change from station data. *International Journal of Climatology*, 40:2986–3007, 2019.

R. Udisti. Multiparametric approach for chemical dating of snow layers from Antarctica. *International Journal of Environmental Analytical Chemistry*, 63:225–244, 1996. ISSN 03067319. doi: 10.1080/03067319608026268.

R. Udisti, S. Becagli, S. Benassai, E. Castellano, I. Fattori, M. Innocenti, A. Migliori, and R. Traversi. Atmosphere-snow interaction by a comparison between aerosol and uppermost snow-layers composition at Dome C, East Antarctica. *Annals of Glaciology*, 39: 53–61, 2004. URL `http://uwamrc.ssec.wisc.edu/aws/`.

U. United Nations Scientific Committee on the Effects of Atomic Radiation. *Sources and effects of ionizing radiation : United Nations Scientific Committee on the Effects of Atomic Radiation : UNSCEAR 2000 report to the General Assembly, with scientific annexes*. United Nations, 2000. ISBN 9211422388.

S. Urbini, M. Frezzotti, S. Gandolfi, C. Vincent, C. Scarchilli, L. Vittuari, and M. Fily. Historical behaviour of Dome C and Talos Dome (East Antarctica) as investigated by snow accumulation and ice velocity measurements. *Global and Planetary Change*, 60: 576–588, 2 2008.

I. G. Usoskin, K. Horiuchi, S. Solanki, G. A. Kovaltsov, and E. Bard. On the common solar signal in different cosmogenic isotope data sets. *Journal of Geophysical Research: Space Physics*, 114, 3 2009.

O. Vaittinen, M. Metsala, S. Persijn, M. Vainio, and L. Halonen. Adsorption of ammonia on treated stainless steel and polymer surfaces. *Applied Physics B*, pages 185–196, 2014.

S. M. Vallina and R. Simo. Strong relationship between DMS and the solar radiation dose over the global surface ocean. *Science*, 315: 506–508, 1 2007. ISSN 00368075. doi: 10.1126/science.1133680.

H. van Loon. The Half-Yearly Oscillations in Middle and High Southern Latitudes and the Coreless Winter. *Journal of the Atmospheric Sciences*, 24, 9 1967.

D. Wagenbach, F. Ducroz, R. Mulvaney, L. Keck, A. Minikin, M. Legrand, J. S. Hall, and E. W. Wolff. Sea-salt aerosol in coastal Antarctic regions. *Journal of Geophysical Research D: Atmospheres*, 103:10961–10974, 1998. ISSN 01480227. doi: 10.1029/97jd01804.

T. Warneke, I. W. Croudace, P. E. Warwick, and R. N. Taylor. A new ground-level fallout record of uranium and plutonium isotopes for northern temperate latitudes. *Earth and Planetary Science Letters*, 203, 11 2002.

O. Watanabe, K. Kamiyama, H. Motoyama, Y. Fujii, H. Shoji, and K. Satow. The paleoclimate record in the ice core at Dome Fuji station, East Antarctica. *Annals of Glaciology*, 29:176–178, 1999.

C. N. Waters, J. Zalasiewicz, C. Summerhayes, A. D. Barnosky, C. Poirier, A. Galuszka, A. Cearreta, M. Edgeworth, E. C. Ellis, M. Ellis, C. Jeandel, R. Leinfelder, J. R. McNeill, D. d. Richter, W. Steffen, J. Syvitski, D. Vidas, M. Wagreich, M. Williams, A. Zhisheng, J. Grinevald, E. Odada, N. Oreskes, and A. P. Wolfe. The Anthropocene is functionally and stratigraphically distinct from the Holocene. *Science*, 351, 1 2016.

D. Weiss, W. Shotyk, and O. Kempf. Archives of Atmospheric Lead Pollution. *Naturwissenschaften*, 86:262–275, 6 1999.

K. A. Welch, P. A. Mayewski, and S. I. Whitlow. Methanesulfonic acid in coastal Antarctic snow related to sea-ice extent. *Geophysical Research Letters*, 20, 3 1993.

R. Weller, F. Traufetter, H. Fischer, H. Oerter, C. Piel, and H. Miller. Postdepositional losses of methane sulfonate, nitrate, and chloride at the European Project for Ice Coring in Antarctica deep-drilling site in Dronning Maud Land, Antarctica. *Journal of Geophysical Research*, 109:D07301–undefined, 2004.

R. Weller, D. Wagenbach, M. Legrand, C. Elsässer, X. Tian-Kunze, and G. König-Langlo. Continuous 25-yr aerosol records at coastal Antarctica - I: Inter-annual variability of ionic compounds links to climate indices. *Tellus, Series B: Chemical and Physical Meteorology*, 63:901–919, 11 2011. ISSN 02806509. doi: 10.1111/j.1600-0889.2011.00542.x.

I. M. Whillans and P. M. Grootes. Isotopic diffusion in cold snow and firn. *Journal of Geophysical Research*, 90, 1985.

S. Whitlow, P. Mayewski, and J. Dibb. A comparison of major chemical species seasonal concentration and accumulation at the South Pole and summit, Greenland. *Atmospheric Environment. Part A. General Topics*, 26, 8 1992.

P.-Y. Whung, E. S. Saltzman, M. J. Spencer, P. A. Mayewski, and N. Gundestrup. Two-hundred-year record of biogenic sulfur in a south Greenland ice core (20D). *Journal of Geophysical Research*, 99, 1994.

D. A. Winski, T. J. Fudge, D. G. Ferris, E. C. Osterberg, J. M. Fegyveresi, J. Cole-Dai, Z. Thundercloud, T. S. Cox, K. J. Kreutz, N. Ortman, C. Buizert, J. Epifanio, E. J. Brook, R. Beaudette,

J. Severinghaus, T. Sowers, E. J. Steig, E. C. Kahle, T. R. Jones, V. Morris, M. Aydin, M. R. Nicewonger, K. A. Casey, R. B. Alley, E. D. Waddington, N. A. Iverson, N. W. Dunbar, R. C. Bay, J. M. Souney, M. Sigl, and J. R. McConnell. The SP19 chronology for the South Pole Ice Core - part 1: Volcanic matching and annual layer counting. *Climate of the Past*, 15:1793–1808, 10 2019.

M. Winstrup, A. M. Svensson, S. O. Rasmussen, O. Winther, E. J. Steig, and A. E. Axelrod. An automated approach for annual layer counting in ice cores. *Climate of the Past*, 8, 11 2012.

M. Winstrup, P. Vallelonga, H. A. Kjær, T. J. Fudge, J. E. Lee, M. H. Riis, R. Edwards, N. A. N. Bertler, T. Blunier, E. J. Brook, C. Buizert, G. Ciobanu, H. Conway, D. Dahl-Jensen, A. Ellis, B. D. Emanuelsson, R. C. A. Hindmarsh, E. D. Keller, A. V. Kurbatov, P. A. Mayewski, P. D. Neff, R. L. Pyne, M. F. Simonsen, A. Svensson, A. Tuohy, E. D. Waddington, and S. Wheatley. A 2700-year annual timescale and accumulation history for an ice core from Roosevelt Island, West Antarctica. *Climate of the Past*, 15, 4 2019.

E. W. Wolff. *Nitrate in Polar Ice*. Springer Berlin Heidelberg, 1995. doi: 10.1007/978-3-642-51172-1_10.

E. W. Wolff, A. M. Rankin, and R. Rothlisberger. An ice core indicator of Antarctic sea ice production? *Geophysical Research Letters*, 30, 11 2003.

E. W. Wolff, C. Barbante, S. Becagli, M. Bigler, C. F. Boutron, E. Castellano, M. de Angelis, U. Federer, H. Fischer, F. Fundel, M. Hansson, M. Hutterli, U. Jonsell, T. Karlin, P. Kaufmann, F. Lambert, G. C. Littot, R. Mulvaney, R. Röthlisberger, U. Ruth, M. Severi, M. L. Siggaard-Andersen, L. C. Sime, J. P. Steffensen,

T. F. Stocker, R. Traversi, B. Twarloh, R. Udisti, D. Wagenbach, and A. Wegner. Changes in environment over the last 800,000 years from chemical analysis of the EPICA Dome C ice core. *Quaternary Science Reviews*, 29:285–295, 1 2010. ISSN 02773791. doi: 10.1016/j.quascirev.2009.06.013.

Y. C. Wu and P. A. Berezansky. Low electrolytic conductivity standards. *Journal of Research - National Institute of Standards & Technology*, 100:521–527, 1995.

K. Yalcin, C. P. Wake, K. J. Kreutz, M. S. Germani, and S. I. Whitlow. Ice core evidence for a second volcanic eruption around 1809 in the Northern Hemisphere. *Geophysical Research Letters*, 33, 7 2006. ISSN 00948276. doi: 10.1029/2006GL026013.

X. Yang, J. A. Pyle, and R. A. Cox. Sea salt aerosol production and bromine release: Role of snow on sea ice. *Geophysical Research Letters*, 35, 8 2008.

X. Yao, P. J. Rehbein, C. J. Lee, G. J. Evans, J. Corbin, and C.-H. Jeong. A study on the extent of neutralization of sulphate aerosol through laboratory and field experiments using an ATOFMS and a GPIC. *Atmospheric Environment*, 45:6251–6256, 11 2011.

G. K. Yue. The formation and growth of sulfate aerosols in the stratosphere. *Atmospheric Environment*, 15:549–556, 1981.

M. Zatko, L. Geng, B. Alexander, E. Sofen, and K. Klein. The impact of snow nitrate photolysis on boundary layer chemistry and the recycling and redistribution of reactive nitrogen across Antarctica and Greenland in a global chemical transport model. *Atmospheric Chemistry and Physics*, 16, 3 2016.

G. A. Zielinski. Use of paleo-records in determining variability within the volcanism climate system. *Quaternary Science Reviews*, 19: 417–438, 2000.